NASA SP-418

LUNAR SAMPLE STUDIES

National Aeronautics and Space Administration

NASA SP-418

LUNAR SAMPLE STUDIES

Prepared by
NASA
LYNDON B. JOHNSON
SPACE CENTER

Scientific and Technical Information Office
NATIONAL AERONAUTICS AND SPACE ADMINISTRATION
Washington, D.C.
1977

Preface

This publication reports the results of five separate investigations of lunar samples which, while heralding no important new discoveries and theories in planetary science, contain nevertheless a wealth of descriptions and compilations valuable by themselves and important enough to be published by NASA. The samples and the nature of their analyses are:

An Apollo 15 breccia (15015), which is thoroughly analyzed as to the nature of the mature regolith from which it derived and the time and nature of the lithification process.

Two Apollo 11 and one Apollo 12 basalts (10069, 10071, and 12008), analyzed in terms of chemistry, Cross-Iddings-Pirsson-Washington norms, mineralogy, and petrography.

Eight Apollo 17 mare basalts (70017, 71055, 74255, 75075, 70215, 71569, 74275, and 75035), also analyzed in terms of chemistry, Cross-Iddings-Pirsson-Washington norms, mineralogy, and petrography. The first seven are shown to be chemically similar although of two main textural groups; the eighth is seen to be distinct in both chemistry and mineralogy.

A troctolitic clast from a Fra Mauro breccia (14321), analyzed and contrasted with other high-temperature lunar mineral assemblages. Two basaltic clasts from the same breccia are shown to have affinities with rock 14053.

And finally, the uranium-thorium-lead systematics of three Apollo 16 samples (60018, 60025, 64435) are determined; serious terrestrial-lead contamination of the first two samples is attributed to bandsaw cutting in the lunar curatorial facility.

The text, tables, and illustrations have been reviewed and approved for publication by a Lunar Samples Studies Editorial Board, chaired by William C. Phinney and Henry E. Clements.

February 1977

WILLIAM C. PHINNEY
Lyndon B. Johnson Space Center

Contents

1. The History of Lunar Breccia 15015

The European Consortium and Friends[a]

Breccia 15015, collected at the Apollo 15 lunar module station, is a coherent, tough soil breccia with an extensive glass surface coating. The wide range of data obtained on this rock is presented. The information concerns the nature of the mature regolith from which the rock was formed and the time and nature of the lithification process.

Lunar breccia 15015 is a coherent, tough breccia; 95 percent of the observable surface is glass coated. This large rock (fig. 1-1) (25 by 15 by 13 cm; 4770 g) was collected about 20 m west of the Apollo 15 lunar module (LM) site. It was first noticed by astronaut Scott during the standup extravehicular activity as unique in appearance and apparently unrelated to any nearby rocks or craters. Although 15015 was not documented during collection, its orientation on the lunar surface is known. A large portion of the rock, particularly the top and sides, is highly vesicular and cindery in texture.

The polarization properties of the rock indicate a ubiquitous vitreous coating on the exterior surfaces. The bulk chemistry of this glass is similar to the bulk composition of the rock and appears, on petrological grounds also, to have been derived from fusion of the rock. The rock contains a wide range of lithic fragments, among them both mare and potassium, rare-earth elements and phosphorus (KREEP[1]) basalts, mineral fragments, and glasses, including devitrified "green glass." These components are typical of the Apollo 15 regolith in general and in detail are characteristic of the surface material at the LM station. Argon-40/argon-39 ($^{40}Ar/^{39}Ar$) ages indicate at least one clast older than 3.7 billion years (b.y.). The

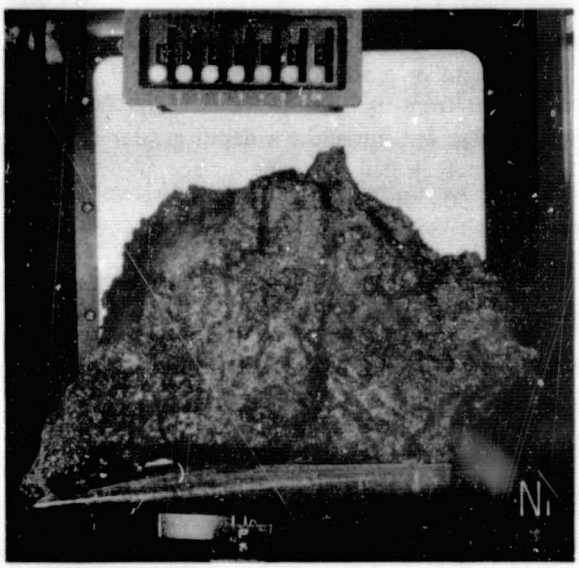

Figure 1-1.- Highly vesicular glassy breccia 15015.

[a]The team composition is listed in Acknowledgments at the end of this section.

[1]Term used to express chemical composition of lunar materials, after Hubbard, N. J.; and Gast, P. W.: Chemical Composition and Origin of Nonmare Lunar Basalts. Proceedings of the Second Lunar Science Conference, vol. 2, MIT Press (Cambridge, Mass.), 1971, p. 999.

$^{38}Ar/^{37}Ar$ ages, noble gases, and track studies indicate an extensive preconsolidation exposure to cosmic rays, and an unusually large exposure age for one clast limits the consolidation age to less than 2.7 b.y. The "isochron age" of frothy vesicular glass tentatively indicates consolidation 1.0 b.y. ago. Carbon (C) data and noble gases show that the constituent grains have been heavily irradiated by solar wind. At some time in its history, possibly during impact lithification, 15015 experienced a nonuniform heating that caused light or more volatile species to be preferentially lost from its upper surfaces. After formation, the breccia was buried at a depth greater than 2 m until it was ejected onto the surface, possibly as recently as 30 million years (m.y.) ago.

SAMPLE PROCESSING

The Consortium allocation, 15015,15 (150 g) was cut from the whole rock as a column to provide material from the top, interior, and bottom of the sample (fig. 1-2). Aliquots of material from each of these locations were studied for their C chemistry, rare-gas content, cosmic ray fission tracks, trace-element composition, and selenochronology. In addition, surface samples from both top and bottom were investigated for their optical properties. Polished thin sections (15015,14,132 to 135) for the mineralogical and petrological studies were prepared from a slice adjacent to the surface sampled for the other measurements.

All sawing operations were performed at the University of Bristol with a water-cooled saw operating in a stainless steel nitrogen-filled glove box situated in a clean-air facility (ref. 1-1). The rock was fed slowly into a 15.2- by 0.05-cm diamond cutting disk by a counterbalance. Chipping operations were conducted directly in the flow of a laminar-flow clean-air bench using a stainless steel hammer and chisels. The nitrogen glove box and all materials coming into contact with the samples (aluminum foil, forceps, chisels, etc.) were precleaned by ultrasonic extraction in redistilled analytical reagent grade toluene methanol (3:1). All processes were documented photographically. The sample allocation plan is shown in table 1-I. The bulk chemical analysis (table 1-II, analysis 1) was performed on the dust generated during sample division.

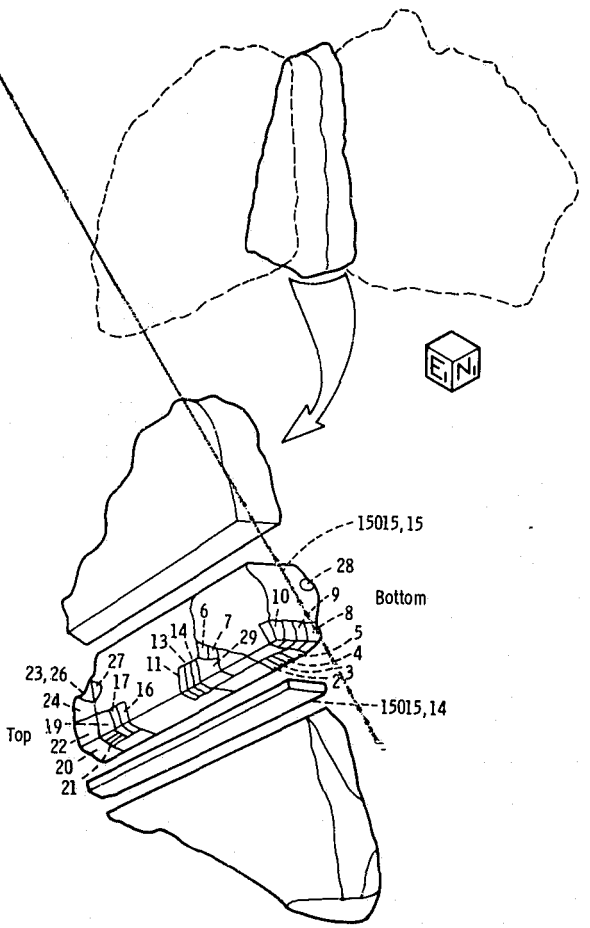

Figure 1-2.- Sample subdivision of lunar breccia 15015.

The procedures used for the determination of methane (CH_4) and carbide (ref. 1-2), rare gases (ref. 1-3), bulk, trace chemistry, and electron microprobe analysis (ref. 1-4), track studies (ref. 1-5), selenochronology (ref. 1-6), and optical properties (ref. 1-7) have been detailed previously elsewhere. Total C, sulfur (S), and nitrogen (N) analyses were performed by submitting samples to complete combustion in a partial atmosphere of oxygen (O). Carbon was collected as carbon dioxide (CO_2), S as sulfur dioxide (SO_2), and N as nitrogen gas (N_2). During this procedure, an attempt was made to measure the volume of helium (He) released; however, the amount released was below the detection limit of the manometer used (0.002 ml, or 5×10^{-3} cc/g of analyzed sample).

TABLE 1-I.- SAMPLE ALLOCATION PLAN

Position of sample	Sample no.	Investigation
Top surface	15015,22	Tracks
	15015,23	Selenochronology
	15015,24	Optical properties
Surface	15015,26	Selenochronology
Clast	15015,27	Rare gases
Top	15015,16	Trace elements
	15015,17	Carbon, nitrogen, sulfur
	15015,19	Selenochronology
	15015,20	Rare gases
	15015,21	Methane and carbide
Middle	15015,6	Methane and carbide
	15015,7	Carbon, nitrogen, sulfur
	15015,11	Trace elements
	15015,13	Selenochronology
	15015,14	Rare gas
	15015,29	X-ray photoelectron spectroscopy
Bottom surface	15015,8	X-ray photoelectron spectroscopy
	15015,9	Optical properties
	15015,10	Tracks
	15015,28	Mineralogy/petrology
Bottom	15015,2A	Methane and carbide
	15015,2B	Trace elements
	15015,3	Carbon, nitrogen, sulfur
	15015,4	Rare gases
	15015,5	Selenochronology
Polished thin section	15014, 132 to 135	Mineralogy/petrology

Samples examined by X-ray photoelectron spectroscopy (XPS) were mounted on the sample holder of an ES200 spectrometer with epoxy adhesive in such a way that four faces could be independently examined. To avoid spurious contributions to the spectra, the adhesive region was covered with gold foil.

RESULTS AND DISCUSSION

Optical Properties

The top surface of breccia 15015 (15015,15,24) is a very-dark hued sample with a highly glassy, specularly reflecting surface. The geometric albedo (measured at a phase angle of 5°) is 0.070 at wavelength λ = 350 nm (3500 Å), 0.073 at 450 nm (4500 Å), and 0.083 at 600 nm (6000 Å). The amount of polarization ($P = (I_{\perp} - I_{\parallel})/(I_{\perp} + I_{\parallel})$) reaches a maximum of 0.415 at a phase angle of 120°, corresponding almost to the Brewster angle of silicates. These polarization properties are characteristic of specular reflection from dark vitreous surfaces of complex structure.

The rate of change of polarization with phase angle (the so-called polarization slope), generally determined at phase angles near 30°, is related to the geometric albedo. In this respect, the extensive glassy top surface of 15015,15,24 conforms to the polarization slope/albedo law previously established for pulverized terrestrial samples, lunar fines, and rough lunar breccia surfaces. This law has been applied to the determination of asteroid diameters (refs. 1-8 and 1-9).

The exposed top surface of breccia 15015,15,24 is outstanding for the ubiquity of its black glass coating, generally smooth and vesicular, and possibly splashed on. Some parts of the thin shell exhibit cavities several millimeters in diameter. Freshly chipped surfaces are rough and do not produce glassy material.

Dimple microcraters, apparently not of impact origin, are abundant at the surface of the glass coating, as seen in figure 1-3. Some areas display a network of mounds (fig. 1-4) of almost equal size – a few tenths of a micron in diameter – and often regularly spaced or alined in chains. These mounds suggest metallic features similar to those postulated (ref. 1-10) to have been produced by reduction.

Chemical Analysis

Chemical analysis for major elements was performed on a homogenized sample, 15015,15, of powder and rock fragments obtained during sawing operations. A small amount of aluminum foil was the only visible contaminant, and this was removed by handpicking during the sieving of the sample.

Classical methods of analysis were used, as described by Scoon in reference 1-4. The values obtained are given as analysis 1, table 1-II, and they agree closely with the matrix samples analyzed by Rhodes (written communication) given as analyses 14 and 15, table 1-II. These values are in close agreement with the <1-mm fraction of the contingency soil sample 15021 from the LM site, analysis 13, table 1-II. This similarity in composition extends to the trace-element abundance determined by reference 1-11.

The composition is intermediate between mare basalts and the Fra Mauro basaltic glasses described by reference 1-12. These relationships are expressed

TABLE 1-II.- CHEMICAL ANALYSES AND CIPW NORMS OF BRECCIA 15015[a]

[Analyses of whole rock and representative glass fragments]

(a) Description of samples

Analysis no.	Sample description
1	15015,15 whole rock analysis; analyst, J. H. Scoon
2	Glass; light brown, from vesicular external skin of 15015,133
3	Glass; light brown, smooth external skin of 15015,15 to 25
4	Glass; light brown, from vesicular vein penetrating sample
5	Glass; very pale brown, finely devitrified broken sphere; green glass spheres (GGS)[b]
6	Glass; somewhat inhomogeneous pale-brown striplike fragment molded on matrix; possibly a ''splash'' glass (mare basalts (M))[b]
7	Glass; very pale green sphere (M)
8	Glass; brownish fragment with single vesicle (high-K Fra Mauro basalt (HK))[b]
9	Glass; brown-tinted, investing hypersthene crystal; a cored ''microbomb'' (HK)[b]
10	Glass; colorless or very pale green fragment of sphere partially devitrified at edge; medium-K Fra Mauro basalt (MK)[b]
11	Glass; colorless sphere
12	Glass; colorless sphere; highland basalt (HB)[b]
13	15021 <1-mm fines; LM site; Apollo 15 Preliminary Examination Team
14	15015,15,2b matrix sample; analyst, J. M. Rhodes
15	15015,15,11, matrix sample; analyst, J. M. Rhodes

[a]Analysis 1 by classical wet procedure; analyses 2 to 12 by electron microprobe; analyses 13 to 15 by X-ray fluorescence.

[b]Class types from reference 1-12.

graphically for certain major elements in figures 1-5 to 1-7.

Breccia 15015 may therefore be a shock-lithified representative of a regolith similar to 15021. Such a regolith could be predominantly derived from the local rocks of the Apollo 15 site, or, if the collection area lies on an ejecta ray, it could reflect in part compositions of rocks from a distant source area. In the former case, one would expect the block 15015 to have been ejected from some local crater whereas, in the latter case, the possibility exists that it was shock-lithified at some distant source and represents a residual boulder in fine-grained ray material deposited at the Apollo 15 site.

Mineralogy and Petrology

Rock 15015 is probably a shock-fused polymict soil breccia. The matrix is composed of glass or its cryptocrystalline devitrification products crowded with minute (1 to 2 μm) mineral fragments in which pyroxene predominates over plagioclase. The glass is gray-brown in sections <15 μm thick but almost black and opaque in thicker sections. The opacity is in part due to submicroscopic iron (Fe) or troilite droplets and "ilmenite" crystallites dispersed in the glass.

Larger rock, mineral, and glass fragments are set in this base. Most of the fragments fall within the fol-

TABLE 1-II.- Continued

(b) Chemical analysis

Compound[c]	Analysis no.[d], wt.%														
	1	2	3	4	5	6	7	8	9	10	11	12	13	14	15
SiO_2	47.11	48.01	48.49	47.45	45.65	47.46	47.03	55.30	50.29	49.74	48.61	46.66	46.56	47.50	47.30
TiO_2	1.90	1.89	1.80	1.92	.37	2.02	2.20	2.16	1.94	1.56	.58	.38	1.75	1.76	1.74
Al_2O_3	14.46	13.43	13.96	13.62	7.53	10.31	12.15	14.16	16.12	16.64	17.61	25.91	13.73	13.99	14.16
Cr_2O_3	.40	.02	.40	(e)	.60	.51	.41	.12	.15	.25	.32	.22	(e)	(e)	(e)
FeO	14.38	12.76	14.37	14.94	20.44	19.50	18.08	11.10	10.66	9.49	8.46	5.28	15.21	14.63	14.56
MnO	.19	(e)	.23	.02	.31	.32	.27	.17	.16	.17	.16	.08	.20	.21	.22
MgO	9.93	10.16	9.56	9.50	17.74	11.52	8.27	4.70	6.38	9.26	14.31	7.48	10.37	10.12	10.09
CaO	10.47	11.16	10.41	9.94	8.25	10.36	11.06	8.91	10.25	10.56	10.82	10.24	10.54	10.52	10.62
Na_2O	.31	.56	.51	.51	.23	.30	.25	1.06	.82	.76	.06	.17	.41	.50	.50
N_2O	.28	.24	.29	.01	.02	.13	.05	1.24	.95	.49	.02	.00	.20	.24	.22
P_2O_5	.22	.05	(e)	(e)	(e)	(e)	(e)	.33	.97	.36	(e)	(e)	.18	.24	.22
Total	99.65	98.28	100.02	97.91	101.14	102.43	99.77	99.25	98.69	99.28	100.95	96.42	99.15	99.71	99.63

TABLE 1-II.- Concluded

(c) CIPW norm[f]

Mineral	Analysis no.[d], wt.%														
	1	2	3	4	5	6	7	8	9	10	11	12	13	14	15
Quartz	--	0.35	0.95	1.04	--	--	0.83	14.02	7.13	3.27	--	--	--	--	--
Orthoclase	1.65	1.39	1.34	.06	0.12	0.77	.30	7.33	5.61	2.90	0.12	--	1.18	1.42	1.30
Albite	4.32	4.74	4.20	4.32	1.95	2.54	2.12	8.97	6.94	6.43	.15	1.44	3.47	4.23	4.23
Anorthite (An)	36.34	33.44	35.11	34.84	19.45	26.40	31.88	30.22	37.50	40.55	47.72	69.93	35.03	35.22	35.74
Plagioclase	40.65	38.18	39.31	39.16	21.40	28.94	34.00	39.19	44.44	46.98	48.23	71.37	38.50	39.45	39.97
Diopside	11.69	17.77	13.69	11.98	17.66	20.77	19.26	9.91	5.81	7.74	4.80	4.59	13.30	12.78	12.81
Hypersthene	38.22	36.86	40.52	42.04	27.13	37.15	40.57	23.76	29.55	34.23	41.85	21.74	36.31	39.44	38.15
Olivine	2.86	--	--	--	33.24	10.22	--	--	--	--	4.38	2.68	6.05	2.69	3.50
Chromite	.59	.03	.60	--	.88	.75	.60	.18	.22	.37	.47	.32	--	--	--
Ilmenite	3.61	3.59	3.41	3.65	.70	3.84	4.18	4.10	3.68	2.96	1.10	.72	3.32	3.34	3.30
Apatite	.47	.11	--	--	--	--	--	.78	2.30	.85	--	--	.43	.57	.52
Mol% FeO+MgO in norm pyroxene	41.60	37.90	42.9	43.80	38.90	46.40	52.40	52.50	44.20	33.00	23.80	26.90	42.70	42.20	42.20
Mol% An in norm plagioclase	88.80	86.90	88.70	88.40	90.90	90.70	93.80	76.00	83.60	85.60	98.90	97.90	90.49	88.70	88.84

[a] Analysis 1 by classical wet procedure; analyses 2 to 12 by electron microprobe; analyses 13 to 15 by X-ray fluorescence.

[b] Glass types from reference 1-12.

[c] SiO_2 = silica; TiO_2 = titania; Al_2O_3 = alumina; Cr_2O_3 = chromic oxide; FeO = ferrous oxide; MnO = manganese monoxide; MgO = magnesia; CaO = lime; Na_2O = soda; K_2O = potash; P_2O_5 = phosphorus pentoxide.

[d] From table 1-II(a).

[e] Not determined.

[f] Cross-Iddings-Pirsson-Washington norms.

lowing size ranges: minerals, 0.02 to 0.3 mm; glass fragments, 0.02 to 1.0 mm; lithic fragments, 0.20 to 1.50 mm. Within the lithic fragments, basalts of several types predominate (84 percent) over metaclastic rocks (16 percent). Sporadic lithic fragments of basaltic composition up to 1 cm in size also occur. The distribution of fragment types is somewhat variable as is seen from the modes of four thin sections given in table 1-III. No distinct banding or segregation can be observed.

One surface of the rock, seen in section 15015,133, is coated by a vesicular glass of cindery appearance. The surface of the rock appears frothy and partially melted to a depth of about 5 mm. In thin section, every surface of the rock is seen to be coated with a thin skin of light-brown-colored glass that, with an increasing amount of resorbed mineral fragments, merges in an irregular manner into the body of the rock. On the opposite surface, the glass 15015,15 to 25 is more in the nature of a glazed skin up to 0.5 mm thick coating the rock. In thin section, the glass is similar in color but less vesicular than the frothy glass. Flow bands are visible in thin section and are accentuated by minute submicron droplets of metallic Fe and troilite. The contact between the glass skin and the rock is smooth, and the transition from one to the other is clear-cut.

The composition of the two glasses is quoted in table 1-II, analyses 2 and 3, along with the composition of a thin vein penetrating the sample (analysis 4). These compositions are similar and close enough to the composition of the whole rock to suggest that they have developed from the melting of the whole rock or of a slightly heterogeneous soil or rock of closely allied composition (figs. 1-5 to 1-7).

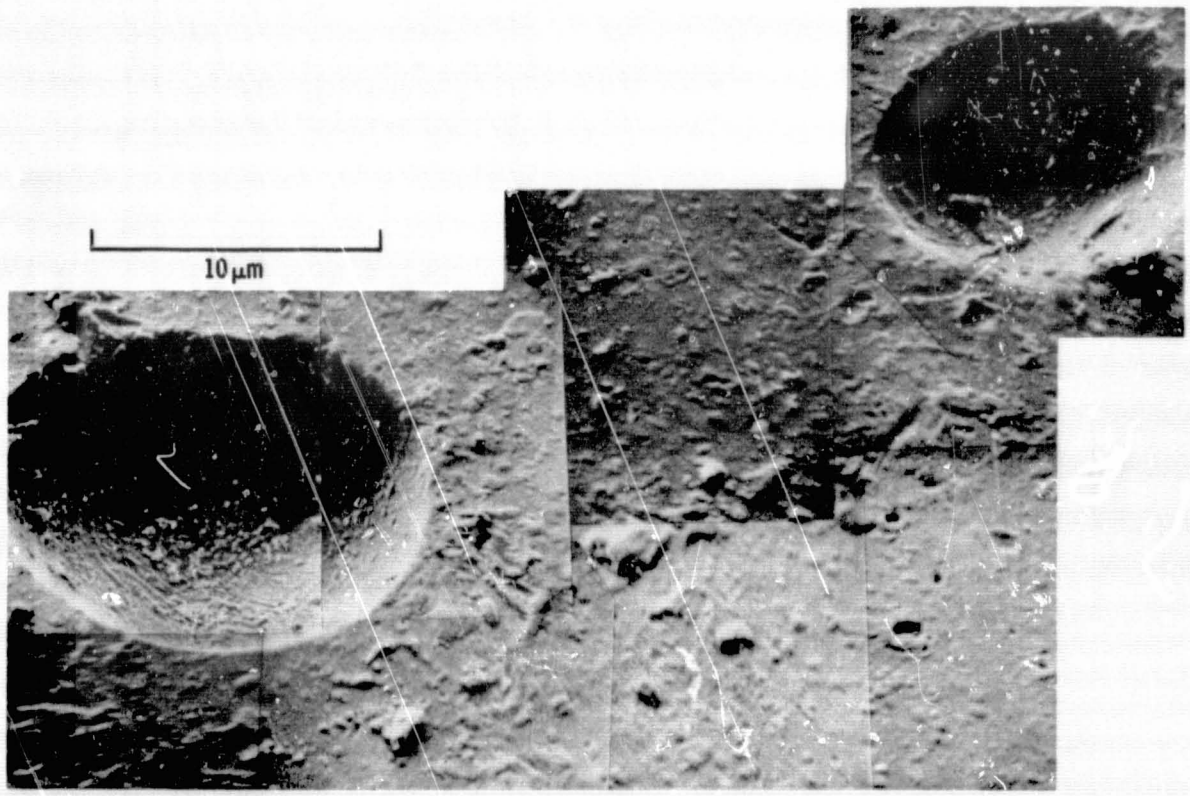

Figure 1-3.- Dimple craters on breccia 15015,15,24.

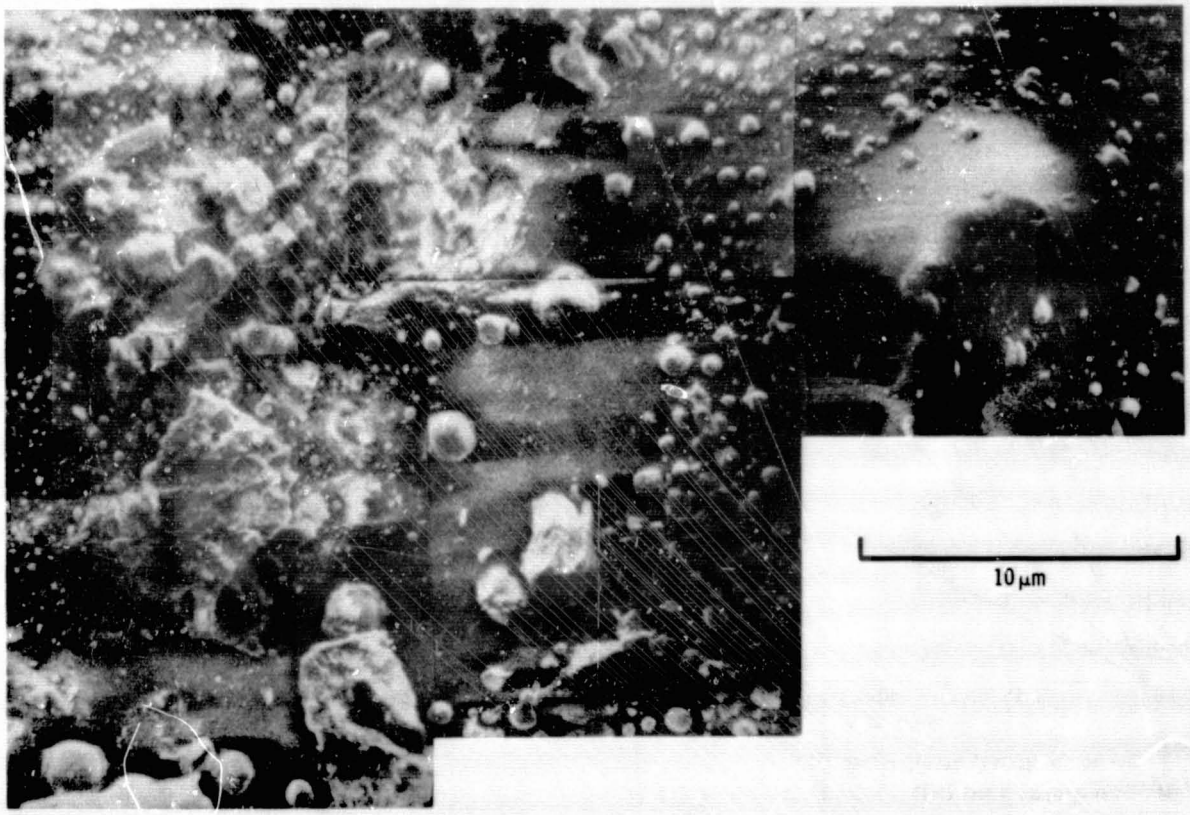

Figure 1-4.- Micromounds on breccia 15015,15,24.

TABLE 1-III.- MODAL MINERALOGY OF BRECCIA 15015

Component	Volume, percent				
	Polished thin section no.				Average
	132	133	135	142	
Rock fragments	16.1	8.8	8.6	8.0	10.4
Pyroxene fragments	16.3	12.2	26.0	21.9	19.1
Plagioclase fragments	5.6	7.2	8.2	10.4	7.8
Glass fragments	9.4	12.7	9.1	8.9	10.0
Metal, oxide, sulfide fragments	1.1	2.2	2.4	.4	1.5
Matrix	51.1	56.9	45.7	50.4	51.2

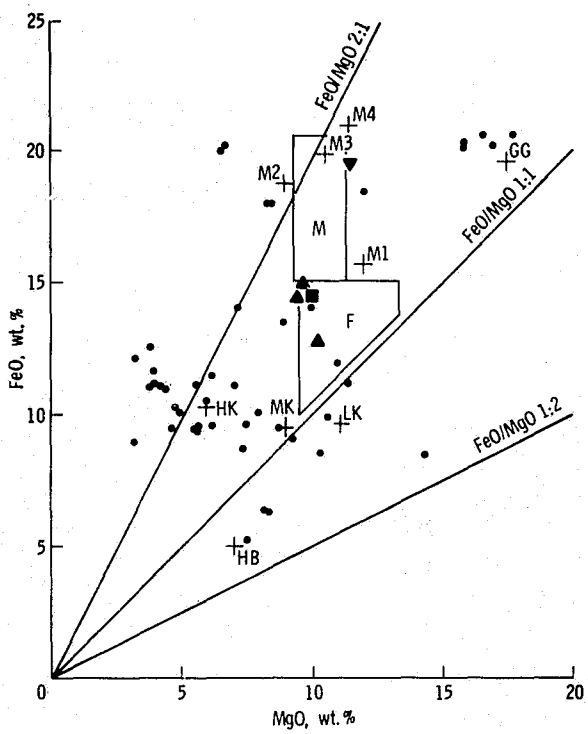

+ Averages of Apollo 15 glass types (ref. 1-12)
■ Three analyses of rock 15015
▲ Bubbly coating glass on 15015
▼ Glass seam in 15015, probably splash glass
• Individual glass fragments
M <1 mm fines, mare sites
F >1 mm fines, Apennine front sites

Figure 1-5.- 15015 glass fragments and coatings, ferrous oxide/magnesium oxide (FeO/MgO). GG = green glass, HB = highland basalt, HK = high-K Fra Mauro basalt, LK = low-K Fra Mauro basalt, MK = medium-K Fra Mauro basalt, and M1 to 4 = mare basalts 1 to 4.

The principal difference between the veining and coating glass and the whole rock is that the latter is just olivine normative (2.5 to 3.5 percent) and the former just quartz normative. Such differences, if the possibility of analytical error is excluded, could be reasonably associated with a minor heterogeneity in the original rocks or with incomplete melting in the production of the coating glass. Molten material might possibly have been added in flight in an impact-produced cloud that was subsequently laid down as a ray deposit. The latter view would be more in accord with the studies of Carter (ref. 1-13), who made a detailed scanning electron microscope (SEM)

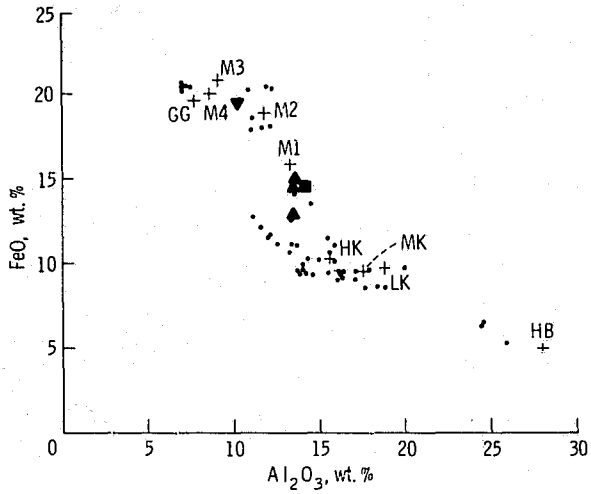

+ Averages of Apollo 15 glass types (ref. 1-12)
■ Three analyses of rock 15015
▲ Bubbly coating glass on 15015
▼ Glass seam in 15015, probably splash glass in original deposit
• Individual glass fragments

Figure 1-6.- 15015 glass fragments and coatings, ferrous oxide/alumina (FeO/Al_2O_3).

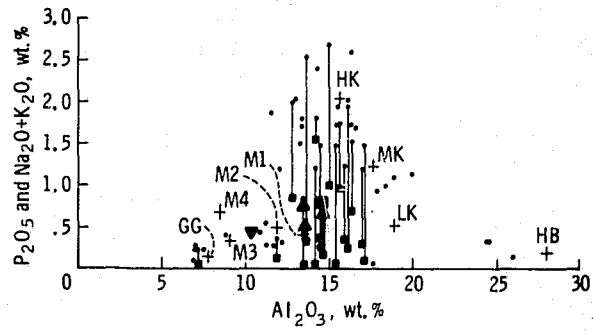

+ Averages of Apollo 15 glasses (ref. 1-12)
■ Three analyses of rock 15015
▲ Bubbly coating glass on 15015
▼ Glass seam in 15015, probably splash glass
• Na_2O+K_2O in individual glass fragments
▪ P_2O_5 in individual glass fragments

Figure 1-7.- 15015 glass fragments and coatings. Composite plot of sodium oxide plus potassium oxide ($Na_2O + K_2O$) and phosphorus pentoxide (P_2O_5) against alumina (Al_2O_3). Tie lines join analyses of individual glass fragments in which the three oxide contents have been determined.

study of the exterior glass from sample 15015,36. He described metallic Fe and troilite mounds, whisker structures, outgassing structures, and low-velocity, hot-target impact structures on the glass surface. The glass coating was interpreted as a siliceous melt generated in a hot, impact-produced cloud. In such a situation, strict comparability of the composition of coating glass and coated rock would not be expected. Reference 1-13 also indicated that the absence of high-velocity, microimpact craters on the glass examined suggests that this sample was from a surface that had been buried or shielded while on the Apollo 15 site.

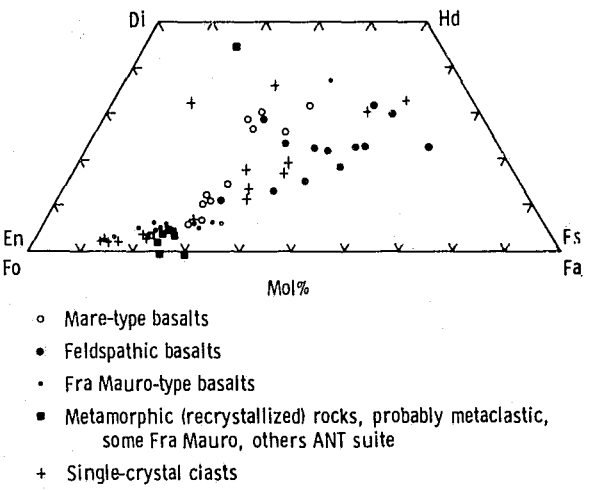

Figure 1-8.- 15015 pyroxenes and olivines from lithic and mineral clasts. (Di - diopside, Fs - ferrosilite, Fo - forsterite, En - enstatite, Fa - fayalite, Hd - hedenbergite.)

Mineral Clasts

Mineral clasts are angular to subangular fragments the maximum grain size of which may be up to three times that found in the same minerals in the lithic clasts. This finding indicates that rocks coarser in grain size than the lithic clasts or the degradation products of such rocks existed in the source areas of the material that contributed to the makeup of rock 15015.

Most of the mineral clasts show evidence of shock metamorphism in their undulose extinction, irregular lamellar features, and, in the case of plagioclase, the presence of felsitic devitrified maskelynite. Rare fragments, usually hypersthene, are coated with a thin layer of brownish glass; this glass has affinities with the Fra Mauro basaltic glasses of reference 1-12. One example is quoted as analysis 9, table 1-II.

Pyroxene clasts cover a wide range of compositions that embrace those of the pyroxenes of the lithic clasts. Analyses of typical examples are quoted in table 1-IV and plotted on the pyroxene quadrilateral in figure 1-8. It is possible that the hypersthenes with >85 percent enstatite (En) are derived from coarsely crystalline rocks of the anorthosite, norite, troctolite (ANT) suite that are proposed here as a source of the plagioclase clasts with approximately 96 percent anorthite (An).

Plagioclase clasts range in composition from 97 to 80 percent An with orthoclase (Or) content from 0.1 to 0.8 percent in the more sodic members. Normally, the clasts are not zoned; a histogram of compositions is given in figure 1-9, along with the composition of the plagioclase in the lithic clasts studied. A population of plagioclase clasts is distinctly richer in An than the feldspars in the lithic clasts. This group with approximately 96 percent An is probably derived from more coarsely crystalline anorthositic rocks of the ANT suite that were not represented among the lithic clasts. The group with 88 to 93 percent An is probably derived from the mare basalts and the feldspathic basalts recognized among the lithic clasts; the group with approximately 88 percent An may have a source in the disintegration of the Fra Mauro basalts recognized among the lithic clasts.

The ferrous oxide (FeO) content of the plagioclase clasts shows some correlation with An content. The majority of the clasts in the range of 90 to 97 percent

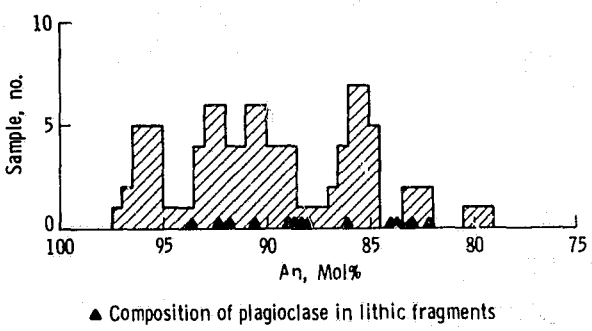

Figure 1-9.- 15015 histogram of plagioclase compositions in mineral clasts, size 100 to 400 μm.

TABLE 1-IV.- ELECTRON MICROPROBE ANALYSES OF BRECCIA 15015 PYROXENE CLASTS

Compound, element, or mineral	Analysis						
	1	2	3	4	5	6	7
	Hypersthene			Subcalcic augite	Subcalcic ferroaugite	Augite	Ferroaugite
SiO_2	54.70	53.76	51.86	49.78	48.86	50.10	47.88
TiO_2	.18	1.31	.25	.92	.64	.80	1.26
Al_2O_3	4.54	1.94	.97	2.04	1.89	2.48	1.10
Cr_2O_3	.51	.33	.74	.58	.74	1.11	.22
FeO	8.80	9.68	14.88	22.99	29.12	17.12	28.15
MnO	.15	.90	.29	.42	.61	.28	.46
MgO	30.28	30.42	26.28	14.40	10.56	11.65	6.57
CaO	1.55	1.22	1.81	8.10	8.14	16.24	13.75
Na_2O	.00	.00	--	.00	.02	--	--
K_2O	.00	.01	--	.00	.01	--	--
Total	100.71	99.57	97.08	99.23	100.59	99.78	99.39
Enstatite (En)	85.7	81.6	73.2	43.2	31.9	35.3	20.2
Ferrosilite (Fs), mol%	13.9	16.0	23.2	39.4	50.4	29.2	49.4
Wollastonite (Wo)	2.3	2.4	3.6	17.4	17.7	35.5	30.4
Unit formulas							
Silicon (Si)	1.907	1.911	1.939	1.929	1.926	1.922	1.937
Titanium (Ti)	.005	.036	.008	.027	.019	.024	.039
Aluminum IV (Al^{IV})	.093	.082	.043	.071	.074	.088	.053
Aluminum VI (Al^{VI})	.094	--	--	.021	.014	.024	--
Chromium (Cr)	.014	.010	.022	.018	.024	.034	.08
Iron (Fe)	.257	.288	.465	.745	.960	.550	.953
Manganese (Mn)	.005	.028	.010	.014	.021	.010	.016
Magnesium (Mg)	1.573	1.612	1.465	.832	.621	.666	.397
Calcium (Ca)	.044	.047	.073	.337	.344	.668	.596
Sodium (Na)	.000	.000	--	.000	.002	--	--
Potassium (K)	.000	.001	--	.000	.001	--	--

An contain less than 0.1 percent FeO, whereas clasts in the range of 80 to 90 percent An show higher concentrations of up to 0.9 percent FeO.

Metallic Fe occurs as sporadic rounded fragments up to 50 μm in diameter. The fragments fall into two subgroups: (1) fragments with <2.0 percent nickel (Ni), 0.1 to 0.6 percent cobalt (Co) and <0.1 percent phosphorous (P), probably derived from basaltic rocks and (2) fragments with 3.0 to 10.0 percent Ni, 0.3 to 0.5 percent Co, and <0.2 percent P, probably of meteoritic origin.

Vitric Clasts

Vitric clasts constitute approximately 10 percent of rock 15015. They include indeterminate plastic forms, twisted and ropey forms, spheres, and broken fragments. One unique clast had the appearance of a splash glass in thin section and a composition similar to that of a mare-type basalt (analysis 6, table 1-II).

The glass fragments may be completely fresh or show partial, usually marginal, devitrification. One type, chemically similar to the green glass spheres described by reference 1-14, is always completely devitrified.

Five main chemical categories of glass fragments may be recognized and can be correlated with the glass types recognized by reference 1-12. Representative analyses of these types are quoted in table 1-II, and these and other glasses from 15015 are plotted in figures 1-5 to 1-7 along with the average compositions of the glass types recognized in the Apollo 15 soils by Reid et al. (ref. 1-12).

The similarity between the bulk composition of 15015 and contingency fines 15021 has already been mentioned. Although fewer glass analyses are available from 15015, it will be seen from comparison of figures 1-5 and 1-6 with figures 2(a) and 2(b) of reference 1-12 that the general similarity extends to the compositions and relative abundances of the glass fragments in the two samples.

These five main chemical categories of glass fragments are grouped as follows.

1. Fra Mauro basaltic glasses are the most abundant: they consist of ropey, plastic, and broken forms; in thin section ranging in color from very pale fawn to pale brown. No glass spheres were observed. Low-, intermediate-, and high-K types are represented. Compared with the contingency fines, 15015 contains a higher proportion of high-K members that are slightly richer in Fe than those of 15021. Phosphorus pentoxide (P_2O_5) has not been determined in all the glass analyses, but in figure 1-7 it is seen that glasses with high sodium oxide plus potassium oxide ($Na_2O + K_2O$) often have high values of P_2O_5, which is a characteristic of Fra Mauro, or KREEP glasses.

2. Agglutinates are a minor group; they tend to be heterogeneous and to have approximately the same composition as the bulk of 15015.

3. Mare-type basaltic glasses are a subordinate group. They usually occur as fragments and occasional spheres with a yellow-brown to green-brown color. Too few have been analyzed to allow the recognition of any significant subdivisions within them.

4. Highland basalt glasses – a few colorless fragments and spheres have been analyzed with the high alumina (Al_2O_3) and calcium oxide (CaO) and low FeO characteristic of this group.

5. Green glass spheres occur as a subordinate glass type but are always represented by devitrified spheres or broken forms composed of fawn-colored cryptocrystalline devitrification products. They form a tight cluster close to the average determined by reference 1-12 for the green glass spheres. This may be seen in figures 1-5 to 1-7.

Such devitrified types of the unique green glass are not uncommon in soils and breccias of the Apollo 15 site. Reid et al. (ref. 1-12) comment on their abundance along with unaltered spheres in 15601; in reference 1-15, their presence is noted as a minor component in 15425 as a green clod dominantly composed of the green glass.

The green glass spheres conceivably are the products of several events operating on identical material. However, their uniformity in composition suggests their formation in a single event, irrespective of magmatic, meteoritic, or impact origin.

The presence of devitrified green glasses implies that annealing occurred in some thermal event subsequent to their initial formation. The event associated with this annealing could have been a secondary

cratering (if 15015 were shock-lithified near the Apollo 15 site) or a primary event if shock-lithification were associated with ejection in the Aristillus or Autolycus ray, of which 15015 may be an integral component. If the green glass is a component of the ray, then it must also either have been a component of the regolith of the Aristillus-Autolycus area or have been generated in the major-impact explosion and devitrified by a secondary cratering event acting on the deposited ray material.

Lithic Clasts

Lithic clasts constitute approximately 10 percent of rock 15015. The following types are recognized: mare basalts (30 percent), Fra Mauro basalts (33 percent), feldspathic basalts (22 percent), and metamorphic (recrystallized) clasts (15 percent).

Mare basalts.— Mare basalts are represented by fragments of porphyritic clinopyroxene-rich basalts, porphyritic pyroxene vitrophyres, and subophitic ilmenite basalts. Insofar as 1-mm fragments are valid for an assessment, these basaltic fragments can be matched texturally with mare basalts collected at the Apollo 15 site. It is significant that olivine-bearing types are rare among the fragments in 15015.

Analyses of minerals from these typical fragments are quoted in table 1-V(a), analyses 1 to 8, and the pyroxene compositions are plotted on figure 1-8. The pyroxenes are commonly zoned and range from early formed, pale-colored, calcium-poor pigeonite with a ratio of Fe to Fe plus magnesium (Mg) approximately 0.30 by way of calcium-rich pigeonites to late ferroaugite with Fe/Fe+Mg approximately 0.55. The late pink-brown ferroaugite may contain up to 2.0 percent titanium dioxide (TiO_2) and 9 percent Al_2O_3.

Fra Mauro basalts.— Fra Mauro basalts are represented by mesostasis-rich (or intersertal), olivine-free basalts with up to 45 percent lathlike, often slightly curved, crystals of plagioclase. The plagioclase in the fragments analyzed is restricted to compositions of approximately $An_{83.5}$, albite (Ab) 15.0, $Or_{1.5}$.

The pyroxenes are zoned from colorless to very pale yellow-brown hypersthene with Fe/Fe+Mg approximately 0.15 to pale yellow-brown calcium-poor pigeonites with Fe/Fe+Mg approximately 0.35. Occasional Fe-rich ferroaugite was observed. Early formed hypersthenes are relatively aluminous compared with the later crystallizing hypersthene and pigeonite. Where a fine-grained mesostasis is present, it is composed of skeletal crystals of ilmenite, pyroxene, and plagioclase with interstitial potash feldspar, cristobalite, and troilite. No quantitative data were obtained from this material.

Analyses of minerals from four typical clasts are quoted in table 1-V(b), analyses 25 to 38, and the pyroxene relationships are plotted in figure 1-8.

Feldspathic basalts.— The feldspathic basalts include fragments that were impossible to assign to either of the two principal groups just described. They are more feldspathic than the unambiguous pyroxene-rich mare basalts, but their plagioclase has a higher An content and their pyroxenes a higher Fe/Fe+Mg ratio than the basalts here classified as of Fra Mauro type. The feldspathic basalts include variolitic, intersertal, and subophitic types of variable grain size in which olivine-bearing types are rare. A common type of clast consists of three or four subparallel crystals of tabular plagioclase with a few interstitial crystals of allotriomorphic pyroxene and minor ilmenite. The plagioclase constitutes 30 to 55 percent of the fragments, and its composition lies within the following ranges: An_{86} to An_{92}, Ab_{13} to Ab_7, $Or_{0.2}$ to $Or_{0.8}$. In some clasts, plagioclase shows normal zoning; in others, it is unzoned. Pyroxenes constitute from 45 to 70 percent of individual clasts, and reference to table 1-V(a), analyses 9 to 24, and to figure 1-8 illustrates their wide range of composition. They range from calcic pigeonites with Fe/Fe+Mg approximately 0.35 to subcalcic ferroaugites or ferroaugites with Fe/Fe+Mg approximately 0.85. Essentially, the pyroxenes cover the field shown by the pyroxenes in the mare basalts of Apollo 15. However, the interpretation of trends in individual clasts is ambiguous. Analyses 10 to 12 (table 1-V(a)) are not unlike those of late-crystallizing pyroxenes of 15085,14, a mare basalt described in reference 1-16, but their trend is also similar to that of the late-crystallizing portion of 14310, which is a Fra Mauro basalt (ref. 1-17).

Gleadow et al. (ref. 1-18) applied chemical discriminant analysis to recognized petrographic types of clasts in Apollo 14 and 15 breccias, including 15015,19. They recognized a distinct field for mare and Fra Mauro basalts but not for a feldspathic group. Most of the feldspathic basalts here recognized

probably have closer affinities with mare basalts and represent olivine-free types with early crystallizing plagioclase.

Metamorphic (recrystallized) clasts.— Two different types of metamorphic (recrystallized) clasts are recognized on the basis of texture.

1. Feldspathic microgranulites are composed of polygonal crystals of plagioclase associated with subordinate granules of pyroxene with or without minor olivine and ilmenite. These may range from almost pure anorthosite to types with only 50 percent plagioclase. They appear to have been produced by thermal recrystallization of an already crystalline rock with no marked differences in grain size.

2. Porphyroclastic rocks have angular porphyroclasts of plagioclase approximately 100 μm in size set in a finer grained matrix of plagioclase and hypersthene with or without minor olivine and ilmenite. The matrix grain size ranges from 5 μm in the least to 30 μm in the most recrystallized examples. Where

TABLE 1-V.- ELECTRON MICROPROBE ANALYSIS OF MINERALS FROM LITHIC CLASTS OF BRECCIA 15015

(a) Description of Samples

Analysis no.	Mineral	Description
	Mare-type, pyroxene-rich basalts with <30 percent plagioclase[a]	
1	Pyroxene - pigeonite core	Porphyritic pyroxene-rich basalt (135I)
2	Pyroxene - augite rim	
3	Pyroxene - pigeonite core	Porphyritic pyroxene vitrophyre (135F)
4	Pyroxene - augite rim	Pyroxene, 46 percent; mesostasis, 54 percent
5	Plagioclase	Pyroxene-rich ilmenite basalt (135K)
6	Pyroxene	Pyroxene, 83 percent; plagioclase, 17 percent
7	Pyroxene	
8	Ilmenite	
	Basalts with >30 percent plagioclase[b]	
9	Plagioclase	Coarse intersertal basalt (135L)
10	Pyroxene - pigeonite core	Pyroxene, 53 percent; plagioclase, 47 percent
11	Pyroxene - augite intermediate	
12	Pyroxene - ferroaugite interstitial	
13	Ilmenite	
14	Plagioclase	Intersertal basalt (133F)
15	Pyroxene - core	Pyroxene, 54 percent; plagioclase, 46 percent
16	Pyroxene - interstitial	
17	Plagioclase	Pyroxene-rich basalt (133D)
18	Pyroxene - core	Pyroxene, 69 percent; plagioclase, 31 percent
19	Pyroxene - rim	
20	Plagioclase	Fine-grained basalt (135AB)
21	Pyroxene	Pyroxene, 45 percent; plagioclase, 55 percent
22	Pyroxene - subcalcic ferroaugite	Dark variolitic basalt (15,5B)
23	Plagioclase	Pyroxene, 50 percent; plagioclase, 40 percent;
24	Ilmenite	Ilmenite, 3 percent; mesostasis, 7 percent

[a] An, 88 mol%; FeO, 1.0 wt.%.

[b] An, 92 to 87 mol%; FeO, 0.6 to 1.4 wt.%.

pyroxene is dominant, it occurs as idioblastic rods set in interstitial plagioclase crystals of irregular outline. In the more feldspathic types, plagioclase forms idioblastic plates, and the pyroxene forms the interstitial crystals.

These porphyroclastic rocks were evidently formed by the recrystallization of fine-grained clastic rocks – including soils. The recrystallization is due to the heat remaining after shock-vitrification (or melting) of originally unconsolidated material. Increase in grain size and changes in texture of the matrix reflect both the temperature attained and the duration of the annealing period.

On the basis of plagioclase composition, the clasts can be tentatively assigned to one of two chemical groups. Those with plagioclase with approximately 93 percent An are possibly recrystallized rocks in which members of the ANT suite or its fragmental associates predominate; e.g., analyses 44 to 47, table 1-V(b). Those with plagioclase approximately 86 percent An

TABLE 1-V.- Continued

(a) Concluded

Analysis no.	Mineral	Description
	Hypersthene "Fra Mauro" basalts[c]	
25	Plagioclase	Mesostasis-rich basalt (133A)
26	Pyroxene - core	Pyroxene, 51 percent; plagioclase, 32 percent;
27	Pyroxene - rim	mesostasis, 17 percent
28	Pyroxene - interstitial	
29	Plagioclase	Mesostasis-poor basalt (135M)
30	Pyroxene - hypersthene	Pyroxene, 60 percent; plagioclase, 31 percent;
31	Pyroxene - pigeonite	mesostasis, 9 percent
32	Plagioclase	Pyroxene, 30 percent; plagioclase, 38 percent;
33	Pyroxene - hypersthene	mesostasis, 32 percent (135H)
34	Pyroxene - hypersthene	Pale, mesostasis-rich basalt (15,23B)
35	Pyroxene - pigeonite	Pyroxene, 30 percent; plagioclase, 20 percent;
36	Plagioclase	mesostasis, 45 percent; ilmenite, 5 percent
37	Cristobalite	
38	Ilmenite	
	Metamorphic (recrystallized) rocks, probably metaclastic[d]	
39	Olivine	Hypersthene-rich metaclastic (135J)
40	Pyroxene - hypersthene	Femic minerals, 74 percent; plagioclase,
41	Plagioclase	26 percent
42	Olivine	Olivine, hypersthene, plagioclase granulite (135B4)
43	Pyroxene - hypersthene	Femic minerals, 49 percent; plagioclase, 51 percent ($An_{85}Ab_{14}Or_1$)
44	Plagioclase	Anorthositic granulite (133E)
45	Pyroxene - salite	Femic minerals, 19 percent; plagioclase, 81 percent
46	Plagioclase	Noritic metaclastic (135G)
47	Pyroxene - hypersthene	Pyroxene, 52 percent; plagioclase, 48 percent

[c] An, 82 to 84 mol%; FeO, 0.4 to 0.6 wt.%.

[d] Numbers 39 to 43: Fra Mauro affinity; An, 85 to 88 mol%; FeO, 0.3 to 0.4 wt.%. Numbers 44 to 47: ANT affinity; An, 92 to 94 mol%; FeO, 0.1 to 0.3 wt.%.

TABLE 1-V.- Continued

(b) Chemical analyses, unit formulas, and atomic ratios

Compound or element	Analysis no.,[a] wt.%											
	1	2	3	4	5	6	7	8	9	10	11	12
SiO_2	53.08	49.39	50.93	48.56	48.26	50.85	51.31	(b)	45.28	50.45	50.08	48.10
TiO_2	.22	1.17	.72	2.01	.02	1.05	.80	51.68	.02	.66	.85	1.10
Al_2O_3	2.49	6.53	5.78	9.21	33.16	3.31	1.34	1.27	32.73	2.71	2.63	1.45
Cr_2O_3	(b)	(b)	(b)	(b)	(b)	(b)	(b)	(b)	(b)	(b)	(b)	(b)
FeO	17.95	16.25	16.87	15.93	1.08	15.77	18.50	46.03	.68	23.21	21.72	30.49
MnO	(b)	(b)	(b)	(b)	(b)	(b)	(b)	(b)	(b)	(b)	(b)	(b)
MgO	22.26	13.49	19.65	13.61	.21	15.15	18.85	.00	.07	15.93	12.91	5.11
CaO	3.46	14.64	5.13	11.68	17.86	13.72	6.88	(b)	18.97	6.25	10.74	12.96
Na_2O	.02	.06	.07	.08	1.28	.05	.30	(b)	.89	.07	.09	.04
K_2O	.02	.02	.02	.02	.05	.02	.02	(b)	.04	.02	.02	.02
Total	99.50	101.55	99.17	101.10	101.92	99.92	98.00	98.98	98.68	99.30	99.04	99.27
Unit formulas												
Si	1.957	1.835	1.885	1.792	2.184	1.911	1.958	--	2.127	1.933	1.938	1.957
Ti	.007	.033	.021	.056	.001	.030	.023	0.985	.001	.020	.025	.034
Al^{IV}	.043	.165	.115	.208	1.769	.089	.042	.038	1.813	.067	.062	.043
Al^{VI}	.066	.122	.138	.193	--	.058	.019	--	--	.056	.059	.027
Cr	--	--	--	--	--	--	--	--	--	--	--	--
Fe	.554	.505	.522	.492	.042	.496	.593	.975	.027	.774	.703	1.038
Mn	--	--	--	--	--	--	--	--	--	--	--	--
Mg	1.223	.747	1.084	.749	.015	.849	1.073	.000	.005	.910	.745	.310
Ca	.137	.583	.204	.462	.866	.553	.282	--	.955	.257	.446	.566
Na	.002	.005	.005	.007	.133	.004	.003	--	.081	.006	.007	.004
K	.002	.002	.002	.002	.003	.002	.002	--	.003	.002	.002	.002
Atomic ratios												
	Mg 63.9 Fe 28.9 Ca 7.2	Mg 40.7 Fe 37.5 Ca 31.8	Mg 59.9 Fe 28.8 Ca 11.3	Mg 44.00 Fe 28.9 Ca 27.1	Ca 88.2 Na 11.5 K .3	Mg 44.7 Fe 26.1 Ca 29.2	Mg 55.1 Fe 30.4 Ca 14.5	Mg 0.00 Fe 100.00	Ca 91.9 Na 7.8 K .3	Mg 47.6 Fe 38.9 Ca 13.5	Mg 39.3 Fe 37.1 Ca 23.6	Mg 16.2 Fe 54.2 Ca 29.6

[a] From table 1-V(a).

[b] Not determined.

TABLE 1-V.- Continued

(b) Continued

Compound or element	Analysis no.,[a] wt.%											
	13	14	15	16	17	18	19	20	21	22	23	24
SiO_2	(b)	45.99	48.81	50.14	46.56	50.97	46.23	47.75	48.82	51.53	47.99	(b)
TiO_2	52.90	.08	1.05	1.01	.08	.46	1.25	.00	1.12	.26	(b)	51.15
Al_2O_3	.13	34.02	2.56	1.32	31.93	1.16	1.16	33.17	2.42	.79	31.51	.37
Cr_2O_3	(b)	(b)	.78	.40	(b)	.87	.02	(b)	(b)	.19	(b)	.12
FeO	46.17	.60	18.25	26.66	1.03	19.61	36.69	1.36	28.09	28.31	.99	46.27
MnO	(b)	(b)	.40	.05	(b)	.35	.48	(b)	(b)	.17	(b)	.06
MgO	.11	.38	14.28	13.15	.01	20.49	3.99	.15	10.08	7.85	.36	.81
CaO	(b)	17.89	13.88	6.86	17.75	5.38	10.32	17.09	7.88	9.46	16.63	(b)
Na_2O	(b)	.99	(b)	(b)	1.15	(b)	(b)	1.23	.25	(b)	1.43	(b)
K_2O	(b)	.04	(b)	(b)	.12	(b)	(b)	.02	.03	(b)	.08	(b)
Total	99.31	99.99	100.01	99.59	98.63	99.29	100.14	100.77	98.69	98.56	98.99	98.78
Unit formulas												
Si	--	2.122	1.873	1.956	2.180	1.927	1.920	2.183	1.943	2.052	2.228	--
Ti	1.007	.003	.031	.030	.003	.014	.040	--	.034	.008	--	0.981
Al^{IV}	.004	1.849	.116	.044	1.762	.052	.058	1.788	.057	--	1.725	.038
Al^{VI}	--	--	.024	.017	--	--	--	--	.057	.037	--	--
Cr	--	--	--	.013	--	.026	.001	--	--	.007	--	.003
Fe	.977	.024	.586	.870	.041	.620	1.274	.052	.935	.943	.039	.987
Mn	--	--	.014	.002	--	.012	.017	--	--	.006	--	.002
Mg	.005	.026	.817	.764	.007	1.155	.027	.011	.598	.466	.025	.031
Ca	--	.885	.571	.287	.891	.218	.460	.837	.337	.404	.828	--
Na	--	.089	--	--	.105	--	--	.110	.020	--	.129	--
K	--	.003	--	--	.008	--	--	.002	.002	--	.005	--
Atomic ratios												
	Mg 0.5 Fe 99.5	Ca 90.6 Na 9.1 K .3	Mg 41.4 Fe 29.7 Ca 28.9	Mg 39.8 Fe 45.3 Ca 14.9	Ca 88.7 Na 10.5 K .8	Mg 58.0 Fe 31.1 Ca 10.9	Mg 12.4 Fe 64.3 Ca 23.2	Ca 88.2 Na 11.6 K .2	Mg 32.0 Fe 50.0 Ca 18.0	Mg 25.7 Fe 52.0 Ca 22.3	Ca 86.1 Na 13.4 K .5	Mg 3.0 Fe 97.0

[a] From table 1-V(a).

[b] Not determined.

TABLE 1-V.- Continued

(b) Continued

Compound or element	Analysis no.,[a] wt.%											
	25	26	27	28	29	30	31	32	33	34	35	36
SiO_2	47.97	53.80	52.84	47.98	48.62	52.44	52.83	48.31	53.43	55.19	53.13	49.36
TiO_2	.10	.57	.78	2.27	.02	.74	.88	.13	.84	.45	.57	(b)
Al_2O_3	31.10	3.79	1.86	1.93	33.00	4.28	2.51	32.05	2.76	2.56	2.66	31.25
Cr_2O_3	(b)	.81	.83	.82	(b)	(b)	(b)	(b)	(b)	.06	.05	(b)
FeO	.49	9.82	14.20	22.18	.45	14.45	19.30	.59	13.70	15.00	19.87	.45
MnO	(b)	.17	.26	.02	(b)	(b)	(b)	(b)	(b)	.21	.22	(b)
MgO	.18	29.43	25.86	8.01	.16	24.72	21.20	.11	25.51	23.81	19.98	.00
CaO	16.48	1.41	2.39	16.43	15.38	2.76	2.89	16.21	2.21	2.11	2.82	16.06
Na_2O	1.70	(b)	(b)	(b)	1.70	.06	.03	1.51	.03	(b)	(b)	1.58
K_2O	.22	(b)	(b)	(b)	.18	.01	.02	.29	.01	(b)	(b)	.20
Total	98.24	99.80	99.02	99.64	99.51	99.46	99.66	99.20	98.49	99.39	99.30	98.90
Unit formulas												
Si	2.242	1.901	1.930	1.907	2.230	1.901	1.95	2.232	1.945	1.994	1.975	2.280
Ti	.004	.016	.022	.068	.001	.021	.02	.005	.023	.013	.016	--
Al^{IV}	1.714	.099	.060	.091	1.784	.099	.04	1.746	.055	.066	.025	1.702
Al^{VI}	--	.059	.021	.000	--	.084	.06	--	.064	.104	.092	--
Cr	--	.023	.024	.003	--	--	--	--	--	.002	.002	--
Fe	.019	.291	.434	.738	.018	.439	.59	.024	.418	.454	.618	.018
Mn	--	.006	.009	.001	--	--	--	--	--	.007	.007	--
Mg	.013	1.550	1.408	.475	.012	1.336	1.16	.008	1.384	1.282	1.107	--
Ca	.826	.054	.094	.700	.756	.108	.11	.803	.087	.082	.113	.795
Na	.155	--	--	--	.152	.005	.00	.135	.003	--	--	.142
K	.014	--	--	--	.011	.001	.00	.018	.002	--	--	.012
Atomic ratios												
	Ca 83.0 Na 15.6 K 1.4	Mg 81.8 Fe 15.4 Ca 2.8	Mg 72.7 Fe 22.4 Ca 4.9	Mg 24.8 Fe 38.8 Ca 36.6	Ca 82.3 Na 16.5 K 1.2	Mg 70.9 Fe 23.3 Ca 5.8	Mg 62.1 Fe 31.7 Ca 6.2	Ca 84.0 Na 14.1 K 1.9	Mg 73.3 Fe 22.1 Ca 4.6	Mg 70.5 Fe 23.0 Ca 4.5	Mg 60.2 Fe 33.6 Ca 6.2	Ca 83.8 Na 15.0 K 1.2

[a]From table 1-V(a).

[b]Not determined.

TABLE 1-V.- Concluded

(b) Concluded

Compound or element	Analysis no.,[a] wt.%										
	37	38	39	40	41	42	43	44	45	46	47
SiO_2	97.99	--	37.84	53.66	45.45	38.20	53.45	44.10	50.51	44.66	53.17
TiO_2	(b)	51.03	.82	.96	.27	.18	.74	.00	2.00	.00	.76
Al_2O_3	1.70	1.84	.05	.80	34.06	.76	2.36	34.54	.92	35.85	1.71
Cr_2O_3	(b)	.14	(b)	(b)	(b)	(b)	(b)	(b)	.29	(b)	(b)
FeO	.27	46.79	26.84	16.30	.39	22.89	13.67	.13	10.03	.32	14.81
MnO	(b)	.10	(b)	(b)	(b)	(b)	(b)	(b)	.22	(b)	(b)
MgO	.00	.19	35.06	25.78	.00	37.33	26.50	.13	12.83	.02	26.66
CaO	.02	(b)	.15	1.61	17.58	.01	1.68	18.78	20.77	18.79	1.80
Na_2O	(b)	(b)	.02	.03	1.20	(b)	.22	.66	(b)	.77	.00
K_2O	(b)	(b)	.02	.02	.19	(b)	.01	.06	(b)	.11	.01
Total	99.98	100.09	100.80	99.16	99.14	99.37	98.63	98.40	97.57	100.52	98.92
Unit formulas											
Si		--	0.997	1.964	2.115	1.000	1.942	2.071	1.944	2.054	1.957
Ti		0.963	.017	.027	.010	.001	.021	--	.058	.000	.022
Al^{IV}		.055	.002	.035	1.868	--	.058	1.912	.042	1.944	.043
Al^{VI}		--	--	--	--	.024	.043	--	.000	--	.032
Cr		.003	--	--	--	--	--	--	.009	--	--
Fe		.981	.591	.499	.016	.502	.416	.006	.323	.013	.456
Mn		.003	--	--	--	--	--	--	.008	--	--
Mg		.008	1.376	1.406	.000	1.457	1.435	.010	.736	.002	1.408
Ca		--	.005	.063	.877	.001	.066	.945	.857	.927	.071
Na		--	.001	.003	.109	--	.016	.061	--	.069	.000
K		--	.001	.002	.012	--	.001	.004	--	.007	.001
Atomic ratios											
		Mg 0.8 Fe 99.2	Mg 70.0 Fe 30.0	Mg 71.4 Fe 25.4 Ca 3.2	Ca 87.9 Na 10.9 K 1.2	Mg 74.4 Fe 25.6	Mg 74.9 Fe 21.7	Ca 93.6 Na 6.0 K .4	Mg 38.3 Fe 17.2 Ca 44.5	Ca 92.4 Na 6.9 K .7	Mg 72.7 Fe 23.6 Ca 3.7

[a] From table 2-V(a).

[b] Not determined.

are possibly recrystallized rocks in which members of the Fra Mauro or KREEP suite or their fragmental associates predominate; e.g., analyses 39 to 43, table 1-V(b). In both groups, homogeneous hypersthene is the dominant ferromagnesian phase. The Fe/Fe+Mg ratio of approximately 0.25 in the hypersthene is within the range of zoned hypersthene in the Fra Mauro basalts. The calcium (Ca) content is marginally lower and the aluminum (Al) content distinctly less in the metamorphic pyroxenes.

No fragments of rocks similar to members of the mare basalt group with a metamorphic texture have been found in 15015. The same is true for the feldspathic basalt group. Reference to figure 1-8 shows an absence of metamorphic pyroxenes with the Fe/Fe+Mg ratios >0.3 that are characteristic of these igneous groups, which reinforces the tentative conclusion that the feldspathic basalts are variants of the mare group of basalts. These basalts should be grouped together as younger effusives that postdated the impact events that were ultimately responsible for the metamorphic nature of a proportion of the clasts here assigned to the Fra Mauro and ANT suite.

A Tentative History of 15015 Based on General Petrology

Breccias 15015 and 15021, nearly identical in chemical composition, were collected on a ray from Aristillus or Autolycus just west of the LM and near the eastern limit of the mare surface overlooked by the mountains of the Apennine front (ref. 1-19). This suggests that the rock 15015 could be a boulder from a distant source, which lay partially buried in the finer grained, less coherent ray material, or that it was buried and reexcavated by some minor cratering event. Alternatively, this boulder may have been formed by shock-lithification of unconsolidated ray material by some local cratering event that deposited it where it was collected. In the first case, lithification was effected by or preceded by the Aristillus event, and the material of the boulder reflects only the lithology of its distant source. In the second and more probable case, during the interval between ray formation and shock-lithification, material of more local origin could have been mixed with the surface layers of the ray material and formed an additional component of the shock-lithified ejecta. Reid et al. (ref. 1-12) have shown that 15021 is enriched in Fra Mauro basalt glass, and Powell et al. (ref. 1-20) have shown that Fra Mauro basalts are more abundant in the <4-mm lithic fragments at the LM site than at other mare sites visited during the Apollo 15 mission. The same features are found in the vitric and lithic clasts of 15015 and are considered diagnostic of the ray. Therefore, the rocks from which these clasts were derived possibly underlie the mare basalts of the Autolycus-Aristillus region. The overlying spectrum of mare basalts should also be found in the ray material. Possibly the feldspathic basalts of 15015, which were assigned previously to the mare basalt group, are the representatives of mare basalts of this distant region.

The small amount of metamorphic rocks in 15015 could be of local (Apennine front) origin or could have come from a distant source: a major crater like Aristillus could be expected to excavate fallback material from the Imbrium event.

The green glass spheres are found as a subordinate component of the glasses in the <1-mm fraction (15021) of the ray soil. They are also a subordinate component in the shock-lithified boulder of soil breccia 15015, but here they are all in a devitrified state. The wide distribution of the green glass spheres and their greater concentration in many of the <1-mm fractions of the surface regolith samples from the Apollo 15 site suggests that they are not a part of the original ray material, but that they were deposited after ray formation and before the cratering event that shock-lithified 15015 and deposited it as a surface boulder.

Selenchronology

Six samples of 15015,15 have been subjected to ^{40}Ar-^{39}Ar analysis. They were: 5c, a 60-mg sample of the dark matrix containing numerous small inclusions; 5b, fragments (33 mg) of a large gray clast chipped from the dark matrix; 23c (52 mg), 23d (19 mg), 26, fragments (24 mg) of bubbly glass chipped from the upper surface of the rock; and 23b, fragments (20 mg) of a white clast embedded in the surface of rock 15015 and partially included in the bubbly glass. The mineralogy of the rock fragments has been described in detail previously. Sample 5b is a dark variolitic basalt with >30 percent plagioclase (feldspathic basalt). Sample 23b is a pale mesostasis-rich basalt (Fra Mauro type). The matrix and glass

were not subjected to a separate mineralogical analysis, though analyses 1 and 2 (table 1-II), respectively, can probably be taken as representative. Details of the irradiation (designated SH15) have been published elsewhere (ref. 1-6).

Each sample was subjected to a stepwise heating experiment, and the Ar-release patterns obtained are summarized in table 1-VI. Apparent K-Ar ages have been calculated from the gas released at each temperature step for the two clasts and are shown in figs. 1-10 and 1-11. The amount of cosmogenic $^{38}Ar_c$ is calculated for each temperature assuming a binary

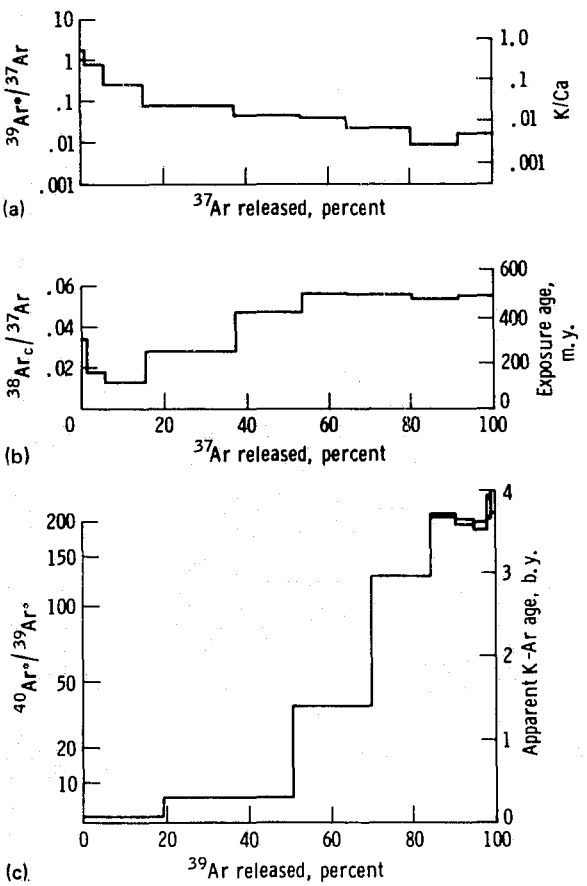

Figure 1-10.- Argon isotope release pattern for Fra Mauro basalt-type fragment 23b, indicating a 75-percent loss of radiogenic ^{40}Ar and a 20-percent loss of cosmogenic $^{38}Ar_c$. The high-temperature $^{40}Ar/^{39}Ar$ age attains a value of 3.7 ± 0.1 b.y. despite the extreme loss and is comparable to, but slightly lower than, more precise ages of other Fra Mauro basalts. A well-defined cosmic ray exposure age of 490 m.y. is determined.

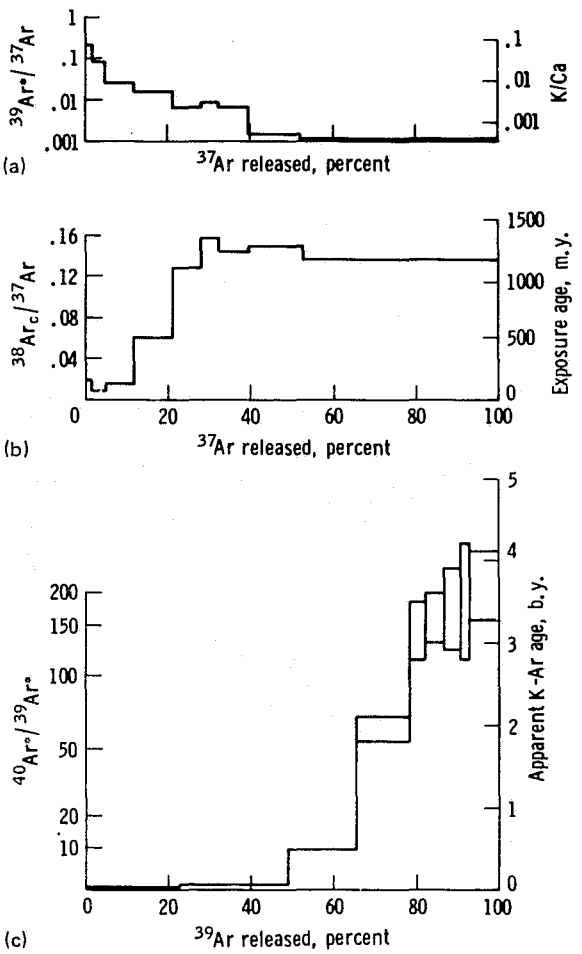

Figure 1-11.- Argon isotope release pattern for variolitic basalt fragment 5b, indicating ^{40}Ar and $^{38}Ar_c$ loss similar to that of fragment 23b. The high-temperature $^{40}Ar/^{39}Ar$ age is imprecise, 3.4 ± 0.2 b.y. The cosmic ray exposure age is well defined and extremely high, 1290 m.y., indicating that 5b received extensive cosmic ray irradiation for at least 800 m.y. after crystallization and before incorporation in the part of the regolith that was later to be lithified to form 15015.

mixture of cosmogenic Ar ($^{36}Ar/^{38}Ar$ = 0.65) and trapped Ar ($^{36}Ar/^{38}Ar$ = 5.35). The ratio $^{38}Ar_c/^{37}Ar$ is plotted also in figures 1-10 and 1-11 and is related directly to the $^{38}Ar_c$/Ca ratio and hence to the cosmic ray exposure age (ref. 1-21).

Also plotted in figures 1-10 and 1-11 is the ratio $^{39}Ar^*/^{37}Ar$, which is proportional to the average K/Ca ratio of the sites releasing Ar at each stage of the experiment[2]. The overall K/Ca ratio for the matrix, 0.024, is identical to that of other matrix samples (analyses 14 and 15, table 1-II) and is slightly smaller than that of the glass, 0.030. The K/Ca ratio of the gray clast (5b) is much lower, 0.0051, while that of the white clast (23b) is high, 0.062, reflecting the presence of a KREEP component.

Both clasts show the effects of extreme radiogenic ^{40}Ar loss, at least 75 percent, based on the maximum $^{40}Ar^*/^{39}Ar^*$ ratios reached in the high-temperature release. Variations in the $^{39}Ar^*/^{37}Ar$ ratio indicate that the loss is associated with low-retentivity, potassium-rich sites. A parallel loss of cosmogenic

[2] $^{40}Ar^*$ and $^{39}Ar^*$ refer to Ar produced by radioactive decay of ^{40}K and (n,p) reactions on 39K, respectively.

TABLE 1-VI.- BRECCIA 15015,15 ARGON-RELEASE PATTERNS

Temperature, K (°C)	$^{36}Ar/^{38}Ar$	$^{38}Ar/^{37}Ar$	$^{38}Ar_c/^{37}Ar$ (a)	$^{39}Ar^*/^{37}Ar$	$^{40}Ar/^{39}Ar^*$	$^{39}Ar^*$ (b)	Apparent age, b.y. (c)
15015,15,23b (white clast, 33.0 mg); J = 0.02982							
773 (500)	0.30 ± 0.05	0.0345 ± 11	--	1.66 ± 3	1.23 ± 0.01	18.6	0.068 ± 0.001
873 (600)	.29 ± .05	.0180 ± 9	--	.806 ± 16	5.81 ± .04	28.1	.301 ± .002
973 (700)	.78 ± .03	.0138 ± 4	0.0134 ± 4	.227 ± 1	37.7 ± .2	18.0	1.42 ± .01
1043 (770)	.93 ± .01	.0303 ± 3	.0285 ± 3	.0762 ± 5	127.3 ± .8	13.6	2.96 ± .01
1123 (850)	1.25 ± .01	.0543 ± 3	.0474 ± 3	.0457 ± 5	206 ± 3	6.1	3.71 ± .02
1193 (920)	1.17 ± .01	.0633 ± 4	.0563 ± 4	.0403 ± 5	194 ± 4	3.7	3.61 ± .03
1303 (1030)	1.04 ± .01	.0609 ± 4	.0558 ± 4	.0211 ± 3	189 ± 5	2.9	3.57 ± .04
1403 (1130)	1.00 ± .01	.0580 ± 5	.0537 ± 5	.0082 ± 2	218 ± 21	.8	3.80 ± .14
1573 (1300)	.80 ± .01	.0571 ± 6	.0553 ± 6	.0156 ± 4	227 ± 20	1.2	3.86 ± .14
Total	1.03	.046	.042	.113	59.8	93.0	1.93
15015,15,5b (gray clast, 20.0 mg); J = 0.02982							
773 (500)	1.14 ± 0.30	0.0211 ± 37	0.0189 ± 40	0.221 ± 12	0.3 ± 0.3	2.0	0.01 ± 0.01
873 (600)	.87 ± .21	.0096 ± 19	.0092 ± 20	.092 ± 6	1.0 ± .3	2.4	.06 ± .01
973 (700)	.90 ± .02	.0177 ± 4	.0168 ± 4	.0253 ± 18	10.4 ± .9	1.9	.51 ± .05
1023 (750)	1.06 ± .01	.0624 ± 5	.0569 ± 5	.0105 ± 14	60.9 ± 7.0	1.1	1.95 ± .15
1073 (800)	.95 ± .01	.1380 ± 12	.129 ± 1	.0087 ± 20	146 ± 40	.58	3.25 ± .35
1123 (850)	1.00 ± .01	.1720 ± 2	.159 ±	.0102 ± 25	156 ± 40	.55	3.25 ± .35
1193 (920)	1.42 ± .01	.1714 ± 6	.143 ± 1	.0055 ± 18	175 ± 60	.39	3.45 ± .55
1343 (1070)	1.28 ± .01	.1719 ± 5	.149 ± 1	.0018 ± 8	180 ± 80	.23	3.5 ± .7
1573 (1300)	1.40 ± .01	.1629 ± 4	.137 ± 1	.0011 ± 3	203 ± 50	.57	3.7 ± .4
Total	1.28	.137	.119	.0093	49.5	9.8	1.71
15015,15,23c (vesicular glass, 51.9 mg); J = 0.0298							
773 (500)	5.11 ± 0.09	1.23 ± 0.22	--	0.352 ± 63	88.6 ± 1.8	0.4	[d]2.08 ± 0.04
873 (600)	5.32 ± .06	.64 ± .04	--	.255 ± 16	44.9 ± .9	1.3	[d]1.18 ± .03
973 (700)	5.32 ± .02	.88 ± .02	--	.157 ± 4	66.2 ± .7	2.5	[d]1.25 ± .02
1043 (770)	5.33 ± .04	1.61 ± .03	--	.113 ± 2	121.0 ± 1.5	2.7	[d]1.29 ± .04
1123 (850)	5.33 ± .03	2.91 ± .03	--	.109 ± 2	194.9 ± 2.7	4.4	[d]1.21 ± .08
1193 (920)	5.31 ± .03	3.46 ± .04	--	.0909 ± 15	269.2 ± 3.6	3.2	--
1343 (1070)	5.17 ± .02	3.73 ± .02	--	.0504 ± 5	481.0 ± 4.9	9.3	--
1573 (1300)	5.11 ± .04	1.56 ± .01	--	.0387 ± 6	268.7 ± 4.3	9.2	--
1743 (1470)	5.14 ± .01	1.80 ± .01	--	.0462 ± 2	261.7 ± 1.1	16.7	--
Total	5.17	2.22	--	.0549	273.4	49.7	--

[a] The $^{38}Ar_c/^{37}Ar$ ratio was calculated assuming that ^{38}Ar originates solely from cosmogenic Ar ($(^{36}Ar/^{38}Ar)_c$ = 0.65) and trapped Ar ($(^{36}Ar/^{38}Ar)_t$ = 5.35). The correspondng $^{38}Ar_c$/Ca ratio is given by $^{38}Ar_c/Ca = 4.14 \times 10^{-3} \times J \times (^{38}Ar/^{37}Ar)$ cm^3 standard temperature pressure (STP)/gm Ca, where J is the irradiation coefficient (ref. 1-21).

[b] Amounts in units of 10^{-8} cm^3 STP/g. Uncertainty in absolute amounts is ±20 percent.

[c] $\lambda = 5.305 \times 10^{-10}$ y^{-1}, $\lambda_e = 0.585 \times 10^{-10} y^{-1}$, $^{40}K/K$ = 0.0119 percent.

$J = (\exp(\lambda t) - 1)/^{40}Ar/^{39}Ar^*)$. No correction applied for trapped/cosmogenic ^{40}Ar except under (d).

[d] Apparent ages calculated assuming $(^{40}Ar/^{36}Ar)_t$ = 0.97 for trapped component in 5c and $(^{40}Ar/^{36}Ar)_t$ = 1.15 for 23c, 23d and 26.

TABLE 1-VI.- Concluded

Temperature, K (°C)	$^{36}Ar/^{39}Ar$	$^{38}Ar/^{37}Ar$	$^{38}Ar_c/^{37}Ar$ (a)	$^{39}Ar^*/^{37}Ar$	$^{40}Ar/^{39}Ar^*$	$^{39}Ar^*$ (b)	Apparent age, b.y. (c)
15015,15,23d (vesicular glass, 19 mg); J = 0.0256							
803 (530)	5.37 ± 0.15	0.903 ± 26	--	0.134 ± 58	720.0 ± 320.0	0.1	--
903 (630)	5.27 ± .10	.830 ± 18	--	.186 ± 18	157.0 ± 16.0	.7	[d]2.8 ± 0.2
993 (720)	5.26 ± .03	1.046 ± 8	--	.136 ± 5	112.2 ± 4.1	2.2	[d]1.9 ± .1
1093 (820)	5.24 ± .03	1.096 ± 7	--	.0979 ± 13	101.0 ± 1.5	4.3	[d]1.2 ± .1
1173 (900)	5.28 ± .04	1.600 ± 15	--	.0852 ± 14	170.1 ± 2.9	3.2	[d]1.7 ± .1
1263 (990)	5.20 ± .01	1.847 ± 12	--	.0736 ± 21	225.2 ± 6.3	2.8	[d]2.0 ± .2
1353 (1080)	5.16 ± .04	2.841 ± 23	--	.0608 ± 4	305.0 ± 1.4	11.8	--
1413 (1140)	5.16 ± .04	1.369 ± 12	--	.0387 ± 3	280.4 ± 1.2	12.9	--
1473 (1200)	4.81 ± .01	.776 ± 4	--	.0275 ± 12	270.0 ± 12.0	1.5	--
1583 (1310)	4.82 ± .08	.653 ± 14	--	.0230 ± 71	840.0 ± 260.0	.2	--
1723 (1450)	4.77 ± .06	.568 ± 13	--	.0254 ± 62	660.0 ± 170.0	.2	--
Total	5.16	1.70		0.054	233.2	40.0	--
15015,15,26 (vesicular glass, 24 mg); J = 0.0256							
803 (530)	5.29 ± 0.11	1.034 ± 35	--	0.239 ± 17	102.8 ± 7.9	0.7	[d]2.0 ± 0.2
903 (630)	5.35 ± .06	.682 ± 11	--	.138 ± 7	50.2 ± 3.2	1.3	[d].77 ± .10
993 (720)	5.34 ± .03	1.315 ± 19	--	.111 ± 3	94.4 ± 2.5	2.1	[d].88 ± .08
1073 (800)	5.25 ± .04	2.467 ± 26	--	.0962 ± 18	181.6 ± 3.1	3.4	[d].99 ± .08
1173 (900)	5.20 ± .01	3.000 ± 19	--	.0819 ± 17	255.9 ± 5.1	2.6	[d]1.3 ± .2
1263 (990)	5.15 ± .03	2.476 ± 21	--	.0500 ± 20	329.6 ± 12.8	1.9	[d]1.2 ± .3
1353 (1080)	5.20 ± .03	4.353 ± 28	--	.0472 ± 3	553.0 ± 2.7	9.1	--
1413 (1140)	5.14 ± .03	2.279 ± 18	--	.0308 ± 9	454.5 ± 12.4	4.1	--
1473 (1200)	4.84 ± .03	.921 ± 9	--	.0098 ± 17	690.0 ± 120.0	.2	--
1723 (1450)	4.91 ± .05	1.068 ± 19	--	.031 ± 9	--	.2	--
Total	5.18	3.04		0.052	365.2	25.6	--
15015,15,5c (matrix, 60 mg); J = 0.02982							
773 (500)	5.25 ± 0.08	0.74 ± 0.15	--	0.45 ± 0.09	31.3 ± 0.9	1.6	[d]0.98 ± 0.03
873 (600)	5.28 ± .05	.45 ± .03	--	.281 ± .019	15.1 ± .2	2.9	[d].35 ± .01
973 (700)	5.31 ± .03	.58 ± .01	--	.153 ± .003	31.4 ± .3	4.3	[d].57 ± .01
1043 (770)	5.27 ± .03	2.31 ± .03	--	.086 ± .002	162.8 ± 2.6	3.9	[d]1.06 ± .02
1123 (850)	5.22 ± .02	4.94 ± .07	--	.060 ± .001	444.7 ± 7.2	2.8	--
1193 (920)	5.25 ± .02	6.08 ± .15	--	.055 ± .002	555.6 ± 8.4	2.4	--
1273 (1000)	5.17 ± .03	3.87 ± .14	--	.034 ± .002	536 ± 28	1.8	--
1343 (1070)	5.25 ± .02	8.71 ± .28	--	.046 ± .003	968 ± 55	11.7	--
1393 (1120)	5.19 ± .02	4.13 ± .05	--	.022 ± .001	950 ± 24	7.7	--
1473 (1200)	5.07 ± .03	1.62 ± .04	--	.014 ± .001	662 ± 46	1.0	--
1553 (1280)	5.19 ± .04	2.18 ± .07	--	.019 ± .001	587 ± 31	.5	--
1743 (1470)	4.89 ± .05	1.42 ± .43	--	--	--	.02	--
Total	5.22	5.0	--	0.044	--	40.6	--

[a]The $^{38}Ar_c/^{37}Ar$ ratio was calculated assuming that ^{38}Ar originates solely from cosmogenic Ar ($(^{36}Ar/^{38}Ar)_c$ = 0.65) and trapped Ar ($(^{36}Ar/^{38}Ar)_t$ = 5.35). The correspondng $^{38}Ar_c/Ca$ ratio is given by $^{38}Ar_c/Ca = 4.14 \times 10^{-3} \times J \times (^{38}Ar/^{37}Ar)$ cm^3 standard temperature pressure (STP)/gm Ca, where J is the irradiation coefficient (ref. 1-21).

[b]Amounts in units of 10^{-8} cm^3 STP/g. Uncertainty in absolute amounts is ±20 percent.

[c]$\lambda = 5.305 \times 10^{-10}$ y^{-1}, $\lambda_e = 0.585 \times 10^{-10} y^{-1}$, $^{40}K/K$ = 0.0119 percent.

$J = (\exp(\lambda t) - 1)/(^{40}Ar/^{39}Ar^*)$. No correction applied for trapped/cosmogenic ^{40}Ar except under (d).

[d]Apparent ages calculated assuming $(^{40}Ar/^{36}Ar)_t$ = 0.97 for trapped component in 5c and $(^{40}Ar/^{36}Ar)_t$ = 1 15 for 23c, 23d and 26.

$^{38}Ar_c$ is in the low-temperature release, evidenced by low $^{38}Ar_c/^{37}Ar$ ratios and suggesting that some of the Ar loss occurred after the main period of cosmic ray exposure of the fragments. The chemical similarity of glass and matrix (section entitled "Mineralogy and Petrology") suggests that the glass was formed by melting and lithification of a preexisting soil. Such an event could certainly account for the extreme Ar loss in this sample. However, it should be noted that 50 percent of the artificially induced $^{39}Ar^*$ was released by 873 K (600° C) in both clasts, and it therefore seems quite possible (ref. 1-22) that

some of the loss could be accounted for by solar heating.

In the last 15 percent of $^{39}Ar^*$ release from 23b, the $^{40}Ar^*/^{39}Ar^*$ ratio reaches a mean value corresponding to an apparent age of 3.71 ± 0.12 b.y. This must be regarded as a lower limit to the original crystallization age. The high-temperature release from 5b (1073 to 1573 K (800° to 1300° C)) corresponds to an ^{40}Ar-^{39}Ar age of 3.4 ± 0.2 b.y. Because of the extreme degree of $^{40}Ar^*$ loss and the low K content of 5b, this age is rather inaccurate and again must be regarded as a lower limit to the original crystallization age.

The major release of cosmogenic Ar occurs at high temperature, and well-defined, but distinct, $^{38}Ar_C/^{37}Ar$ plateaus are obtained for both clasts. Based on a nominal $^{38}Ar_C$ production rate of 1.4×10^{-8} cm^3 standard temperature pressure (STP)/g Ca/m.y. (ref. 1-21), exposure ages of 490 m.y. (23b) and 1290 m.y. (5b) are calculated. Ages based on total $^{38}Ar_C/^{37}Ar$ are respectively 400 m.y. and 1050 m.y. and reflect some 20 percent $^{38}Ar_C$ loss.

The Ar data for the matrix (5c) and the glasses (23c, 23d, 26) are dominated by trapped Ar, and age information is less clear. A graph of $^{40}Ar/^{36}Ar$ against $^{39}Ar^*/^{36}Ar$ (fig. 1-12) reveals an apparent correlation for glasses 23c and 26, corresponding to isochron ages of 1.2 b.y. and 0.8 b.y. The correlations are largely defined by relatively low temperature points (<9273 K (9000° C)) and are subject to numerous interpretations. Sample 23d shows no correlation. The frothy glass contains many small lithic and mineral inclusions, and it is suspected that the low-temperature release, being relatively low in trapped Ar, may be dominated by these inclusions while the glass itself may be responsible for the greater proportion of trapped Ar in the high-temperature Ar. It seems likely that the isochron ages may represent at best an upper limit to the age of the glass, on the assumption that the lithic clasts were largely outgassed at the time the glass was melted. The $^{40}Ar/^{36}Ar$ ratio of the trapped Ar in the glass is 1.17 ± 0.04, as indicated by the intercept in figure 1-12. This is 0.20 ± 0.06, higher than the corresponding ratio for the matrix. The difference could have resulted from the homogenization of trapped Ar and radiogenic Ar within the glass at the time of its formation and to this extent is consistent with the glass being relatively recent.

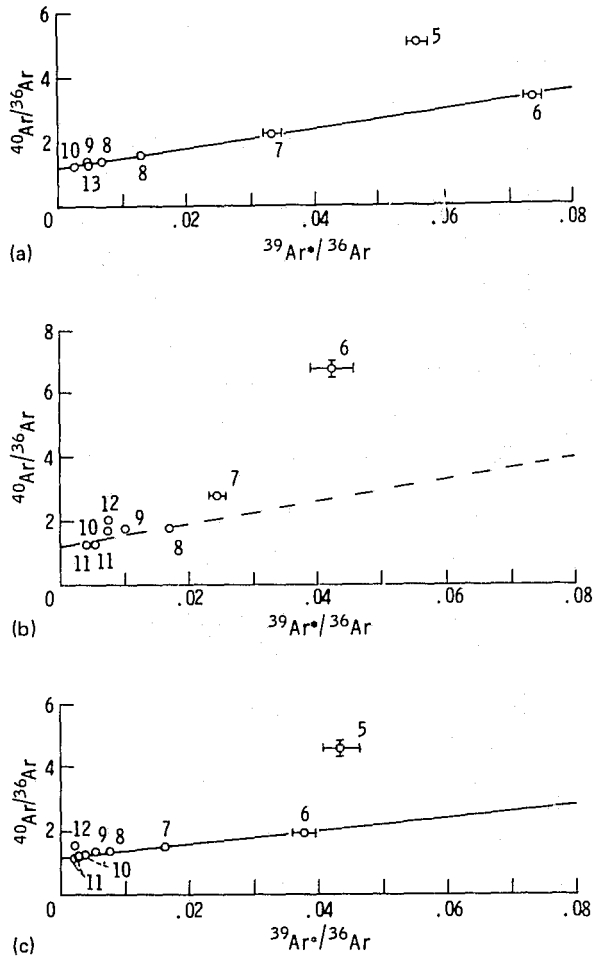

Figure 1-12.- Isochron diagram of $^{40}Ar/^{36}Ar$ and $^{39}Ar^*/^{36}Ar$ for Ar from vesicular glasses 23c, 23d, and 26. The numbers represent temperature in units of 100° C ($T_K = T_C + 273.15$). The slopes of the isochron for 23c and 26 correspond to ages of 1.2 and 0.8 b.y., respectively. No correlation is observed for 23d, and the dashed line drawn corresponds to the same apparent age as 23c. The correlations appear to indicate outgassing of the glass or of inclusions within the glass within the last 1.0 b.y. It has been tentatively inferred that the glass formed at 1.0 b.y. or later, but the correlations could reflect recent solar heating. (a) Sample 15015,23c. (b) Sample 15015,23d. (c) Sample 25025,26.

The matrix sample (5c) does not yield a well-defined correlation of $^{40}Ar/^{36}Ar$ and $^{39}Ar^*/^{36}Ar$. Above 1223 K (950° C), the yield is entirely domi-

nated by trapped Ar with a $^{40}Ar/^{36}Ar$ ratio of 0.97 ± 0.04. Apparent ages for the low-temperature release steps are calculated assuming a trapped component of this composition and are included in table 1-VI. The apparent ages are low, reflecting Ar loss, as observed for the clasts and possibly for the glass.

The predominance of trapped Ar in the matrix and glass precludes an accurate estimation of an ^{38}Ar exposure age for these samples. The $^{36}Ar/^{38}Ar$ ratio (table 1-VI) decreases by a few percent in the high-temperature release, which is consistent with a small cosmogenic contribution. An $^{38}Ar/^{36}Ar$ and $^{37}Ar/^{36}Ar$ correlation diagram (fig. 1-13) appears to indicate the absence of cosmogenic ^{38}Ar in the low-temperature release (approximately 10 percent of total ^{37}Ar release). The $^{38}Ar/^{36}Ar$ ratio in the high-temperature release increases with increasing $^{37}Ar/^{36}Ar$ in a fashion approximately consistent with the presence of cosmogenic ^{38}Ar. The data for both matrix and glass do not appear to be in conflict with an exposure age similar to that of 23b, but the total variation in $^{38}Ar/^{36}Ar$ is only a few percent. In view of the possibility of fractionation effects at this level due to thermal diffusion, it is not possible to make any precise comments on the exposure age data of matrix and glass.

The results of these measurements provide a number of constraints for models of the possible history of 15015, but they do not define a unique history. The constraints are as follows.

1. The high-temperature $^{40}Ar^*/^{39}Ar^*$ ratios from the Fra Mauro basalt clast (23b) indicate that the parent rock crystallized at 3.7 ± 0.1 b.y. or earlier, predating the Hadley Rille mare basalts (refs. 1-23 to 1-26).

2. The variolitic basalt (5b) crystallized at 3.4 ± 0.2 b.y. or earlier.

3. Although no mare basalt clasts from 15015 have been dated, their presence (section entitled "Mineralogy and Petrology") indicates that the breccia formed after the basalt flows had crystallized. If the mare basalt fragments are locally derived, this would imply that the breccia formed more recently than 3.3 b.y. ago (refs. 1-23 to 1-26).

4. The variolitic basalt clast (5b) has an exposure age of 1290 m.y., greatly in excess of that of the Fra Mauro basalt clast 23b, 490 m.y., and also greatly in excess of neon-21 (^{21}Ne) exposure ages inferred for the matrix (noble gas data). This implies a preirradiation of clast 5b for at least 800 m.y. before incorporation in the breccia. Such a history of preirradiation combined with the $^{40}Ar^*/^{39}Ar^*$ age indicates that 15015 was formed more recently than 2.6 ± 0.2 b.y. ago from a mature regolith. Petrologic considerations (discussed earlier) suggest that this regolith was locally derived. In view of the late date of the lithification in comparison to the time of basalt extrusion, it appears likely that lithification resulted from meteorite impact.

5. The ^{40}Ar-^{39}Ar isochron ages of 23c and 26, around 1.0 b.y., may represent the formation time of

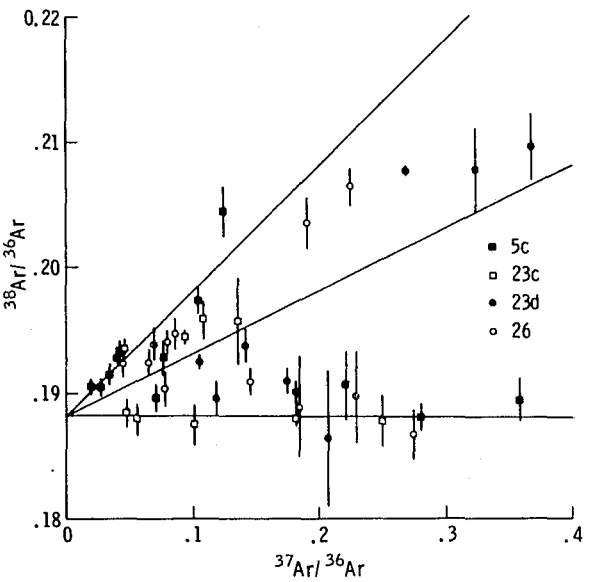

Figure 1-13.- Correlation diagram of $^{38}Ar/^{36}Ar$ and $^{37}Ar/^{36}Ar$ for matrix 5c and glasses 23c, 23d, and 26. The Ar is a mixture of trapped Ar ($^{38}Ar/^{36}Ar$ = 0.188, $^{37}Ar/^{36}Ar$ = 0) and cosmogenic Ar produced predominantly from the bombardment of Ca ($^{38}Ar/^{36}Ar \simeq 1.6$, $^{37}Ar/^{36}Ar \neq 0$, inversely proportional to exposure age). For all samples, the low-temperature release lies on a horizontal line, reflecting the absence in these (Ca) sites of cosmogenic $^{38}Ar_c$ and ^{36}Ar. The higher temperature points show the release of cosmogenic $^{38}Ar_c$ and ^{36}Ar in amounts approximately proportional to the amount of ^{37}Ar (= Ca). The upper line corresponds to an exposure age of 1000 m.y. irradiation coefficient (J = 0.0298) or 1160 m.y. (J = 0.0256). The slope of the middle line corresponds to an exposure age of half this. The absence of cosmogenic Ar in the low-temperature points appears to be at odds with the observations of radiogenic ^{40}Ar (fig. 1-12).

the glass and also the time of the lithification, although this interpretation is speculative. If the glass does date from this time, it is apparent from the track and ^{3}He measurements (discussed in following sections) that the sample remained buried at depth until quite recently.

Cosmic Ray Tracks

Combined high-voltage and scanning electron microscopy, previously applied to Apollo 11 and 14 breccias (refs. 1-27 and 1-28) have been used to study both radiation damage features and various textural features in individual grains from breccia 15015.

Preliminary 1-MeV electron microscope examination of micron-sized grains extracted from the bottom chip, 15015,15,10, yields the following results.

1. Less than 10 percent of the grains appear as totally amorphous, but a much higher proportion shows evidence of shock (i.e., diffraction patterns indicative of disorder and deformation bands in pyroxenes).

2. No evidence exists for ultrathin amorphous coatings or high densities of latent tracks characteristic of highly irradiated particles in mature soil samples.

3. Approximately 30 percent of the grains contain microcrystallites (fig. 1-14) similar to those found both in artificially heated lunar dust grains and in mildly metamorphosed Apollo 11 and 14 breccias belonging to groups 1 and 2 (ref. 1-29).

Polished sections from two exterior chips, 15015,15,10 (bottom) and 15015,15,22 (top), have been irradiated with a californium (^{252}Cf) source to induce fission-fragment tracks and then examined by

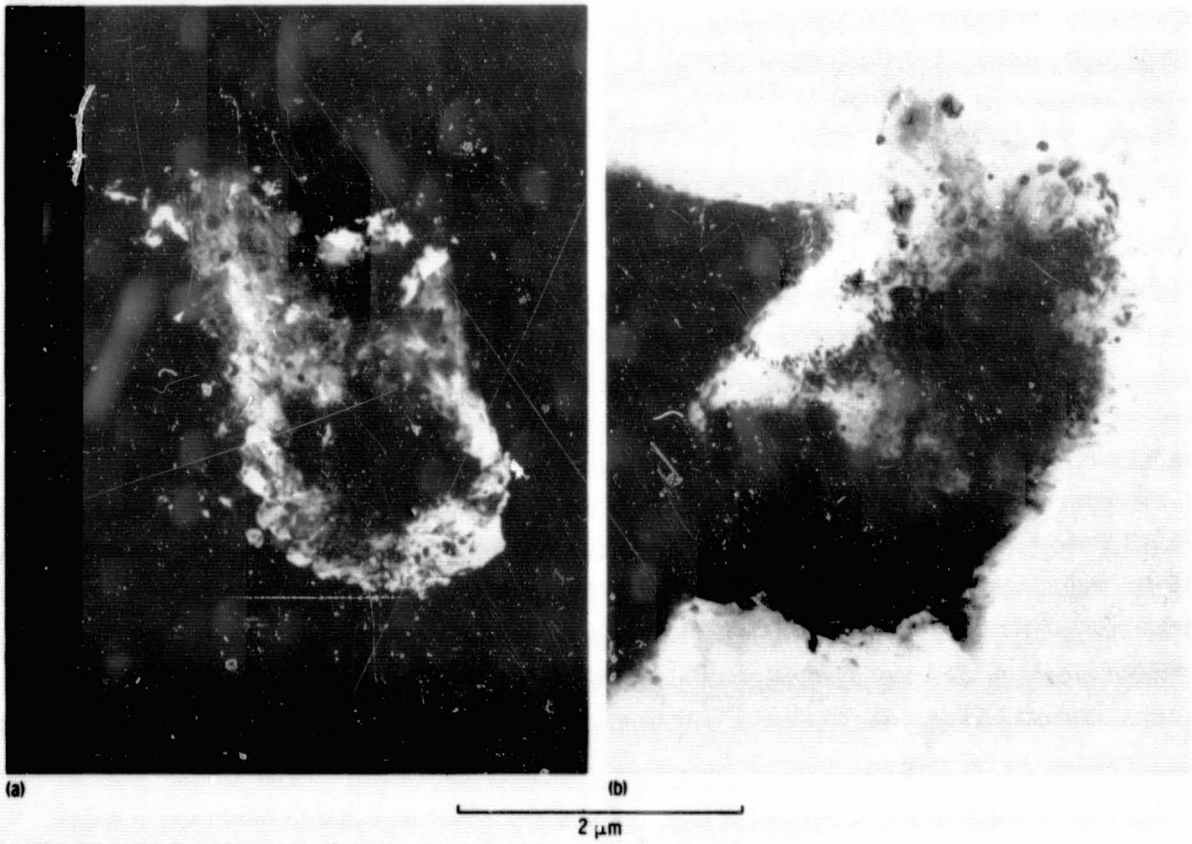

Figure 1-14.- 1-MeV electron micrographs of crystalline grains loaded with microcrystallites. (a) Dark field. (b) Bright field.

an SEM. Gradual etching was used to reveal both artifical and fossil tracks successively in glass, feldspars, and pyroxenes (each mineral phase being identified with the electron microprobe attachment of the SEM). The main results are as follows.

1. A very slight etching quickly dissolves the fine-grained matrix that presumably consists of glassy or highly disordered grains. Glass is also found in vesicular veins and in numerous angular clasts, and constitutes the external coatings of the two chips. All interior glassy grains have fossil track densities of approximately 10^6 tracks/cm^2. It is almost impossible to use the exterior glass coating as a track detector because high concentrations of vesicular bubbles are superimposed on the track distribution. Therefore, no track density gradient can be identified, and an approximate estimate indicates the density ρ is of the order of 10^7 tracks/cm^2. The very heavy exposure age of the glass coating is therefore $<10^7$ years.

2. Feldspar grains are very scarce, very small (<10 μm), and surrounded by a much larger area of disordered mineral phase of anorthosite composition (fig. 1-15). Eleven such grains have been found with track densities at the centers ranging from 10^7 to 4×10^9 tracks/cm^2.

3. Pyroxene grains are highly fractured and have track densities at the center ranging from about 10^6 to 4×10^8 tracks/cm^2.

In a previous study of Apollo 11 and 14 breccias, two distinct groups of breccias were defined in terms of track metamorphism (refs. 1-27 and 1-28) as follows.

1. The mildy metamorphosed breccias still contain radiation damage features due to the individual irradiation of their constituent grains in solar nuclear particle fluxes before brecciation. Such features appear either as high densities of latent nuclear particle tracks (approximately 10^{11} tracks/cm^2) or as very small crystallites similar in size to those formed in artificially heated mature lunar dust grains. These

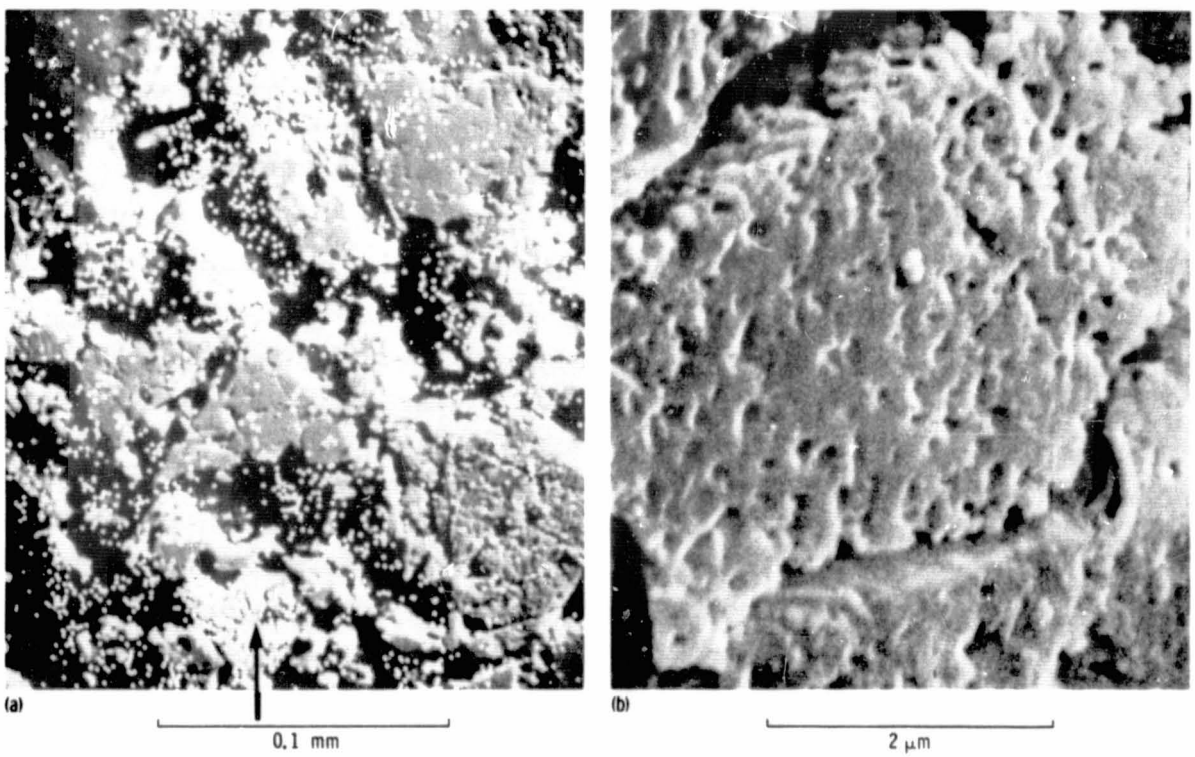

Figure 1-15.- Scanning electron micrographs of a polished section that has been etched to reveal tracks in feldspars. (a) Aluminum X-ray scan superimposed on a backscattered electron scan. The arrow indicates the location of a feldspar grain of high track density in a rich Al-bearing mineral phase. (b) Micrograph of the same feldspar grain of high track density.

breccias are also characterized by high densities (approximately 10^9 tracks/cm^2) of etched tracks at the center of 100-μm grains.

2. In the strongly metamorphosed breccias, no remnant of the prebreccia solar irradiation is found, and the track densities of about 10^7 tracks/cm^2 seem to be due to the exposure of the whole breccia to galactic cosmic rays.

Rock 15015 is intermediate between these two extreme groups. It contains microcrystallites similar to those observed in mildly metamorphosed breccias but much larger in size. Furthermore, the track densities in feldspars and pyroxenes are spread over two orders of magnitude, in striking contrast to the narrow range of values observed for the second group of breccias. These "intermediate" characteristics suggest either that the breccia has been formed from a mixture of mature and nonmature soil or that a nonthermal process has also been responsible for the track metamorphism. At present, the second explanation is preferred, because several textural features (extensive fracturing, lattice disorder) support the hypothesis that rock 15015 has suffered a strong shock event that could have severely affected its track distribution.

Noble Gases

Concentrations and isotopic compositions of He, Ne, and Ar were determined by mass spectrometry of three matrix samples and of one clast sample of 15015,15 (table 1-VII).

The spallogenic and trapped Ne components are evaluated by assuming a $^{22}Ne/^{21}Ne$ ratio of 1.10 ± 0.05 in spallogenic Ne and one of 32 ± 1 in trapped Ne. These calculated concentrations are given in table 1-VII. Together with the chemical composition given in table 1-II and respective elemental production rates, the ^{21}Ne exposure ages are computed (table 1-VII). Within limits of error, the ^{21}Ne exposure ages of the three matrix samples and the clast sample agree with each other. Unfortunately, the chemical composition of the clast was not determined, which renders the ^{21}Ne exposure age uncertain despite the comparatively small error of the spallogenic ^{21}Ne component.

The predominance of trapped Ar renders the calculation of the spallogenic Ar components uncertain, except for the clast sample. Assuming an $^{36}Ar/^{38}Ar$ ratio of 5.35 ± 0.05 for trapped Ar and one of 0.65 ± 0.03 for spallogenic Ar, a concentration of spallogenic ^{38}Ar approximately 30×10^{-8} cm^3 STP/g is calculated for the clast. Spallogenic ^{38}Ar is also clearly present in the bottom and top samples, but the quantities are uncertain. With a Ca concentration in the clast assumed to be equal to that in the matrix, an exposure age of 290 ± 20 m.y. is determined. Using the formula for the production rate of ^{38}Ar given by reference 1-31, an exposure age of 203 ± 56 m.y. is obtained. An evaluation of the radiogenic and trapped ^{40}Ar components is not possible. As seen from the measured $^{40}Ar/^{36}Ar$ ratios, a single $^{40}Ar/^{36}Ar$ ratio in the Ar initially trapped and a constant concentration of radiogenic ^{40}Ar can both be ruled out. This is presumably due to an inhomogeneous K distribution. With the K concentration given in table 1-II, approximately 10^{-4} cm^3 STP/g of radiogenic ^{40}Ar would be expected if the sample had retained Ar for 4 b.y. Clearly, the clast sample has either retained Ar for a shorter period or is depleted in K.

Concerning the composition of the He in the 15015 samples, the following observations are made. The $^4He/^3He$ ratios of trapped He in lunar fines are around 2800, and the $^3He/^{21}Ne$ ratio of spallogenic gas, around 6. Thus, a substantial deficit of ^3He is evident in all samples. Also, the measured $^4He/^{20}Ne$ ratios are low compared to lunar soil values of approximately 20 to 50. This indicates also a substantial deficit of ^4He. Taken together and considering that in linear heating experiments trapped He is more readily released than spallogenic ^3He (refs. 1-32 and 1-33), it is concluded that only a minor fraction of trapped He initially present has been retained. Thus, precise determination of the components is not possible because of the substantial loss of He in all three cases.

With respect to the different events recorded by the noble gases in the breccia, these findings can be interpreted as follows. The occurrence of solar Ne and Ar indicates that the matrix of the breccia 15015 contains constituents that were exposed to solar irradiation as finely dispersed material before formation of the breccia. The ^{21}Ne and ^{38}Ar exposure ages of the matrix and the clast are 280 ± 25 m.y. The deficit of spallogenic ^3He indicates a recent degassing event. Compared to solar He, Ne, and Ar in lunar fines, the breccia contains not only concentrations lowered to a variable degree but also severely altered

TABLE 1-VII.- NOBLE GASES RELEASED FROM 15015,15, TOGETHER WITH CALCULATED EXPOSURE AGES

[All units in 10^{-8} cm^3 STP/g unless otherwise indicated]

Sample	^3He	^4He	^{20}Ne	^{21}Ne	^{22}Ne	^{36}Ar	^{38}Ar	^{40}Ar
Top (15015,15,20); 3.06 mg								
Total	32.8 ± 1.8	21 400 ± 1000	9620 ± 450	63 ± 3	820 ± 40	11 900 ± 600	2240 ± 110	23 00 ± 1000
Spallogenic	≤32.8	--	37 ± 7	39 ± 6	42 ± 7	--	--	--
Trapped	--	--	9580 ± 450	24 ± 7	780 ± 43	11 890 ± 600	2220 ± 110	--
Exposure ages, m.y.[a]	≤33	--	--	250 ± 40	--	--	--	--
Middle (15015,15,14); 3.04 mg								
Total	68 ± 4	167 000 ± 9000	24 900 ± 1300	104 ± 7	2030 ± 120	Lost	--	--
Spallogenic	≤68	--	40 ± 20	42 ± 19	46 ± 20	--	--	--
Trapped	--	--	24 900 ± 1300	62 ± 20	1990 ± 122	--	--	--
Exposure ages, m.y.[a]	≤68	--	--	270 ± 120	--	--	--	--
Bottom (15015,15,4); 3.35 mg								
Total	100 ± 4	274 000 ± 10 000	45 000 ± 1600	160 ± 8	3620 ± 150	24 500 ± 900	4640 ± 200	23 900 ± 1000
Spallogenic	≤100	--	47 ± 11	59 ± 10	54 ± 11	--	--	--
Trapped	--	--	45 000 ± 1600	111 ± 13	3570 ± 150	24 500	4570 ± 250	--
Exposure ages, m.y.[a]	≤100	--	--	310 ± 70	--	--	--	--
Clast (15015,15,27); 16.57 mg								
Total	23.0 ± 0.3	29 300 ± 300	251 ± 3	41.2 ± 0.6	60.9 ± 0.9	169 ± 2	56.6 ± 0.9	5600 ± 250
Spallogenic	≤23	--	38.7 ± 2.7	40.7 ± 2.0	44.8 ± 3.1	20.0 ± 1.7	30.8 ± 2.2	--
Trapped	--	--	212 ± 5	0.5 ± 2.0	16.1 ± 3.2	149 ± 2.6	27.8 ± 2.5	--
Radiogenic	--	--	--	--	--	--	--	~5400
Exposure ages m.y.[a]	≤23	--	--	260 ± 12	--	--	[b]203 ± 56 290 ± 20	--

[a]Production rates from Bogard et al. (ref. 1-30), but P(38) = 1.4×10^{-8} cm^3 STP $(g\ Ca)^{-1}$ $m.y.^{-1}$.

[b]Production rated according to Weber (ref. 1-31).

abundance patterns. The bottom sample shows the least depletion and the clast, the largest.

It is interesting that the degree of depletion is paralleled by an alteration of the element abundances. This change in the element abundances shows that the varying concentrations are not solely caused by differences in matrix grain size. It is tempting to invoke thermal differences as the reason for the solar gas pattern observed. The loss of spallogenic ^3He seems to be larger in samples closer to the top of the rock. A concentration gradient is also observed for trapped noble gases. The loss of noble gases may have occurred during the heating caused by the coating of the rock with glass. However, comparison of the noble gas abundance patterns in 15015 to those in lunar fines shows larger variations than those observed during linear heating experiments. This may indicate that shock events played an essential role in the alteration of the initial abundance patterns.

Carbon, Nitrogen, and Sulfur

Three small samples of the breccia from the top, middle, and bottom of the rock were analyzed for C, S, and N (table 1-VIII). The value for C is in the range of other measurements of C content for Apollo 15 samples (ref. 1-34). Little variation was found, and the average value for three samples (table 1-VIII) is 121 parts per million (ppm). This C content is only 29 ppm lower than the measured value of four fines from the same station (station LM, ref. 1-34). The average S content of the three samples is 630 ppm and is not significantly different from the S content of the fines at the same station (ref. 1-35). The average N content of the three samples is 54 ppm; approximately half the N content measured in the fines (refs. 1-35 and 1-36). The C/N ratio in the breccia is 2.24, whereas in the fines it is 1.41.

All three elements show isotopic depletion of the heavy isotopes relative to the measured values for fines samples 15012 and 15013 from the same station. Fines average δC^{13} = +11 per mill; breccia = −4.3 per mill; δS^{34} fines = +8.1 per mill; breccia = +7.1 per mill; δN^{15} fines = +35.6 per mill; breccia = +0.9 per mill. The greatest difference between isotopic values in the fines and breccias is for N, followed by C, with the least change in S.

Petrographic and microscopic studies (previously discussed) indicate that coincident with, or subsequent to, formation of the breccia, thermal annealing may have occurred. The conclusion that heating occurred is also supported by the very low content of ^4He. The temperature of the sample heating can be estimated by comparing pyrolysis profiles obtained in the experiments on fines sample 15012 (ref. 1-35). It is evident from this study that, at 1073 K (800° C), >90 percent He, 45 percent N_2, and 20 percent C are lost from the sample. At this temperature, S is negligibly affected. Furthermore, C preferentially enriched in C^{13} and N enriched in N^{15} are released at temperatures of heating from 873 to 1073 K (600° to 800° C). The relatively greater losses of N_2 from the top of the rock (samples closest to 15015,15,17) suggest that this section may have undergone heating to a slightly higher temperature or remained heated for a longer period.

TABLE 1-VIII.- CARBON, SULFUR, AND NITROGEN IN BRECCIA 15015, OBTAINED BY COMBUSTION IN PARTIAL OXYGEN ATMOSPHERE

Sample no.	Location in consortium slab	Weight, g	C, ppm	δC^{13} PDB (a)	S, ppm	δS^{34} C.D. (b)	N, ppm	δN^{15} air	He, ppm
15015,15,17	Top	0.5568	131	[c]-2.8	673	7.4	42	-1.5	[d]<1
15015,15,7	Middle	.6393	121	-4.5	586	7.6	61	3.2	<1
15015,15,3	Bottom	.4607	110	-5.5	628	6.3	59	(e)	<1
Average		--	121	-4.3	630	7.1	54	.9	

[a] PDB = Pee Dee belemnite.

[b] C.D. = Canyon Diablo.

[c] CO_2 repurified.

[d] Below detection limit.

[e] Impure.

Methane and Carbide

Interior samples from the top, middle, and bottom of the slab were examined by dissolution in deuterium chloride (DCl) (38 percent in deuterium oxide); the CH_4 and CD_4 released were analyzed quantitatively by gas chromatography (table 1-IX). The amount of carbide (hydrolyzable C) indicated by the CD_4 is essentially the same in each sample; however, the CH_4 (methane trapped gas) concentration is much less in samples from the highly vesicular top portion and from the center of the rock. This observation is paralleled by the light rare-gas concentrations and total N measurements (discussed earlier). The ratio of volatile to involatile C (CD_4/CH_4 ratio; bottom 7.3, middle 26.0, and top ∞) suggests that a preferential loss of the volatile species CH_4 from the uppermost sections of 15015 occurred and that presumably this rock has experienced a thermal gradient.

These results are consistent with the following history for 15015. The rock is a metamorphic breccia; unlike the Apollo 14 metamorphic breccias, which were formed from a soil containing only a small portion of mature regolith (ref. 1-37), it was compacted from very mature fines.

The material constituting the top of 15015 has experienced a process more violent (higher temperatures or longer time) than during the formation of highly vesicular glassy agglutinates. Aliquots of such particles selected by microscopic appearance or by density/magnetic properties from the lunar fines show considerable fractionation of volatile CH_4 relative to carbide; CD_4/CH_4 ratios up to approximately 21 have been observed (refs. 1-38 and 1-39). The highly vesicular appearance of the top surface of 15015 is strongly indicative of a thermal mechanism rather than a shock process for the removal of volatile species. The materials comprising the interior and bottom of 15015 have progressively less violent histories. Even so, the middle underwent a process similar to agglutination and the bottom, an event like that usually accompanying the formation of group 0 to 1 regolith breccias or soil microbreccias. Unmetamorphosed breccias exhibit low CD_4/CH_4 ratios (approximately 4.0) approximately equal to the ratios observed for bulk soil and constant with volatile CH_4 retention (refs. 1-38 and 1-39).

Formation of 15015 from local soil (15041; CD_4: 23.5 μg/g; CH_4: 4.6 μg/g) by lithification at a temperature of approximately 1073 K (800° C) would result in the observed reduction in the carbide content (ref. 1-40). Indeed, the material constituting the matrix of the breccia has a bulk chemistry that is identical to that of the local soil (15041) (ref. 1-11); thus, 15015 may have been formed by an impact occurring at the Apollo 15 site. The similarity in the absolute amounts of carbide for the three sections of 15015 suggests that volatile fractionation resulted from the top section of the rock being at an elevated temperature for a longer time (i.e., the bottom of the rock had a more rapid rate of cooling) rather than from an increased temperature. The circumstances leading to the observed temperature gradient within 15015 are presently not understood.

TABLE 1-IX.- QUANTITIES OF METHANE AND DEUTERIUM CARBIDE RELEASED BY DISSOLUTION IN DEUTERIUM CHLORIDE

Sample no.	Location in consortium slab	Weight, g	CD_4, µg/g	CH_4, µg/g	CD_4/CH_4
15015,15,21	Top	0.0728	14.6	<0.01	∞
15015,15,21	Top	.0573	15.3	<.01	∞
15015,15,6	Middle	.0098	16.6	.64	26
15015,15,2A	Bottom	.0082	15.0	2.0	7.3

X-Ray Photoelectron Spectroscopic Studies

Three types of sample surface from two chips of rock, 15015,15,8 and 15015,15,29, were examined. These were an exterior glass face from the bottom of the rock and interior chipped and sawn surfaces.

Intense signals due to oxygen (O) and C were obtained in the XPS analysis of the exterior surface. Other peaks identified included Ca, silicon, (Si), Al, Fe, and Mg. The presence of all elements was confirmed by detailed high-resolution spectra from the appropriate kinetic energy regions of the spectrum. Etching at 1333.22^{-5} N/m^2 (10^{-5} torr) for 20 minutes using Ar ion bombardment (removal of very approximately 2 nm (20 Å of material) reduced the C signal to a level just above the background noise and constant with a slow buildup of contamination from residual gases in the spectrometer. The major C peak in the unetched sample was presumably due to surface contamination.

The analysis of a chipped surface (greater in area than the collection area of the spectrometer to ensure maximum sensitivity) again revealed a spectrum dominated by C. This C signal was removed by 30 minutes etching with Ar ions. An examination of cut faces yielded similar results, except in one case when the C/O ratio suggested that contamination from the diamond saw was occurring.

No evidence for the presence of the carbidic C giving rise to CD_4 on DCl dissolution (discussed earlier) was found, although XPS evidence for this species has been reported for fines and a breccia from Apollo 16 (ref. 1-41). It was also impossible to determine the valence state of Fe from either its peak profile or position, even in cases when the etching procedure enhanced the signal due to Fe. Detailed high-resolution study of the appropriate region of the spectrum also failed to reveal the presence of the N that was observed by pyrolysis (discussed previously).

In conclusion, it appears that XPS is not sufficiently sensitive, at present, to detect the low concentrations of C, free Fe, and N that occur in lunar fines and breccias.

CONCLUSIONS

The consortium investigation allows the following tentative history for 15015 to be drawn.

Breccia 15015 is petrologically assigned to Warner's group 2. It was formed from a well-mixed soil; the many fragment types recognized suggest an origin from a shallow depth of regolith. The bulk chemistry of the matrix is similar to that of the local soil, and presumably 15015 was derived at the Apollo 15 site rather than being deposited there from elsewhere. The soil here could itself still have a large component of disintegrated "ray" material even though the breccia was generated at the Apollo 15 site.

The varying exposure ages of both clasts and matrix indicate a complex history before lithification. The presence of large amounts of noble gases, carbon compounds, and nitrogen, together with etchable tracks and microcrystallites, suggests a considerable exposure of the constituent grains to solar wind.

The ^{40}Ar retention ages and ^{38}Ar exposure ages considered together indicate that 15015 was not consolidated earlier than 2.7 ± 0.2 b.y. However, the 0.8- to 1 2-b.y. age of the frothy vesicular glass estimated from a $^{40}Ar/^{39}Ar$ "isochron" very tentatively suggests that lithification occurred considerably later. During consolidation, the maximum temperature reached was approximately 1073 K (800°C) based on carbon chemistry and noble gas measurements. Both suggest, however, that 15015 exhibits a unique thermal gradient and that the top of the rock was maintained at a higher temperature or was heated considerably longer than the bottom. Shock events may also have played a part in the preferential fractionation of volatile components from the upper regions of the breccia.

Helium-3 and the track density in the coating glass indicate that after consolidation 15015 was buried at a depth greater than 2 m until it was ejected onto the lunar surface possibly as recently as 30 m.y. ago.

ACKNOWLEDGMENTS

The membership of the European Consortium and friends is as follows. G. Eglinton, B. J. Mays, and C. T. Pillinger, School of Chemistry, University of Bristol, England; S. O. Agrell, J. H. Scoon, J. V. P. Long, J. E. Agrell, and A. A. Arnold, Department of Mineralogy and Petrology, University of Cambridge, England; I. R. Kaplan and C. Petrowski, Department

of Geology, University of California at Los Angeles; J. W. Smith C.S.I.R.O., North Ryde, New South Wales, Australia; P. W. Gast and L. E. Nyquist, NASA Lyndon B. Johnson Space Center; J. C. Dran, M. Maurette, Laboratoire Rene Bernas, 91406, Orsay, France; E. Bowell and A. Dollfus, Observatoire de Paris, 92190, Meudon, France; J. E. Geake, University of Manchester, Institute of Science and Technology, England; G. Turner, P. H. Cadogan, C. J. Yonge, Department of Physics, University of Sheffield, England; L. Schultz and P. Singer, Swiss Federal Institute of Technology, 8006, Zurich, Switzerland; and E. L. Evans and M. J. Tricker, Department of Chemistry, University College of Aberystwyth, Wales.

We would like to thank the Science Research Council for a grant (SGS02320) towards the installation and operation of the sample distribution facility at Bristol. The following agencies have provided funds to support the analyses: the Science Research Council (SGS128 and B/RG/26562), the National Environment Research Council (Grant Nos. GR/3/1715 and GR/3/1144), the Swiss National Science Foundation (Grant No. 2.589.71), NASA (NGR 05-007-221), Centre National de la Recherche Scientifique and Centre National d'Etude Spatiale.

We are indebted to the Institut d'Optique Electronique du C.N.R.S., Toulouse, and the B.R.G.M., Orléans, for the use of the 1-MeV and scanning electron microscopes, respectively.

We are particularly grateful to the staff of the School of Chemistry, University of Bristol, Engineering Workshop, who helped design and assemble the rock-cutting equipment and to Mr. I. Manning and Mrs. A. P. Gowar for technical assistance.

REFERENCES

1-1. Abell, P. I.; Draffan, G. H.; et al.: Organic Analysis of the Returned Apollo 11 Lunar Sample. Proceedings of the Apollo 11 Lunar Science Conference, vol. 2, Pergamon Press (New York), 1970, pp. 1757-1773.

1-2. Cadogan, P. H.; Eglinton, G.; et al.: Survey of Lunar Carbon Compounds: II. The Carbon Chemistry of Apollo 11, 12, 14, and 15 Samples. Proceedings of the Third Lunar Science Conference, vol. 2, MIT Press (Cambridge, Mass.), 1972, pp. 2069-2090.

1-3. Nyquist, L. E.; Hubbard, N. J.; et al.: Rb-Sr Systematics for Chemically Defined Apollo 15 and 16 Materials. Proceedings of the Fourth Lunar Science Conference, vol. 2, Pergamon Press (New York), 1973, pp. 1823-1846.

1-4. Agrell, S. O.; Scoon, J. H.; et al.: Observations on the Chemistry, Mineralogy and Petrology of Some Apollo 11 Lunar Samples. Proceedings of the Apollo 11 Lunar Science Conference, vol. 1, Pergamon Press (New York), 1970, pp. 93-128.

1-5. Borg, J.; Dran, J. C.; et al.: High Voltage Electron Microscope Studies of Fossil Nuclear Particle Tracks in Extraterrestrial Matter. Earth Planet. Sci. Letters, vol. 8, 1970, pp. 379-386.

1-6. Turner, G.; Cadogan; P. H.; and Yonge, C. J.: Argon Selenochronology. Proceedings of the Fourth Lunar Science Conference, vol. 2, Pergamon Press (New York), 1973, pp. 1889-1914.

1-7. Bowell, E.; Dollfus, A.; Zellner, B.; and Geake, J. E.: Polarimetric Properties of the Lunar Surface and Its Interpretation. Part 6: Albedo Determinations From Polarimetric Characteristics. Proceedings of the Fourth Lunar Science Conference, vol. 3, Pergamon Press (New York), 1973, pp. 3167-3174.

1-8. Bowell, Edward; and Zellner, Ben: Polarizations of Asteroids and Satellites. Planets, Stars and Nebulae Studied with Photopolarimetry, T. Gehrels, ed., The Univ. of Arizona Press (Tucson, Ariz.), 1974, pp. 381-404.

1-9. Bowell, E.; Dollfus, A.; Geake, J. E.; and Zellner, B.: Optical Polarizations of Lunar Samples, With Applications to the Study of Asteroids and Planetary Satellites. (Abs. of papers presented at the Fourth Lunar Science Conference (Houston, Tex.), Mar. 5-8, 1973), pp. 85-87.

1-10. Carter, James L.; and McKay, David S.: Metallic Mounds Produced by Reduction of Material of Simulated Lunar Composition and Implications on the Origin of Metallic Mounds on Lunar Glasses. Proceedings of the Third Lunar Science Conference, vol. 1, MIT Press (Cambridge, Mass.), 1972, pp. 953-970.

1-11. Laul, J. C.; and Schmitt, R. A.: Chemical Composition of Apollo 15, 16 and 17 Samples. Proceedings of the Fourth Lunar Science Conference, vol. 2, Pergamon Press (New York), 1973, pp. 1349-1367.

1-12. Reid, A. M.; Warner, J. L.; Ridley, W. I.; and Brown, R. W.: Major Element Composition of Glasses in Three Apollo 15 Soils. Meteoritics, vol. 7, Sept. 30, 1972, pp. 395-415.

1-13. Carter, J. L.: Morphology and Chemistry of Probable VLS (Vapor-Liquid-Solid)-Type of Whisker Structures and Other Features on the Surface of Breccia 15015,36. Proceedings of the Fourth Lunar Science Conference, vol. 1, Pergamon Press. (New York), 1973, pp. 413-421.

1-14. Ridley, W. I.; Reid, A. M.; Warner, J. L.; and Brown, R. W.: Apollo 15 Green Glasses. Phys. Earth and Planet. Interiors, vol. 7, 1973, pp. 133-136.

1-15. Agrell, S. O.; Agrell, J. E.; Arnold, A. R.; and Bristol, C. C.: Observations on Glass From 15425, 15426, 15427. (Abs. of papers presented at the Fourth Lunar Science Conference (Houston, Tex.), Mar. 5-8, 1973), pp. 12-14.

1-16. Brown, G. M.; Emeleus, C. H.; et al.: Mineral-Chemical Variations in Apollo 14 and Apollo 15 Basalts and Granitic Fractions. Proceedings of the Third Lunar

Science Conference, vol. 1, MIT Press (Cambridge, Mass.), 1972, pp. 141-157.

1-17. Bence, A. E.; and Papike, J. J.: Pyroxenes as Recorders of Lunar Basalt Petrogenesis: Chemical Trends Due to Crystal-Liquid Interaction. Proceedings of the Third Lunar Science Conference, vol. 1, MIT Press (Cambridge, Mass.), 1972, pp. 431-469.

1-18. Gleadow, A. J. W.; Lemaitre, R. W.; Sewell, D. K. B.; and Lovering, J. F.: Chemical Discrimination of Petrographically Defined Clast Groups in Apollo 14 and 15 Lunar Breccias. (Abs. of papers presented at the Fourth Lunar Science Conference (Houston, Tex.) Mar. 5-8, 1973), pp. 289-291.

1-19. Swann, G. A.; Bailey, N. G.; et al.: Preliminary Geologic Investigation of the Apollo 15 Landing Site. Sec. 5 of the Apollo 15 Preliminary Science Report. NASA SP-289, 1972.

1-20. Powell, B. N.; Aitken, F. K.; and Weiblen, P. W.: Classification, Distribution and Origin of Lithic Fragments From the Hadley-Apennine Region. Proceedings of the Fourth Lunar Science Conference, vol. 1, Pergamon Press (New York), 1973, pp. 445-460.

1-21. Turner, G.; Huneke, J. C.; Podosek, F. A.; and Wasserburg, G. J.: ^{40}Ar-^{39}Ar Ages and Cosmic Ray Exposure Ages of Apollo 14 Samples. Earth Planet. Sci. Letters, vol. 12, 1971, pp. 19-35.

1-22. Turner, Grenville: ^{40}Ar-^{39}Ar Ages From the Lunar Maria. Earth Planet. Sci. Letters, vol. 11, 1971, pp. 169-191.

1-23. Alexander, E. C., Jr.; Davis, P. K.; and Lewis, R. S.: Argon 40-Argon 39 Dating of Apollo Sample 15555. Science, vol. 175, no. 4020, 1972, pp. 417-419.

1-24. Husain, L.; Schaeffer, O. A.; Funkhouser, J.; and Sutter, J.: The Ages of Lunar Material From Fra Mauro, Hadley Rille and Spur Crater. Proceedings of the Third Lunar Science Conference, vol. 2, MIT Press (Cambridge, Mass.), 1972, pp. 1557-1568.

1-25. Podosek, F. A.; Huneke, J. C.; and Wasserburg, G. J.: Gas-Retention and Cosmic-Ray Exposure Ages of Lunar Rock 15555. Science, vol. 175, no. 4020, 1972, pp. 423-425.

1-26. York, Derek; Kenyon, W. John; and Doyle, Roy J.: ^{40}Ar-^{39}Ar Ages of Apollo 14 and 15 Samples. Proceedings of the Third Lunar Science Conference, vol. 2, MIT Press (Cambridge, Mass.), 1972, pp. 1613-1622.

1-27. Dran, J. C.; Duraud, J. P.; and Maurette, M.: Low Energy Solar Nuclear Particle Irradiation of Lunar and Meteoritic Breccias. The Moon, Harold C. Urey and Stanley Keith Runcorn, eds., 1972, pp. 309.

1-28. Dran, J. C.; Duraud, J. P.; et al.: Track Metamorphism in Extraterrestrial Breccias. Proceedings of the Third Lunar Science Conference, vol. 3, MIT Press (Cambridge, Mass.), 1972, pp. 2883-2903.

1-29. Warner, Jeffrey L.: Metamorphism of Apollo 14 Breccias. Proceedings of the Third Lunar Science Conference, vol. 1, MIT Press (Cambridge, Mass.), 1972, pp. 623-643.

1-30. Bogard, D. D.; Funkhouser, J. G.; Schaeffer, O. A.; and Zähringer, J.: Noble Gas Abundances in Lunar Material – Cosmic Ray Spallation Products and Radiation Ages From the Sea of Tranquility and the Ocean of Storms. J. Geophys. Res., vol. 76, no. 11, 1971, pp. 2757-2779.

1-31. Weber, H.: Bestrahlungsalter und radiogene Edelgasalter von Mondmaterial. Thesis, Univ. of Mainz, 1973.

1-32. Huneke, J. C.; Nyquist, L. E.; et al.: The Thermal Release of Rare Gases From Separated Minerals of the Mocs Meteorite. Meteorite Research, P. Millman, ed., D. Reidel Publ. Co. (Dordrecht, Holland), 1969, pp. 901-921.

1-33. Frick, U.; Baur, H.; et al.: Diffusion Properties of Light Noble Gases in Lunar Fines. Proceedings of the Fourth Lunar Science Conference, vol. 2, Pergamon Press (New York), 1973, pp. 1987-2002.

1-34. Moore, C. B.; Lewis, C. F.; et al.: Total Carbon, Nitrogen and Sulphur in Apollo 14 Lunar Samples. Proceedings of the Third Lunar Science Conference, vol. 2, MIT Press (Cambridge, Mass.), 1972, pp. 2051-2058.

1-35. Chang, S.; Smith, J.; et al.: Carbon, Nitrogen and Sulfur Release During Pyrolysis of Bulk Apollo 15 Fines. The Apollo 15 Lunar Samples, Lunar Science Institute (Houston, Tex.), 1972, pp. 291-293.

1-36. Kothari, B. K.; and Goel, P. S.: Total Nitrogen Abundances in Five Apollo-15 Samples (Hadley-Apennine Region) by Neutron Activation Analysis. The Apollo 15 Lunar Samples, Lunar Science Institute (Houston, Tex.), 1972, pp. 282-283.

1-37. Eglinton, G.; Mays, B. J.; et al.: The European Consortium: The History of Lunar Breccia 14267. Proceedings of the Fifth Lunar Science Conference, vol. 2, Pergamon Press (New York), 1974, pp. 1159-1180.

1-38. Cadogan, P. H.; Eglinton, G.; Maxwell, J. R.; and Pillinger, C. T.: Distribution of Methane and Carbide in Apollo 11 Fines. Nature Phys. Sci., vol. 241, 1972, pp. 81-82.

1-39. Cadogan, P. H.; Eglinton, G.; et al.: Location of Methane and Carbide in Apollo 11 and 16 Lunar Fines. Proceedings of the Fourth Lunar Science Conference, vol. 2, Pergamon Press (New York), 1973, pp. 1493-1508.

1-40. Billetop, M. C. J.; Eglinton, G.; et al.: Pyrolysis-Acid Dissolution Studies of Lunar Carbon Chemistry. (Abs. of papers presented at the Seventh Lunar Science Conference (Houston, Tex.), Mar. 15-19, 1976), pp. 61-63.

1-41. Modzeleski, Judith E.; Modzeleski, Vincent E.; et al.: Types of Carbon Compounds Examined in Apollo 16 Lunar Samples by Vacuum Pyrolysis-Mass Spectrometry and by Photoelectron Spectroscopy. (Abs. of papers presented at the Fourth Lunar Science Conference (Houston, Tex.), Mar. 5-8, 1973), pp. 531-533.

2. Composition of Lunar Basalts 10069, 10071, and 12008

E. Jarosewich[a] and Brian Mason[a]

Chemical analyses, Cross-Iddings-Pirsson-Washington norms, and mineralogical and petrographical data are presented for lunar basalts 10069 and 10071 (from the Apollo 11 mission) and 12008 (from the Apollo 12 mission).

As part of the program for filling gaps in the analytical base for some of the early Apollo missions, samples of basaltic rocks 10069, 10071, and 12008, collected during the Apollo 11 and 12 missions, were allocated for analysis. The results are reported in table 2-I with their Cross-Iddings-Pirsson-Washington (CIPW) norms.

DISCUSSION

Approximately 0.5 g of sample was taken for each chemical analysis. Silica, magnesia (MgO), lime (CaO), total iron (Fe) as ferrous oxide (FeO), titania (TiO_2), and manganese oxide (MnO) were determined by using the general procedure for silicate analysis (ref. 2-1). Aluminum (Al) was determined gravimetrically by precipitation with 8-hydroxyquinoline on an aliquot from the R_2O_3 solution after removal of interfering ions by means of the mercury electrode. Sodium (Na) and potassium (K) were determined by flame photometry; and phosphorus (P) and chromium (Cr) were determined colorimetrically with molybdenum blue (ref. 2-2) and diphenyl carbazide

[a]Smithsonian Institution.

TABLE 2-I.- CHEMICAL ANALYSES AND CIPW NORMS OF LUNAR BASALTS[a]

Compound or mineral (b)	Sample no.		
	10069	10071	12008
Compound abundance, wt.%			
SiO_2	40.41	40.47	42.58
TiO_2	11.97	12.31	4.82
Al_2O_3	8.22	8.08	8.49
Cr_2O_3	.36	.33	.53
FeO	19.76	19.79	22.40
MnO	.27	.26	.28
MgO	7.75	7.56	11.99
CaO	10.50	10.63	9.10
Na_2O	.55	.54	.24
K_2O	.31	.32	.14
P_2O_5	.21	.18	.05
Total	100.31	100.47	100.62
CIPW norm, wt.%			
Quartz	2.08	2.28	--
Orthoclase	1.84	1.89	.83
Albite	4.66	4.56	2.04
Anorthite	18.94	18.63	21.65
Diopside	26.09	27.08	19.26
Hypersthene	22.61	21.69	27.73
Olivine	--	--	19.02
Chromite	.53	.49	.78
Ilmenite	22.70	23.30	9.13
Apatite	.50	.44	.10
Fem[c]	.40	.40	.46

[a]E. Jarosewich, analyst.

[b]SiO_2 = silica, Al_2O_3 = alumina, Cr_2O_3 = chromic oxide, Na_2O = soda, K_2O = potash, and P_2O_5 = phosphorus pentoxide.

[c]Fem = FeO/FeO+MgO mole ratio in normative silicates.

(ref. 2-3), respectively. Summations are somewhat greater than 100.00; this feature has been noted by other analysts of lunar rocks. Some of this excess can be ascribed to the presence of metallic Fe, whereas all Fe is reported as FeO. It is possible that titanium (Ti) and Cr may be present in lower valence states than reported. It was noted that ignition of the samples in air results in a weight gain, which is evidently the result of combination with oxygen (O). To economize on the consumption of material, sulfur (S) was not determined. Similar Apollo 11 rocks average 0.2 percent S, and 12051, a rock similar to 12008, contains 0.09 percent S (ref. 2-4).

ROCK SAMPLES 10069, 10071

Schmitt et al. (ref. 2-5) describe 10069 as a 120-g specimen of very fine grained, vuggy to vesicular, glass-bearing granular basalt aggregate (type A), and 10071 as a 195-g specimen of fine-grained, vesicular to vuggy, glass-bearing plumose basalt aggregate (type AB). Basically, these are hand-specimen descriptions. James and Jackson (ref. 2-6) have provided more detailed descriptions based on thin-section examinations. They classify both rocks as intersertal basalts – 10069 as a very fine grained hornfels, and 10071 as unmetamorphosed. Their modal analysis of 10069 by volume percentage is pyroxene, 54.3; plagioclase, 22.4; ilmenite, 14.9; troilite, 0.9; cristobalite, 4.1; myrmekite and residual glass, 3.2; and apatite, 0.2. For 10071, the modal analysis is olivine, 1.7; pyroxene, 51.5; plagioclase, 20.6; ilmenite, 16.8; armalcolite, trace; troilite, 0.1; cristobalite, 2.8; myrmekite and residual glass, 6.2; apatite, trace; and others, 0.1. The chemical analyses (table 2-I) show that the two rocks are essentially identical in composition. The potash (K_2O) content shows that the rocks belong to the high K, rubidium (Rb), zirconium (Zr), barium (Ba), cerium (Ce), thorium (Th), uranium (U) geochemical group of the Apollo 11 basalts (ref. 2-7, p. 120). A noteworthy feature is the presence of quartz in the norms and cristobalite in the modes despite the low silicon dioxide (SiO_2) content. This feature is related to the high TiO_2 content, which combines with much of the FeO as ilmenite.

A considerable amount of chemical data has been published concerning these two rocks. Major element data for 10069 are given by Ehmann and Morgan (ref. 2-8), Goles et al. (ref. 2-9), and Tera et al. (2-10). Minor and trace element data are provided by Goles et al. (ref. 2-9), Tera et al. (ref. 2-10), Annell and Helz (ref. 2-11), Murthy et al. (ref. 2-12), and Lovering and Butterfield (ref. 2-13).

Major element data for 10071 are given by Ehmann and Morgan (ref. 2-8) and Goles et al. (ref. 2-9); minor and trace element data, by Goles et al. (ref. 2-9), Annell and Helz (ref. 2-11), Gast et al. (ref. 2-14), and Tatsumoto (ref. 2-15). These data are compiled in tables 2-II and 2-III. For sample 10069, marked discrepancies exist between the data of the authors of this paper and those of Ehmann and Morgan, and Goles et al. for O, magnesium (Mg), Al, and Fe. In all instances, the authors' measurements are greater than those obtained by instrumental neutron activation analysis by the other investigators. The authors believe their data are to be preferred, because they alone provide a summation close to 100 percent. The large discrepancy between the oxygen data seems certainly to be due to an error in the instrumental analysis, because Ehmann and Morgan record 40.3 percent O in 10071, a rock essentially identical to 10069. Agreement between the authors' measurements and those of other investigators for 10071 is good to excellent.

ROCK SAMPLE 12008

Rock 12008 is a 58-g specimen collected along the traverse route between the lunar module and Middle Crescent crater during the first extravehicular activity on the Apollo 12 mission. Warner (ref. 2-16) classifies rock 12008 along with 12009 and 12015 as type I of the group I lunar basalts. These are porphyritic basalts with skeletal and euhedral olivine phenocrysts in a dark, glassy matrix and have been described as olivine vitrophyres. A polished thin section (fig. 2-1) provided with the analyzed sample shows equant and prismatic olivine phenocrysts (0.1 to 0.2 mm in cross section, up to 0.6 mm long) in a black, opaque groundmass that contains dendritic skeletal olivine crystals (up to 1 mm long, but only 0.03 mm across) and some red-brown titanaugite with a feathery texture suggesting formation by devitrification. The rock contains 21 volume percent olivine phenocrysts, determined by point counting. The compositions of the interiors of the olivine phenocrysts range from 28 to

TABLE 2-II- ELEMENTAL ABUNDANCES IN LUNAR BASALT 10069

Element	Abundance as determined by –						
	Jarosewich and Mason	Ehmann and Morgan (ref. 2-8)	Goles et al. (ref. 2-9)	Tera et al. (ref. 2-10)	Annell and Helz (ref. 2-11)	Murthy et al. (ref. 2-12)	Lovering and Butterfield (ref. 2-13)
Lithium, ppm	--	--	--	17.2	18	--	--
Beryllium, ppm	--	--	--	--	3.3	--	--
Boron, ppm	--	--	--	--	<10	--	--
Oxygen, percent	40.83	37.6	--	--	--	--	--
Sodium, ppm	4100	--	3650	3400	--	--	--
Magnesium, percent	4.67	--	3.7	--	--	--	--
Aluminum, percent	4.35	3.7	3.8	--	--	--	--
Silicon, percent	18.89	18.3	18.3	--	--	--	--
Phosphorus, ppm	900	--	--	--	<2000	--	--
Potassium, ppm	2600	--	--	2438	--	2295	--
Calcium, percent	7.50	--	7.1	7.20	--	--	--
Scandium, ppm	--	--	72.4	--	94	--	--
Titanium, percent	7.18	--	7.2	--	--	--	--
Vanadium, ppm	--	--	87	--	72	--	--
Chromium, ppm	2500	--	2130	--	2760	--	--
Manganese, ppm	2100	--	1600	--	2390	--	--
Iron, percent	15.36	--	14.1	--	--	--	--
Cobalt, ppm	--	--	26.0	--	30	--	--
Nickel, ppm	--	--	--	--	6.7	--	--
Copper, ppm	--	--	12	--	8.7	--	--
Zinc, ppm	--	--	--	--	<4	--	--
Gallium, ppm	--	--	--	--	4.9	--	--
Germanium, ppm	--	--	--	--	<1	--	--
Arsenic, ppm	--	--	--	--	<4	--	--
Rubidium, ppm	--	--	--	5.70	5.5	5.60	--
Strontium, ppm	--	--	--	155.6	130	165	--
Yttrium, ppm	--	--	--	--	164	--	--
Zirconium, ppm	--	--	520	--	566	--	--
Niobium, ppm	--	--	--	--	20	--	--
Molybdenum, ppm	--	--	--	--	<2	--	--
Silver, ppm	--	--	--	--	<.2	--	--
Cadmium, ppm	--	--	--	--	<8	--	--
Indium, ppm	--	--	--	--	<1	--	--
Tin, ppm	--	--	--	--	<10	--	--
Antimony, ppm	--	--	--	--	<100	--	--
Tellurium, ppm	--	--	--	--	<300	--	--
Cesium, ppm	--	--	--	.163	<1	--	--
Barium, ppm	--	--	250	288	420	277	--
Lanthanum, ppm	--	--	23.7	--	27	--	--
Cerium, ppm	--	--	65	--	<100	--	--
Neodymium, ppm	--	--	--	--	<100	--	--
Samarium, ppm	--	--	18.0	--	--	--	--
Europium,ppm	--	--	2.04	--	--	--	--
Terbium, ppm	--	--	4.8	--	--	--	--
Holmium, ppm	--	--	6.9	--	--	--	--
Ytterbium, ppm	--	--	20.8	--	--	--	--
Lutetium, ppm	--	--	2.67	--	--	--	--
Hafnium, ppm	--	--	17.8	--	<20	--	--
Tantalum, ppm	--	--	2.7	--	<100	--	--
Tungsten, ppm	--	--	--	--	<200	--	--
Rhenium, ppm	--	--	--	--	<30	--	[a]1.18
Osmium, ppb	--	--	--	--	--	--	[a].897
Platinum, ppm	--	--	--	--	<3	--	--
Gold, ppm	--	--	--	--	<.2	--	--
Mercury, ppm	--	--	--	--	<8	--	--
Thallium, ppm	--	--	--	--	<1	--	--
Lead, ppm	--	--	--	--	<1	--	--
Bismuth, ppm	--	--	--	--	<1	--	--
Thorium, ppm	--	--	--	--	<100	--	--
Uranium, ppm	--	--	.78	--	<500	--	--

[a]In ppb.

TABLE 2-III.- ELEMENTAL ABUNDANCES IN LUNAR BASALT 10071

Element	Abundance as determined by –					
	Jarosewich and Mason	Ehmann and Morgan (ref. 2-8)	Goles et al. (ref. 2-9)	Annell and Helz (ref. 2-11)	Gast et al. (ref. 2-14)	Tatsumoto (ref. 2-15)
Lithium, ppm	--	--	--	17	--	--
Beryllium, ppm	--	--	--	3.0	--	--
Boron, ppm	--	--	--	<10	--	--
Oxygen, percent	40.70	40.3	--	--	--	--
Sodium, ppm	4000	--	3640	--	3900	--
Magnesium, percent	4.56	--	4.4	--	--	--
Aluminum, percent	4.28	4.2	4.5	--	--	--
Silicon, percent	18.92	19.1	19.1	--	--	--
Phosphorus, ppm	800	--	--	<2000	--	--
Potassium, ppm	2700	--	--	--	2770	--
Calcium, percent	7.60	--	7.2	--	--	--
Scandium, ppm	--	--	73.2	97	--	--
Titanium, percent	7.38	--	7.0	--	--	--
Vanadium, ppm	--	--	92	78	--	--
Chromium, ppm	2300	--	2170	3060	--	--
Manganese, ppm	2000	--	1650	2230	--	--
Iron, percent	15.38	--	14.9	--	--	--
Cobalt, ppm	--	--	27.1	33	--	--
Nickel, ppm	--	--	--	7.0	--	--
Copper, ppm	--	--	11	14	--	--
Zinc, ppm	--	--	--	<4	--	--
Gallium, ppm	--	--	--	4.8	--	--
Germanium, ppm	--	--	--	<1	--	--
Arsenic, ppm	--	--	--	<4	--	--
Rubidium, ppm	--	--	--	5.2	5.93	--
Strontium, ppm	--	--	--	140	160.9	--
Yttrium, ppm	--	--	--	162	--	--
Zirconium, ppm	--	--	210	644	--	--
Niobium, ppm	--	--	--	24	--	--
Molybdenum, ppm	--	--	--	<2	--	--
Silver, ppm	--	--	--	<.2	--	--
Cadmium, ppm	--	--	--	<8	--	--
Indium, ppm	--	--	--	<1	--	--
Tin, ppm	--	--	--	<10	--	--
Antimony, ppm	--	--	--	<100	--	--
Tellurium, ppm	--	--	--	<300	--	--
Cesium, ppm	--	--	--	<1	.170	--
Barium, ppm	--	--	450	470	327	--
Lanthanum, ppm	--	--	25.8	27	28.8	--
Cerium, ppm	--	--	84	<100	83.5	--
Neodymium, ppm	--	--	--	<100	64.5	--
Samarium, ppm	--	--	20.0	--	22.7	--
Europium, ppm	--	--	2.12	--	2.32	--
Gadolinium, ppm	--	--	--	--	29.3	--
Terbium, ppm	--	--	5.7	--	--	--
Dysprosium, ppm	--	--	--	--	33.5	--
Holmium, ppm	--	--	9.2	--	--	--
Erbium, ppm	--	--	--	--	21.3	--
Ytterbium, ppm	--	--	20.8	--	20.5	--
Lutetium, ppm	--	--	3.08	--	2.87	--
Hafnium, ppm	--	--	19.1	<20	--	--
Tantalum, ppm	--	--	2.0	<100	--	--
Tungsten, ppm	--	--	--	<200	--	--
Rhenium, ppm	--	--	--	<30	--	--
Platinum, ppm	--	--	--	<3	--	--
Gold, ppm	--	--	--	<.2	--	--
Mercury, ppm	--	--	--	<8	--	--
Thallium, ppm	--	--	--	<1	--	--
Lead, ppm	--	--	--	<1	--	1.71, 1.67
Bismuth, ppm	--	--	--	<1	--	--
Thorium, ppm	--	--	--	<100	--	3.43, 3.29
Uranium, ppm	--	--	.69	<500	--	.873, .845

Figure 2-1.- Photomicrograph (transmitted light) of a thin section of lunar basalt 12008, showing phenocrysts of olivine (maximum length 0.6 mm) in opaque groundmass.

35 mol% fayalite, with an average of 32 mol%. In reflected light, the groundmass is seen to contain occasional small euhedral chromite grains and rare minute metal particles.

The analysis of 12008 is comparable with analyses of other Apollo 12 basalts, such as 12022 (ref. 2-17), 12051 (ref. 2-4), and 12063 (ref. 2-18). The TiO_2 content (4.82 percent) is somewhat higher than many of the Apollo 12 basalts, the average for which is approximately 3 percent. The amount of normative olivine is somewhat less than the modal amount, indicating that the groundmass may be slightly oversaturated. In the classification of James and Wright (ref. 2-19), 12008 belongs in group IIA, ilmenite-bearing olivine basalts. It is evidently a quenched sample of this subordinate magma type at the Apollo 12 site.

Anders et al. (ref. 2-20) provide trace element data for 15 elements in 12008.

ACKNOWLEDGMENTS

This work has been supported by a grant (NGR 09-015-146) from the National Aeronautics and Space Administration. We thank Drs. Odette B. James and S. R. Taylor for helpful reviews of the manuscript.

REFERENCES

2-1. Peck, Lee C.: Systematic Analysis of Silicates. U.S. Geol. Survey Bull. 1170, 1964.

2-2. Boltz, David F., ed.: Colorimetric Determination of Nonmetals. Chemical Analysis Series, vol. 8, Wiley Interscience (New York), 1958.

2-3. Sandell, Ernest B.: Colorimetric Determination of Trace Metals. Chemical Analysis Series, vol. 3, Wiley Interscience (New York), 1954.

2-4. Compston, W.; Berry, H.; et al.: Rubidium-Strontium Chronology and Chemistry of Lunar Material From the Ocean of Storms. Proceedings of the Second Lunar Science Conference, vol. 2, MIT Press (Cambridge, Mass.), 1971, pp. 1471-1485.

2-5. Schmitt, H. H.; Lofgren, G; Swann, G. A.; and Simmons, G.: The Apollo 11 Samples: Introduction. Proceedings of the Apollo 11 Lunar Science Conference, vol. 1, Pergamon Press (New York), 1970, pp. 1-54.

2-6. James, Odette B.; and Jackson, Everett D.: Petrology of the Apollo 11 Ilmenite Basalts. J. Geophys. Res., vol. 75, no. 29, 1970, pp. 5793-5824.

2-7. Mason, Brian; and Melson, William G.: The Lunar Rocks. Wiley Interscience (New York), 1970.

2-8. Ehmann, W. D.; and Morgan, J. W.: Oxygen, Silicon and Aluminum in Apollo 11 Rocks and Fines by 14 MeV Neutron Activation. Proceedings of the Apollo 11 Lunar Science Conference, vol. 2, Pergamon Press (New York), 1970, pp 1071-1079.

2-9. Goles, G. G.; Randle K.; et al.: Elemental Abundances by Instrumental Activation Analyses in Chips From 27 Lunar Rocks. Proceedings of the Apollo 11 Lunar Science Conference, vol. 2, Pergamon Press (New York), 1970, pp. 1165-1176.

2-10. Tera, F.; Eugster, O.; Burnett, D. S.; and Wasserburg, G. J.: Comparative Study of Li, Na, K, Rb, Cs, Ca, Sr, and Ba Abundances in Achondrites and in Apollo 11 Lunar Samples. Proceedings of the Apollo 11 Lunar Science Conference, vol. 2, Pergamon Press (New York), 1970, pp. 1637-1658.

2-11. Annell, C. S.; and Helz, A. W.: Emission Spectrographic Determination of Trace Elements in Lunar Samples from Apollo 11. Proceedings of the Apollo 11 Lunar Science Conference, vol. 2, Pergamon Press (New York), 1970, pp. 991-994.

2-12. Murthy, V. R.; Evensen, N. M.; and Coscio, M. R., Jr.: Distribution of K, Rb, Sr, and Ba and Rb-Sr Isotopic Relations in Apollo 11 Lunar Samples. Proceedings of the Apollo 11 Lunar Science Conference, vol. 2, Pergamon Press (New York), 1970, pp. 1393-1406.

2-13. Lovering, J. F.; and Butterfield, D.: Neutron Activation of Rhenium and Osmium in Apollo 11 Lunar Material. Proceedings of the Apollo 11 Lunar Science Conference, vol. 2, Pergamon Press (New York), 1970, pp. 1351-1356.

2-14. Gast, P. W.; Hubbard, N. J.; and Wiesmann, H.: Chemical Composition and Petrogenesis of Basalts from Tranquillity Base. Proceedings of the Apollo 11 Lunar Science Conference, vol. 2, Pergamon Press (New York), 1970, pp. 1143-1163.

2-15. Tatsumoto, M.: Age of the Moon: An Isotopic Study of U-Th-Pb Systematics of Apollo 11 Lunar Samples—II. Proceedings of the Apollo 11 Lunar Science Conference, vol. 2, Pergamon Press (New York), 1970, pp. 1595-1612.

2-16. Warner, J. L.: Lunar Crystalline Rocks: Petrology and Geology. Proceedings of the Second Lunar Science Conference, vol. 1, MIT Press (Cambridge, Mass.), 1971, pp. 469-480.

2-17. Kushiro, Ikuo; and Haramura, Hiroshi: Major Element Variation and Possible Source Materials of Apollo 12 Crystalline Rocks. Science, vol. 171, no. 3977, 1971, pp. 1235-1237.

2-18. Willis, J. P.; Ahrens, L. H.; et al.: Some Interelement Relations Between Lunar Rocks and Fines, and Stony Meteorites. Proceedings of the Second Lunar Science Conference, vol. 2, MIT Press (Cambridge, Mass.), 1971, pp. 1123-1138.

2-19. James, Odette B.; and Wright, Thomas L.: Apollo 11 and 12 Mare Basalts and Gabbros: Classification, Compositional Variations, and Possible Petrogenetic Relations. Geol. Soc. America Bull., vol. 83, no. 8, 1972, pp. 2357-2382.

2-20. Anders, E.; Ganapathy, R.; et al.: Volatile and Siderophile Elements in Lunar Rocks: Comparison With Terrestrial and Meteoritic Basalts. Proceedings of the Second Lunar Science Conference, vol. 2, MIT Press (Cambridge, Mass.), 1971, pp. 1021-1036.

3. Composition of Eight Apollo 17 Basalts

Brian Mason[a], E. Jarosewich[a], Sara Jacobson[a], and G. Thompson[b]

Chemical analyses, Cross-Iddings-Pirsson-Washington norms, and mineralogical and petrographical data are presented for eight mare basalts collected on the Apollo 17 mission. Seven of these have very similar chemical compositions but can be divided into two textural groups: medium to coarse grained (70017, 71055, 74255, 75075) and fine grained (70215, 71569, 74275). The eighth, 75035, has a distinctive chemical and mineralogical composition (lower titania, higher silica, quartz in the norm, and cristobalite in the mode), and evidently represents a different flow probably underlying the high-titanium basalts at Camelot Crater.

The authors received samples of the following Apollo 17 basalts for analysis:

1. Sample 70017: A 2957-g, coarse-grained, vuggy basalt collected close to the lunar module (LM)
2. Sample 70215: An 8110-g, dense, fine-grained, nonvesicular basalt collected approximately 50 m northeast of the LM
3 Sample 71055: A 669-g, medium-grained, very vesicular basalt collected at station 1a
4. Sample 71569: A 289-g, fine-grained basalt collected at station 1a (rake fragment)
5. Sample 74255: A 737-g, coarse-grained, vuggy basalt collected at station 4 (south rim of Shorty Crater)
6. Sample 74275: A 1493-g, dense, fine-grained basalt collected at station 4
7. Sample 75035: A 1235-g, medium-grained basalt collected at station 5 (southwest rim of Camelot Crater)
8. Sample 75075: A 1008-g, coarse-grained, vuggy basalt collected at station 5

Approximately 0.5 g of sample was taken for each of the chemical analyses listed in table 3-I. Silica (SiO_2), magnesia (MgO), lime (CaO), total iron (Fe) as ferrous oxide (FeO), titania (TiO_2), and manganese monoxide (MnO) were determined according to the general procedure for silicate analysis (ref. 3-1). Alumina (Al_2O_3) was determined gravimetrically by precipitation with 8-hydroxyquinoline on an aliquot from the R_2O_3 solution after removal of interfering ions by means of the mercury electrode. Soda (Na_2O) and potash (K_2O) were determined by flame photometry, and phosphorus (P) and chromium (Cr) were determined colorimetrically with molybdenum blue (ref. 3-2) and diphenyl carbazide (ref. 3-3), respectively. Summations often are somewhat greater than 100.00; this feature has been noted by other analysts of lunar rocks. Some of this excess can be ascribed to the presence of metallic Fe, whereas all Fe is reported as FeO. It is also possible that titanium (Ti) and Cr may be present in lower valence states than reported. Ignition of the samples in air resulted in a weight gain, evidently the result of combination with oxygen (O). To economize on the consumption of material, sulfur (S) was not determined; analyses reported by the Apollo 17 preliminary examination team (ref., 3-4) show about 0.17 percent S in the Apollo 17 basalts, which is equivalent to approximately 0.5 percent troilite.

Modal analyses were made of most of the rocks by the point-counting technique. In general, the modal analyses were in good agreement with the normative composition, which is to be expected in view of the close correspondence between normative and ob-

[a]Smithsonian Institution.

[b]Woods Hole Oceanographic Institution.

TABLE 3-I.- CHEMICAL ANALYSES AND CIPW NORMS OF APOLLO 17 BASALTS, IN ORDER OF MgO CONTENT[a]

Compound or mineral (b)	Sample no.							
	74255	74275	75075	70017	71569	71055	70215	75035
	Compound abundance, wt.%							
SiO_2	37.98	38.21	37.45	37.62	38.63	37.30	37.71	41.29
TiO_2	12.55	12.42	13.96	13.90	12.75	13.27	13.48	10.40
Al_2O_3	8.94	8.62	8.59	8.85	7.99	9.45	9.08	9.52
Cr_2O_3	.56	.55	.51	.54	.42	.40	.40	.23
FeO	18.64	18.67	19.82	19.60	20.05	20.00	20.01	18.78
MnO	.29	.27	.27	.29	.29	.26	.26	.25
MgO	10.73	10.63	9.58	9.42	8.99	8.44	8.23	6.50
CaO	10.09	10.19	9.83	9.81	10.31	10.52	10.71	13.07
Na_2O	.39	.37	.37	.41	.39	.43	.42	.46
K_2O	.08	.08	.06	.07	.07	.06	.05	.07
P_2O_5	.04	.03	.04	.04	.04	.10	.07	.05
Total	100.29	100.04	100.48	100.55	99.93	100.23	100.42	100.62
	CIPW norm, wt.%							
Quartz	--	--	--	--	.16	--	--	1.60
Orthoclase	0.47	.47	.35	.41	.41	.35	.28	.39
Albite	3.30	3.13	3.13	3.47	3.30	3.64	3.51	3.88
Anorthite	22.41	21.62	21.60	22.10	19.85	23.68	22.71	23.60
Diopside	22.19	23.29	21.86	21.37	25.40	22.80	24.52	33.91
Hypersthene	20.97	21.98	24.97	25.19	25.89	20.86	22.61	16.94
Olivine	6.21	5.08	1.21	.72	--	2.88	.37	--
Chromite	.82	.81	.75	.80	.62	.59	.59	.34
Ilmenite	23.84	23.59	26.51	26.40	24.22	25.20	25.50	19.80
Apatite	.09	.07	.09	.09	.09	.23	.17	.10
Fem[c]	.28	.28	.30	.30	.35	.35	.35	.45

[a] E. Jarosewich, analyst.

[b] SiO_2 = silica, TiO_2 = titania, Al_2O_3 = alumina, Cr_2O_3 = chromic oxide, FeO = ferrous oxide, MnO = manganese monoxide, MgO = magnesia, CaO = lime, Na_2O = soda, K_2O = potash, P_2O_5 = phosphorus pentoxide.

[c] Fem = FeO/FeO+MgO mole ratio in normative silicates.

served mineralogy. Modal pyroxene is a few percent higher than normative pyroxene, because of the incorporation of minor amounts of Al_2O_3 and TiO_2; and, because not all Al_2O_3 is combined as plagioclase, the modal amount of the latter is slightly less than the normative amount. When olivine is present in the norm, even in amounts less than 1 percent, it is seen in thin sections. It is also present as small phenocrysts in 71569, although the analysis is slightly quartz-normative; interstitial cristobalite (or tridymite) was detected in the groundmass with the microprobe. Cristobalite is a prominent accessory in 75035, amounting to about 5 percent, although only 1.6 percent quartz is in the norm; the additional SiO_2 is evidently provided by substitution of aluminum (Al) for silicon (Si) in pyroxene.

Trace element determinations on aliquots of the analyzed samples are reported in table 3-II. The technique used is described by Thompson and Bankston (ref. 3-5). Trace element variations within these basalts are not great, which is consistent with the limited range in the major element composition. Compared to data on Apollo 15 basalts (ref. 3-6), the Apollo 17 basalts have lower Cr, cobalt (Co), and nickel (Ni) and higher gallium (Ga), strontium (Sr), vanadium (V), and zirconium (Zr). The higher V can probably be correlated with the high Ti content of the Apollo 17 rocks.

TABLE 3-II.- TRACE ELEMENT ANALYSES OF APOLLO 17 BASALTS[a]

Element	Sample no.							
	74255	74275	75075	70017	71569	71055	70215	75035
	Abundance, ppm							
Barium	130	100	45	45	80	50	55	150
Lead	10	6	--	--	18	--	--	3
Strontium	275	190	120	140	145	130	130	295
Yttrium	135	135	--	--	145	--	--	155
Zirconium	125	145	320	235	175	240	240	220
Nickel	19	33	20	20	25	28	11	22
Cobalt	12	13	16	23	5	27	21	8
Zinc	<2	<2	5	4	4	5	6	<2
Copper	9	7	30	17	8	25	16	7
Lithium	9	9	9	10	10	13	10	12
Chromium	>2000	>2000	3100	2950	>2000	2950	3050	1500
Vanadium	240	270	290	260	280	315	320	140
Gallium	13	10	13	9	13	11	11	10
Boron	<2	<2	1	1	<2	2	3	<2

[a]G. Thompson, analyst.

PETROLOGY

Table 3-I shows that the basalts analyzed are remarkably uniform in composition, with the exception of 75035. Omitting the latter from consideration for the present, the remaining seven basalts can be clearly divided into two distinct textural groups as follows.

1. Samples 70017, 71055, 74255, and 75075 are medium- to coarse-grained basalts with ophitic to subophitic textures.

2. Samples 70215, 71569, and 74275 are fine-grained basalts with acicular ilmenite crystals and skeletal and/or subequant phenocrysts of olivine in a groundmass of plagioclase and pyroxene.

Despite the textural differences, the compositions may be essentially identical (as for 74255 and 74275), suggesting that the differences reflect different cooling histories. Other investigators have also distinquished these two groups of Apollo 17 basalts; group A corresponds to type 3 of Papike and Bence (ref. 3-7) and mare basalts III of Brown et al. (ref. 3-8), whereas group B corresponds to type 2 of Papike and Bence and mare basalts I of Brown et al. Brown et al. classify 75035 as mare basalt II, and it probably belongs to type I of Papike and Bence. It is therefore convenient to describe the petrology of the samples in terms of these three groupings.

ROCK SAMPLES 70017, 71055, 74255, AND 75075

Samples 70017, 71055, 74255, and 75075 are all medium-to coarse-grained basalts (maximum length of plagioclase crystals, 1 to 4 mm) with ophitic to subophitic textures. The principal minerals are calcic and subcalcic augite, plagioclase, and ilmenite, with minor amounts (1 to 5 percent) of olivine; some cristobalite is usually present as late crystallization. Trace constituents are armalcolite (in ilmenite), chromian ulvöspinel, troilite, and metallic Fe. Brown, silica-rich ($SiO_2 \sim 70$ percent) and potassium-rich ($K_2O \sim 5$ percent) mesostasis is present in small amounts. Plagioclase is very uniform in composition, averaging 82 mol% anorthite (An_{82}); some of the larger crystals are weakly zoned, the maximum range noted being from An_{85} (core) to An_{77} (margin). Olivine shows a

moderate range in composition 28 to 38 mol% fayalite (Fa_{28} to Fa_{38}); the olivine in 74255 is more magnesian than that in the other rocks; this correlated with the lower fem[1] value (0.28) for this rock (table 3-I). The pyroxene (fig. 3-1) is largely calcic to subcalcic augite, with minor amounts of pigeonite; the pigeonite occurs sometimes as cores to large augite crystals, and sometimes pigeonite and augite are complexly zoned with each other.

Additional information has been obtained regarding Ti and Al concentrations in the pyroxenes in 70017 and 74275. As can be seen in figure 3-2, the Ti:Al ratio (atomic) straddles the 1:2 line, indicating the presence of a $CaTiAl_2O_6$ component. The pyroxenes in 74275 are notably richer in both Ti and Al than those in 70017; this suggests later crystallization of ilmenite and plagioclase in 74275 than in 70017, whereby the pyroxene in 74275 crystallized from a magma rich in Ti and Al. A few of the pyroxenes in 70017 fall between the 1:2 and 1:1 line, suggesting that a small amount of Ti_3 (as the component $CaTiAlSiO_6$) may be present. On the other hand, the pyroxenes in 74275 plot between the 1:2 and the 1:4 line, indicating the presence of the $CaAl_2SiO_6$ component.

ROCK SAMPLES 70215, 71569, AND 74275

Samples 70215, 71569, and 74275 are basalts with microphenocrysts of olivine and acicular ilmenite in a fine-grained groundmass of augite and plagioclase. They are indistinguishable in bulk chemistry from the preceding group. The compositions of their constituent minerals are very uniform (fig. 3-3). Olivine ranges from Fa_{21} to Fa_{34}; individual crystals are sometimes zoned from magnesium-rich cores to more iron-rich margins. The pyroxene is a strongly colored reddish-brown augite of remarkably uniform composition. (Most compositions are within a field 37 to 47 mol% Wollastonite (Wo_{37} to Wo_{47}), 16 to 22 mol% ferrosilite (Fs_{16} to Fs_{22}). Plagioclase occurs as small laths in the groundmass; its composition is also very uniform, An_{77} to An_{80}. Some of the olivine includes small crystals of chromian ulvöspinel. A little tridymite or cristobalite was detected in the groundmass with the microprobe. Among these three rocks, 70215 is texturally distinctive for the presence of long (up to 2 mm) skeletal olivine crystals.

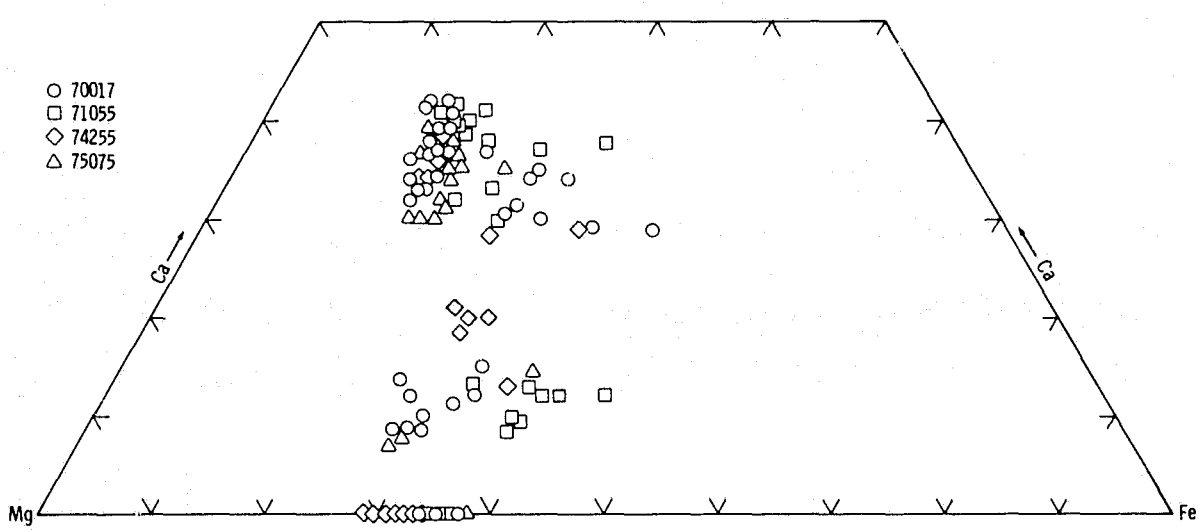

Figure 3-1.- Composition of olivine and pyroxenes in mare basalts 70017, 71055, and 75075.

[1]Fem = FeO/FeO+MgO mole ratio in normative solicates.

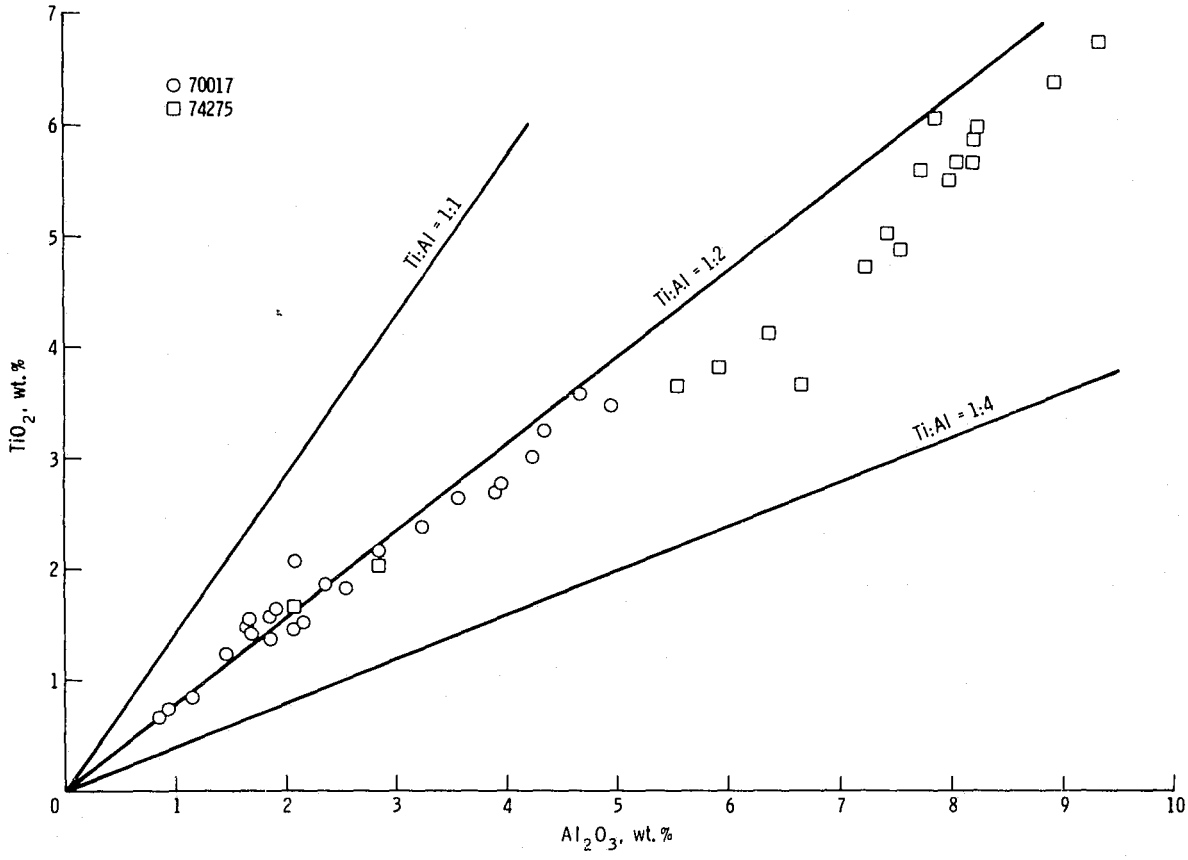

Figure 3-2.- TiO_2 and Al_2O_3 content of clinopyroxenes in mare basalts 70017 and 74275.

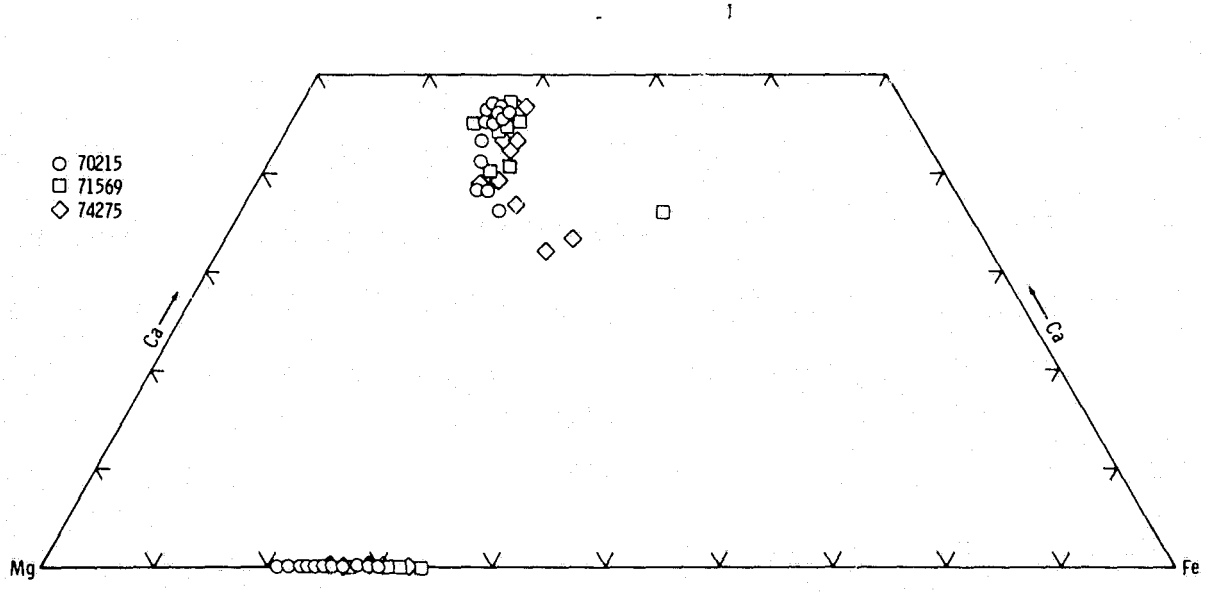

Figure 3-3.- Composition of olivine and pyroxenes in mare basalts 70215, 71569, and 74275.

ROCK SAMPLE 75035

Rock 75035 is a medium-grained (augite grains up to 0.6 mm across, plagioclase laths up to 1.5 mm long), ophitic, vesicular basalt from the southwest rim of Camelot Crater near the center of the Taurus-Littrow valley. The primary assemblage is strongly zoned calcic to subcalcic augite (fig. 3-4), plagioclase (unzoned to weakly zoned, ranging in composition from An_{86} in the centers of large crystals to An_{77} at their margins), and ilmenite in lathy to blocky crystals. Olivine is absent, and cristobalite is a prominent accessory (~5 percent). The pyroxenes are zoned toward increasing Fe and somewhat diminishing calcium (Ca), going from cores to margins; the zoning does not appear in thin section as discrete bands but as rounded, irregular patches. Many of the pyroxene crystals are rimmed by pyroxferroite. Meyer and Boctor (ref. 3-9) give a detailed account, with analyses, of the opaque minerals in 75035; ilmenite is the major opaque mineral, but ulvöspinel, metallic Fe, troilite, tranquillityite, baddeleyite, and zirconolite are also present in small amounts.

Sample 75035 is unique among the basalts analyzed by the author. Its fem value of 0.45 (table 3-I) is considerably higher than the other basalts, and it has the lowest TiO_2 and MgO and the highest CaO contents. Its mineralogy is notable for the absence of olivine, the presence of appreciable cristobalite, and the presence of pyroxferroite. All these features suggest a more strongly fractionated magma as the source material.

DISCUSSION

Papike and Bence (ref. 3-7) comment that their type 2 and type 3 basalts, equivalent respectively to the B and A groups of this paper, have essentially identical chemistry and could represent different cooling histories in the same basalt flow. This observation is certainly true for 74255 and 74275, as can be seen from tables 3-I and 3-II. All the major elements and most of the minor elements are identical within the range of probable error. The only exceptions are Ni (19 and 33 ppm) and Sr (275 and 190 ppm); the Ni values are probably controlled by the erratic occurrence of minute metal particles, but the cause for the variation in Sr is not obvious. If the Sr variation is dismissed as a chance artifact, then 74255 and 74275 may well be parts of the same flow, 74275 representing a rapidly crystallized marginal phase. These two rocks were collected close together on the rim of Shorty Crater.

The remaining rocks of groups A and B (70017, 70215, 71055, 71569, and 75075) were collected either at, or within approximately 1 km of, the LM, in the central part of the Taurus-Littrow valley. They show some range in major element chemistry, the

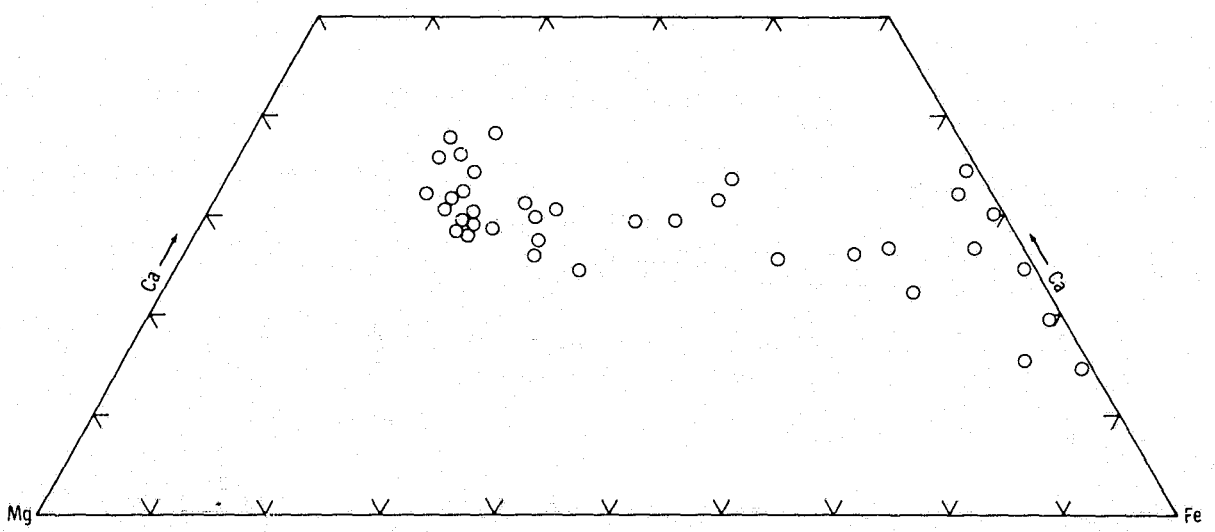

Figure 3-4.- Composition of pyroxenes and pyroxferroite in mare basalt 75035.

principal variable being MgO (9.58 to 8.23 percent), resulting in fem values from 0.30 to 0.35. Most of the trace elements are relatively uniform throughout, exceptions being Co (5 to 27 ppm), copper (Cu; 8 to 30 ppm), Ni (11 to 28 ppm), and Zr (175 to 320 ppm). The variations in these trace elements seem random and unrelated to the MgO and fem variation. Cobalt, copper, and nickel are probably concentrated in rare metal particles, and Zr, in an accessory mineral such as baddeleyite; the variation may be more apparent (affected by sampling), rather than a significant effect. All these samples could well be fragments from a single flow or a sequence of thin flows of similar composition.

Rock 75035 is clearly a basalt of distinctive composition. The only comparable rock thus far described from the Apollo 17 mission is 75055, from the same location, the analysis of which (ref. 3-4) is essentially identical. It thus appears that Camelot Crater excavated both high-titanium basalts (75075, 13.96 percent TiO_2) and low-titanium basalts (75035, 10.40 percent TiO_2). Camelot Crater is one of the largest craters in the Taurus-Littrow valley, and it may have penetrated a greater depth of the mare lava flows than the other craters visited. Such an occurrence would suggest that 75035 and 75055 are samples of a deeper, older lava than the basalts of groups A and B.

ACKNOWLEDGMENT

We are indebted to our colleagues, Drs. W. G. Melson and T. Simkin, for their constructive comments. This research has been supported by a grant (NGR 09-015-146) from the National Aeronautics and Space Administration.

REFERENCES

3-1. Peck, Lee C.: Systematic Analysis of Silicates. U.S. Geol. Survey Bull. 1170, 1964.

3-2. Boltz, David L.: Colorimetric Determination of Nonmetals. Chemical Analysis Series, vol. 8, Wiley Interscience (New York), 1958.

3-3. Sandell, Ernest B.: Colorimetric Determination of Trace Metals. Chemical Analysis Series, vol. 3, Wiley Interscience (New York), 1954.

3-4. Apollo 17 Preliminary Examination Team: Apollo 17 Lunar Samples: Chemical and Petrographic Description. Science, vol. 182, no. 4113, 1973, pp. 659-672.

3-5. Thompson, Godfrey; and Bankston, Donald C.: Technique for Trace Element Analysis of Powdered Materials Using The d.c. Arc and Photoelectric Spectrometry. Spectrochim. Acta 24, series B, vol. 24, no. 7, 1969, pp. 335-350.

3-6. Mason, Brian; Jarosewich, E.; Melson, W. G.; and Thompson, G.: Mineralogy, Petrology and Chemical Composition of Lunar Samples 15085, 15256, 15271, 15471, 15475, 15476, 15535, 15555, 15556. Proceedings of the Third Lunar Science Conference, vol. 1, MIT Press (Cambridge, Mass.), 1972, pp. 785-796.

3-7. Papike, J. J.; and Bence, A. E.: Basalts From the Taurus-Littrow Region of the Moon. (Abs. of papers submitted to the Fifth Lunar Science Conference (Houston, Tex.) Mar. 18-22, 1974), pp. 586-588.

3-8. Brown, G. M.; Peckett, A.; Emeleus, C. H.; and Phillips, R.: Mineral-Chemical Properties of Apollo 17 Mare Basalts and Terra Fragments. (Abs. of papers submitted to the Fifth Lunar Science Conference (Houston, Tex.) Mar. 18-22, 1974), pp. 89-91.

3-9. Meyer, Henry O. A.; and Boctor, Nabil Z.: Opaque Mineralogy: Apollo 17, Rock 75035. Proceedings of the Fifth Lunar Science Conference, vol. 1, 1974, pp. 707-716.

4. Troctolitic and Basaltic Clasts from a Fra Mauro Breccia

N. G. Ware[a] and D. H. Green[a]

A troctolitic clast removed from breccia 14321 is a well-equilibrated subsolidus mineral assemblage of olivine (86 mol% forsterite) and plagioclase (95 mol% anorthite) with accessory whitlockite, chrome spinel, ilmenite, armalcolite, and barian potassium-rich feldspar. This clast is a low-temperature-equilibrated example of the spinel troctolite compositional grouping and contrasts with the high-temperature, quenched mineral assemblages of most rocks in this group. Two basaltic clasts from the same breccia have affinities with rock 14053.

Lunar sample 14321 is a partly annealed but coherent clastic breccia found near the rim of Cone Crater in the Fra Mauro region; it is included in the classification of Chao, Minkin, and Best (ref. 4-1) as a "moderately annealed Fra Mauro breccia" and in the classification of Warner (ref. 4-2) as a "medium grade partly annealed breccia." Grieve et al. (ref. 4-3) have examined the petrology in detail and identify several generations of brecciation culminating in the incorporation of basaltic and other clasts, including anorthosite, in an unrecrystallized light friable matrix.

A troctolitic clast weighing 0.5 g and two basaltic fragments weighing 0.15 g each were removed from the light matrix in consortium sample 14321,88 (W. Compston, consortium leader). The rare-earth element (REE) abundances have been determined by Taylor et al. (ref. 4-4): the basaltic clasts are enriched by factors of 100 to 50 (lanthanum to ytterbium (La/Yb)) relative to chondrites with a moderate negative europium anomaly, and the troctolite is enriched by corresponding factors of 50 to 12 (La/Yb) with a positive europium anomaly. Compston et al. (ref. 4-5) report rubidium to strontium (Rb/Sr) mineral ages of 4.08 ± 0.1 and 4.05 ± 0.08 billion years (b.y.) for the basalts and 3.74 ± 0.17 b.y. for the troctolite.

[a]Research School of Earth Sciences, Australian National University.

TECHNIQUES

A 5- by 4-mm polished thin section and a 0.05-g fused glass bead were made from the troctolite fragment. After using the small basaltic clasts for Rb/Sr mineral age determination and for spark source mass spectrography, insufficient material remained for preparation of thin sections; therefore, electron-probe analysis was performed on selected grains from mineral separates.

All electron-probe analyses reported herein were performed using an Applied Research Laboratories EMX microanalyzer and techniques described by Lovering and Ware (ref. 4-6). Measurements also were made using a Technisch Physische Dienst microprobe fitted with a silicon (lithium-activated) detector (ref. 4-7); these additional data confirmed the earlier conventional probe analyses.

TROCTOLITE CLAST 8A

The Cross-Iddings-Pirsson-Washington (CIPW) norm calculated from the electron-probe analysis of the fused glass bead from troctolite clast 8A of sample 14321,88 is given in table 4-I. The CIPW norm is in good agreement with the observed mineralogy in

TABLE 4-I.- COMPARISON OF TROCTOLITE CLAST 8A AND AVERAGE SPINEL TROCTOLITE[a]

Compound or mineral	Troctolite clast 8A	Spinel troctolite
Compound abundance, wt.%		
Silicon dioxide (SiO_2)	43.50	43.7
Titanium dioxide (TiO_2)	.19	.17
Aluminum oxide (Al_2O_3)	23.29	22.7
Iron oxide (FeO)	4.56	4.9
Manganese oxide (MnO)	.06	.07
Magnesium oxide (MgO)	15.82	14.7
Calcium oxide (CaO)	12.27	13.1
Sodium oxide (Na_2O)	.28	.39
Potassium oxide (K_2O)	.06	.05
Chromium oxide (Cr_2O_3)	.03	.11
Phosphorus pentoxide (P_2O_5)	--	.04
Total	100.06	99.93
CIPW norm, wt.%		
Corundum	0.5	0
Orthoclase	.4	.3
Albite	2.4	3.4
Anorthite	60.8	58.1
Olivine	29.7	31.2
Diopside	0	3.6
Hypersthene	5.9	3.0
Ilmenite	.4	.3
Chromite	.04	.1

[a]Spinel troctolite of Prinz et al. (ref. 4-8).

the thin section, which contains approximately 35 percent olivine (86 mol% forsterite (Fo_{86}), table 4-II) set in plagioclase (95 mol% anorthite (An_{95}), table 4-III). Whitlockite (table 4-IV), which constitutes approximately 1 percent by volume and occurs in groups of 50-μm euhedral grains within the plagioclase, is the main accessory phase. Lesser amounts of ilmenite and aluminous chrome spinel are distributed randomly throughout the clast, and three grains of armalcolite were found associated with ilmenite (fig. 4-1, table 4-V). A few 40-μm anhedral grains within plagioclase were identified as barian potassium-rich feldspar (K-feldspar) (table 4-III).

The plagioclase, the whitlockite, and the ilmenite are remarkably homogeneous and unzoned, and the compositional scatter in the

TABLE 4-II.- OLIVINE ANALYSES

Compound, element, or mineral	Basalt clasts		Troctolite and basalt fusion crust		
	4A	6A	Clast 8A	Glassy basaltic fragment	Contact zone rim[a]
Compound abundance, wt.%					
SiO_2	36.05	37.05	40.06	35.29	35.39
FeO	36.23	29.63	12.89	35.86	37.20
MnO	.28	.31	.13	.27	.33
MgO	27.52	32.73	46.39	28.52	26.54
CaO	.15	.14	.03	<.02	.17
Cr_2O_3	.20	.22	<.03	<.03	<.03
Total	100.43	100.08	99.50	99.94	99.63
No. grains	1	7	14	1	3
Molecular proportion[b]					
Si	1.001	0.999	1.000	0.985	0.998
Fe	.841	.668	.269	.837	.877
Mn	.007	.007	.003	.006	.008
Mg	1.139	1.316	1.727	1.187	1.115
Ca	.005	.004	.001	.0	.005
Cr	.004	.005	.0	.0	.0
Mineral abundance, mol%					
Total Fo	57.5	66.3	86.5	58.6	56.0
Max. Fo	--	68.0	87.1	--	--
Min. Fo	--	63.9	85.1	--	--

[a]Analysis at rim to glass.

[b]On the basis of four oxygen ions.

spinel analyses is considerably less than that found in aluminous lunar chromites from other rocks. A small but significant compositional scatter of olivine is evident, but zoning was not observed within individual grains excepting those, described later, at the edge of the clast.

The presence of magnesian armalcolite is unusual; this mineral is usually formed as a liquidus phase in titanium-rich magmas, and any associated chrome spinel has a very high titanium content reflecting the concentration in the liquid. For example, the primary spinel in the armalcolite-bearing rock 70035 contains as much as 23 percent titanium dioxide (TiO_2). The olivine (86 mol% magnesium (Mg_{86})), armalcolite ($Mg_{61.5}$), spinel (Mg_{53}), and ilmenite ($Mg_{37.5}$) association in the troctolite is a subsolidus-equilibrated assemblage that is believed by the authors to be unique among the anorthosite and troctolite samples investigated.

TABLE 4-III.- FELDSPAR ANALYSES

Compound, element, or mineral	Basalt clasts		Troctolite clast 8A		Glassy basaltic fragment
	4A	6A	Plagioclase	K-feldspar	
			Compound abundance, wt.%		
SiO_2	47.24	46.87	44.91	63.01	47.87
Al_2O_3	33.14	33.55	34.94	19.98	32.40
FeO	.49	.45	.07	<.03	.53
MgO	.18	.19	.04	<.03	.49
CaO	17.54	17.71	19.20	.45	17.02
SrO	<.04	<.04	<.04	.04	<.04
BaO[a]	<.04	<.04	<.04	3.00	<.04
Na_2O	1.14	1.13	.45	.45	1.63
K_2O	.15	.13	.08	13.15	.29
Total	99.88	100.03	99.69	100.08	100.23
No. grains	23	10	15	3	1
			Molecular proportion[b]		
Si	8.701	8.267	8.318	11.733	8.794
Al	7.194	7.278	7.627	4.385	7.015
Fe	.076	.069	.011	.0	.081
Mg	.049	.052	.011	.0	.134
Ca	3.461	3.492	3.810	.090	3.350
Sr	.0	.0	.0	.004	.0
Ba	.0	.0	.0	.219	.0
Na	.407	.403	.162	.163	.581
K	.035	.031	.019	3.124	.068
Total	19.923	19.592	19.958	19.718	20.023
			Mineral abundance, mol%		
Total An	88.7	88.9	95.5	2.5	83.8
Total Or[c]	.9	.8	.5	86.9	1.7
Max. An	91.8	93.4	95.7	--	--
Min. An	80.0	85.0	95.0	--	--

[a]BaO = barium oxide.

[b]On the basis of 32 oxygen ions.

[c]Or = orthoclase.

TABLE 4-IV.- WHITLOCKITE IN TROCTOLITE CLAST[a]

Compound or element	Abundance, wt.%
Primary detections	
P_2O_5	44.50
SiO_2	.23
TiO_2	.04
Al_2O_3	.32
FeO	.52
MnO	.04
MgO	3.47
CaO	42.13
Na_2O	.31
K_2O	.03
Y_2O_3[b]	2.52
Cl[b]	.02
Total	94.13
Additional detections[c]	
Cerium oxide (Ce_2O_3)	2.0
Neodymium oxide (Nd_2O_3)	1.5
Gadolinium oxide (Gd_2O_3)	.5
Dysprosium oxide (Dy_2O_3)	.5
Erbium oxide (Er_2O_3)	.5
Lanthanum oxide (La_2O_3)	.8

[a]Mean of six analyses.

[b]Y_2O_3 = yttrium oxide, Cl = chlorine.

[c]Approximate values.

Gooley et al. (ref. 4-9) describe a troctolite of similar bulk composition, having slightly higher magnesian olivine content (Fo_{88}), in which the discrete spinel grains are compositionally variable with lower TiO_2 and aluminum oxide (Al_2O_3), higher chromium oxide (Cr_2O_3), and a lower magnesium value (Mg_{45}); titanium-rich phases such as ilmenite and armalcolite are absent, and whitlockite is an extremely rare accessory mineral. The symplectic intergrowth of diopside, enstatite, and spinel observed by Gooley et al. is not present in troctolite fragment 8A, and the spinel is an equilibrium phase associated with olivine and anorthite.

Roedder and Weiblen (ref. 4-10) describe a spinel troctolite fragment from Luna 20 soil samples having similar bulk composition, but the olivine in this sample is Fo_{91} and the spinel (Mg_{82}) contains 70 percent Al_2O_3 and 1.7 percent Cr_2O_3. This sample has an igneous, quenched texture. In an earlier report, Roedder and Weiblen (ref. 4-11) described a slightly shocked olivine anorthosite (sample 14303,51) containing spinel (Mg_{53}) of very similar composition to those in troctolite clast 8A with 18 percent Al_2O_3 and 46 percent Cr_2O_3, but these spinels coexist with olivine of composition Fo_{74} to Fo_{77}.

TABLE 4-V.- OPAQUE ANALYSES

Compound or element	Basalt clast 4A		Troctolite clast 8A			Glassy basaltic fragment spinel
	Spinel	Ilmenite	Spinel	Ilmenite	Armalcolite	
Compound abundance, wt.%						
SiO_2	0.14	<0.03	0.12	0.07	0.03	<0.09
TiO_2	4.28	52.98	1.96	57.16	74.13	5.50
ZrO_2[a]	--	--	<.04	<.04	.52	--
Al_2O_3	16.22	.09	25.54	.08	1.74	15.60
V_2O_3[a]	.96	<.03	.27	.03	<.05	--
Cr_2O_3	40.24	.40	41.92	.30	1.20	42.14
FeO	32.76	43.55	18.31	31.39	11.51	33.02
MnO	.30	.39	.19	.32	.03	.26
MgO	4.22	2.47	11.69	10.62	10.34	3.19
CaO	.15	.12	.13	.10	.11	.22
Total	99.27	100.00	100.13	100.07	99.61	99.93
No. grains	1	4	6	7	3	1
Molecular proportion						
O	4.000	6.000	4.000	6.000	5.000	4.000
Si	.005	0	.004	.003	.001	0
Ti	.109	1.978	.045	1.998	1.965	.139
Zr	--	--	.0	.0	.009	--
Al	.646	.005	.916	.004	.072	.620
V	.026	0	.007	.001	0	--
Cr	1.075	.016	1.009	.011	.033	1.123
Fe	.926	1.808	.466	1.220	.339	.931
Mn	.009	.016	.005	.013	.001	.007
Mg	.213	.183	.530	.734	.543	.160
Ca	.005	.006	.004	.005	.004	.008
Total cations	3.014	4.012	2.986	3.989	2.967	2.988
Ratio[b]	18.7	9.2	53.1	37.6	61.5	14.7

[a] ZrO_2 = zirconium dioxide, V_2O_3 = vanadium oxide.

[b] 100 Mg/Mg+Fe.

The large partition coefficient for Mg and iron (Fe) for coexisting olivine and spinel in sample 8A contrasts with much smaller partition coefficients in the two other "igneous" samples quoted. From this difference and from the very strongly selective partition against TiO_2 and zirconium dioxide (ZrO_2) in spinel and against ZrO_2 and Cr_2O_3 in ilmenite, the authors infer that the troctolite mineral assemblage equilibrated at comparatively low temperatures, well below the solidus but possibly above the temperature of equilibration of olivine and spinel and that of reaction between olivine and plagioclase in the troctolite described by Gooley et al. (ref. 4-9).

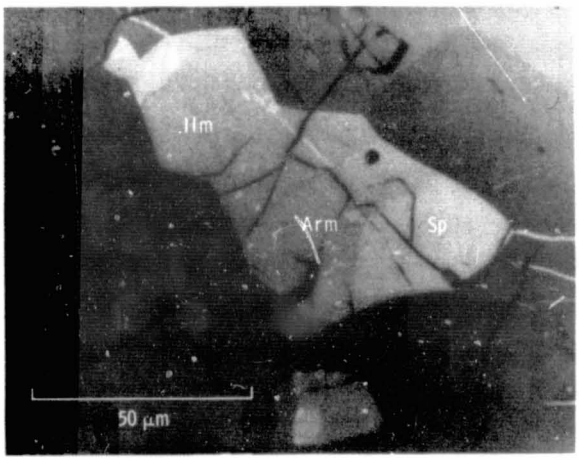

Figure 4-1.- Reflected light photomicrograph showing the association of spinel (Sp), ilmenite (Ilm), and armalcolite (Arm) in clast 8A; the stringers and small inclusions within the ilmenite are spinel.

The texture of the troctolite clast is shown in figure 4-2. Brown et al. (ref. 4-12) have observed 2- to 3-mm-size fragments of olivine (Fo_{86}) and plagioclase (An_{95}) intergrowths in breccia sample 14320,4 and describe their texture as crescumulate, similar to the layered ultra-basic rocks of Rhum (ref. 4-13). The long, branching olivines characteristic of crescumulates are absent in clast 8A; olivine occurs as chains of randomly oriented, interlocking crystals set in a matrix of polycrystalline plagioclase. These chains could be remnants of a coarser, crescumulate texture, but, if so, recrystallization has been completed. Alternatively, deformations followed by complete annealing could produce the observed texture.

A glassy fragment fused to the troctolite clast along a 2-mm boundary in the thin section seems to be partly remelted mare basalt. This fragment contains plagioclase, spinel, and pigeonite (tables 4-III, 4-V, and 4-VI) typical of such

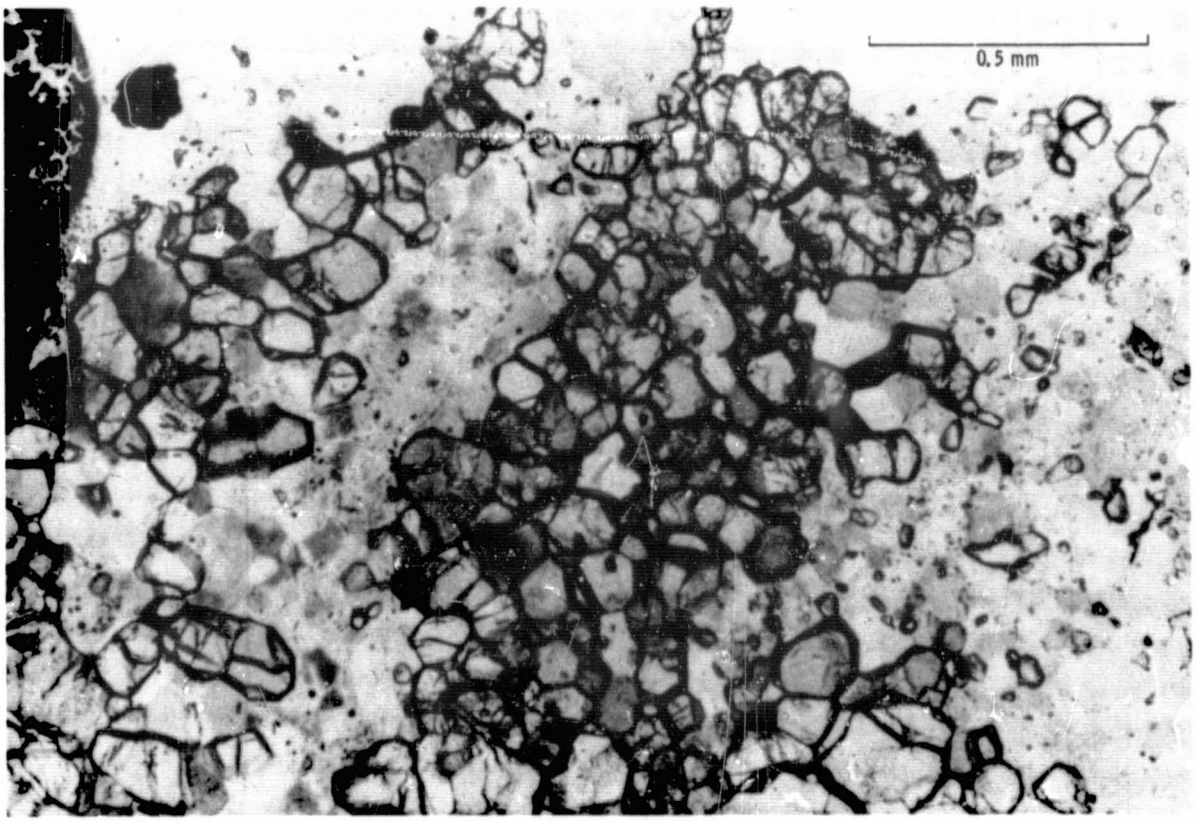

Figure 4-2.- Ordinary light photomicrograph of troctolite clast 8A showing polycrystalline aggregates of olivine and plagioclase.

TABLE 4-VI.- PYROXENE ANALYSES

Compound, element, or mineral	Basalt clast 4A			Basalt clast 6A			Contact zone, enstatite	Glassy basalt, pigeonite
	Pigeonite	Mg-augite	Fe-augite	Pigeonite	Mg-augite	Fe-augite		
Compound abundance, wt.%								
SiO_2	53.01	50.53	48.60	52.67	50.45	50.11	56.61	52.39
TiO_2	.46	1.12	1.37	.55	1.09	1.62	.35	.61
Al_2O_3	1.79	1.50	1.26	1.92	3.45	1.91	1.59	1.46
FeO	15.99	22.54	29.89	16.76	15.76	22.56	9.99	18.22
MnO	.22	.33	.43	.31	.31	.40	.11	.26
MgO	23.35	14.06	4.64	22.57	19.00	12.98	30.54	21.15
CaO	4.24	9.23	12.53	4.91	8.86	10.64	.49	5.07
Na_2O	<.04	<.04	.07	<.04	<.04	.06	<.04	<.04
Cr_2O_3	.84	.38	.06	.86	1.26	.56	.31	.64
Total	99.90	99.69	98.85	100.55	100.18	100.84	99.99	99.80
Molecular proportion[a]								
Si	1.942	1.946	1.979	1.930	1.876	1.919	1.982	1.947
Al^{IV}	.058	.054	.021	.070	.124	.081	.018	.053
Al^{VI}	.019	.014	.040	.013	.027	.005	.048	.011
Ti	.013	.032	.042	.015	.031	.047	.009	.017
Fe	.490	.726	1.018	.514	.490	.722	.292	.566
Mn	.007	.011	.015	.010	.010	.013	.003	.008
Mg	1.275	.807	.282	1.234	1.053	.741	1.593	1.172
Ca	.166	.381	.547	.193	.353	.437	.018	.202
Na	0	0	.006	0	0	.005	0	0
Cr	.024	.012	.002	.025	.037	.017	.009	.019
Total	3.994	3.983	3.952	4.004	4.001	3.987	3.972	3.995
Mineral abundance, mol%								
Enstatite	66.0	42.2	15.3	63.6	55.6	29.0	83.7	60.4
Ferrosilite	25.4	37.9	55.1	26.5	25.8	38.0	15.4	29.2
Wollastonite	8.6	19.9	29.6	9.9	18.6	23.0	.9	10.4

[a]On the basis of six oxygen ions.

basalts, although an olivine grain, unusual in containing neither calcium (Ca) nor chromium, is also included. (See table 4-II for limits of detection.) Troctolite minerals at the boundary have interacted with the glassy basalt. Contacting olivine grains are strongly zoned. One large grain of typical Fo_{86} composition adjacent to the troctolite plagioclase is zoned to Fo_{56} at the glassy contact. A few homogeneous enstatite (En) grains (table 4-VI) are formed only along this contact region. Plagioclase, however, is not altered. These reactions are confined to the contact zone and do not influence the center of the clast. The reactions could have been caused by an event affecting the fragment edge before basalt attachment or, more probably, by "contact metamorphism" produced by the basalt glass coating. Mineral grains in the glassy basalt are not zoned, but available data are not sufficient to determine any possible annealing history.

The troctolite clast preserves evidence of an early low-temperature recrystallization and equilibration and a later contact with a fused but rapidly chilled basalt, which did not cause penetrative reequilibration of the troctolite. The troctolite clast was finally incorporated into the light matrix of the breccia. Grieve et al. (ref. 4-3) and Duncan et al. (ref. 4-14) recognize three generations of recrystallization in fragments within the breccia, the first at a mean temperature of approximately 1273 K (1000° C) and the second and third at 973 K (700° C). This thermal history does not fit neatly with that of the troctolite, although the lower temperature could correspond to that of equilibration.

BASALT CLASTS 4A AND 6A

Basalt clasts 4A and 6A of sample 14321,88 are rounded fragments containing grains larger than 200 μm. Clast 4A contains approximately 3 percent olivine, 5 percent opaque minerals, and more pyroxene than plagioclase, whereas clast 6A contains approximately 20 percent olivine and equal quantities of plagioclase and pyroxene with fine-grained ilmenite. Only one olivine grain was successfully extracted from clast 4A (table 4-II), and the only spinel (table 4-V) analyzed was included in this grain. Because the entire small, high-density separate of clast 6A was required for Rb/Sr dating, no ilmenite analyses were obtained for this clast. The pyroxene data for both fragments are summarized in figure 4-3, and representative analyses are given in table 4-VI. Average plagioclase analyses are given in table 4-III.

The olivine in clast 4A is considerably richer in Fe than the early pigeonite (fig. 4-3); consequently, the included spinel, although obviously a primary phase may not represent the initial chromite composition that crystallized. Nevertheless, if the titanium partitioning is comparable to that in Apollo 12 basalts, then the titanium content of the spinel indicates that the TiO_2 content of the magma was approximately 3 percent. The pyroxene zoning of clast 4A is similar to that of the type VI lunar basalt classification of Bence and Papike (ref. 4-15). The representative of the type is sample 14053, an aluminous rock having a very low oxygen fugacity in the late stages of crystallization and apparently itself once a clast in a breccia. The spinel analysis may be matched precisely by primary nonreduced 14053 spinels analyzed in the authors' laboratory; however, the 14053 olivines are much more magnesian (Fo_{67} to Fo_{69}) and the feldspars more calcic (An_{84} to An_{94}). Pyroxenes composed of 35 mol% wollastonite (Wo_{35}) and En_{45} found in sample 14053 are absent in the specimen removed from clast 4A. Nevertheless, the evidence is that the clast has a bulk composition and an

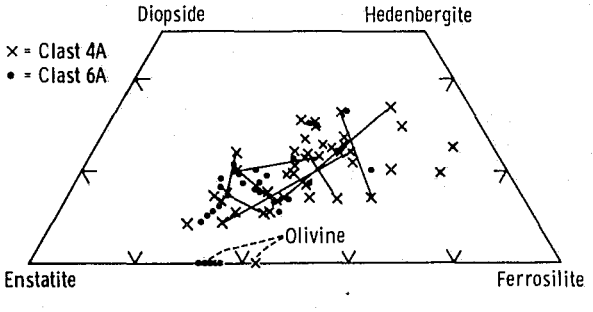

Figure 4-3.- Pyroxene zoning in basaltic clasts 4A (crosses) and 6A (dots). Core and rim (greater ferrosilite content) analyses are joined.

initial crystallization history similar to those of sample 14053 but continued to precipitate olivine to lower temperatures. Late-stage pyroxenes are zoned toward hedenbergite and were precipitated together with ilmenite. Unfortunately, no data exist for the final stages, which are characterized in sample 14053 by very low oxygen fugacities and recorded by subsolidus oxide reduction reactions.

The olivine in clast 6A is of similar Mg/Fe content to the most magnesian pigeonite, and the early subcalcic augite contains as much as 3.5 percent Al_2O_3. Apart from the Al_2O_3 content, the chemical trends in the pyroxenes are similar to those in clast 4A and sample 14053, although zoning in the pyroxene quadrilateral does not extend as far in the hedenbergite direction. Clast 6A seems to be another high-Al_2O_3 basalt preserving minerals of a crystallization temperature earlier than those of minerals in clast 4A.

RELATIONSHIP OF TROCTOLITE CLAST TO OTHER LUNAR HIGHLAND COMPOSITIONS

Prinz et al. (ref. 4-8) have described, analyzed, and classified 157 lithic fragments from the lunar highland region sampled by the Luna 20 spacecraft. The rock type classified as spinel troctolite has an average composition close to that of the troctolite 8A clast (table 4-I). The mineralogy given for spinel troctolite (table 2 and figs. 8 to 13 of ref. 4-8) shows olivine averaging Fo_{83} and plagioclase averaging An_{96} but spinel typically with more than 60 percent Al_2O_3 and less than 5 percent Cr_2O_3. Prinz et al. noted that, in bulk composition and mineralogy, the spinel troctolite fragments form a tightly clustered group. Troctolite clast 8A therefore assumes a greater significance in exemplifying the subsolidus equilibrated mineralogy of this bulk compositional grouping. The discussions in references 4-8 and 4-16 of crystallization in the Fo-rich olivine/anorthite/silica system illustrate that the spinel troctolite bulk composition will crystallize as an equilibrated assemblage of olivine and anorthite plus accessory minerals, including chromium-rich spinel and minor orthopyroxene. However, if this assemblage is partly or completely melted in an impact event, the mineralogy will contain highly aluminous spinel as a major phase. Thus, the principal differences between the mineralogy of troctolite 8A and that of the spinel-bearing troctolites described in references 4-8 and 4-9 are due to differences in temperature of crystallization.

The primary origin of troctolite clast 8A may have been as a cumulate from magnesian, high-Al_2O_3 basalts of the "Fra Mauro type" (ref. 4-17). If this origin is valid, the presence of accessory titanium-rich minerals, whitlockite, and barian K-feldspar establishes a link with the geochemical characteristics of the alkali-rich members of this basalt suite (e.g., high-K Fra Mauro basalts; potassium, rare-earth elements, and phosphorus (KREEP)). The cumulus origin would imply interstitial entrapment of source parent liquid and equilibration of this unit with the cumulus phases at subsolidus temperatures.

An alternative to the preceding genetic relationship is to interpret the Fra Mauro basalts as having been formed by varying degrees of incomplete melting of a parent troctolite composition. Results of experimental studies (refs. 4-16 and 4-18) show that olivine (Fo_{80} for KREEP, Fo_{88} for sample 14310) and plagioclase are the near-liquidus phases for "Fra Mauro basalt" types at low pressure and would be the residual phases during partial melting. Incomplete melting of the troctolite would leave olivine ($Fo_{86.5+}$) and plagioclase ($An_{95.5+}$) as residual phases and eliminate phases such as barian K-feldspar, whitlockite, and ilmenite. Comparison of REE data for troctolite clast 8A and Fra Mauro basalts (ref. 4-4) shows that REE data, applied with current uncertainties in partition coefficients and assuming partial melting or crystallization in equilibrium, are consistent with either interpretation.

REFERENCES

4-1. Chao, E. C. T.; Minkin, Jean A.; and Best, Judith B.: Apollo 14 Breccias: General Characteristics and Classification. Proceedings of the Third Lunar Science Conference, vol. 1, MIT Press (Cambridge, Mass.), 1972, pp. 645-660.

4-2. Warner, Jeffrey L.: Metamorphism of Apollo 14 Breccias. Proceedings of the Third Lunar Science Conference, vol. 1, MIT Press (Cambridge, Mass.), 1972, pp. 623-644.

4-3. Grieve, R.; McKay, G.; Smith, H.; and Weill, D.: Mineralogy and Petrology of Polymict Breccia 14321. Lunar Science III (Abs. of papers presented at the Third Lunar Science Conference (Houston, Tex.) Jan 10-13, 1972), pp. 338-340.

4-4. Taylor, S. R.; Kaye, Maureen; et al.: Composition of the Lunar Uplands: Chemistry of Apollo 14 Samples From Fra Mauro. Proceedings of the Third Lunar Science Conference, vol. 2, MIT Press (Cambridge, Mass.), 1972, pp. 1231-1250.

4-5. Compston, W.; Vernon, M. J.; et al.: Apollo 14 Mineral Ages and the Thermal History of the Fra Mauro Formation. Proceedings of the Third Lunar Science Conference, vol. 2, MIT Press (Cambridge, Mass.), 1972, pp. 1487-1502.

4-6. Lovering, J. F.; and Ware, N. G.: Electron-Probe Microanalyses of Minerals and Glasses in Apollo 11 Lunar Samples. Proceedings of the Apollo 11 Lunar Science Conference, vol. 1, Pergamon Press (New York), 1970, pp. 633-654.

4-7. Reed, Stephen J. B.; and Ware, N. G.: Quantitative Electron Microprobe Analysis Using a Lithium Drifted Silicon Detector. X-Ray Spectrom., vol. 2, no. 2, 1973, pp. 69-74.

4-8. Prinz, Martin; Dowty, Eric; Keil, Klaus; and Bunch, T. E.: Mineralogy, Petrology and Chemistry of Lithic Fragments From Luna 20 Fines: Origin of the Cumulate ANT Suite and Its Relationship to High-Alumina and Mare Basalts. Geochim. Cosmochim. Acta, vol. 37, 1973, pp. 979-1006.

4-9. Gooley, R.; Brett, Robin; Warner, Jeff; and Smyth, J. R.: A Lunar Rock of Deep Crustal Origin: Sample 76535. Geochim. Cosmochim. Acta, vol. 38, 1974, pp. 1329-1339.

4-10. Roedder, Edwin; and Weiblen, Paul W.: Petrology of Some Lithic Fragments From Luna 20. Geochim. Cosmochim. Acta, vol. 37, 1973, pp. 1031-1052.

4-11. Roedder, Edwin; and Weiblen, Paul W.: Occurrence of Chromian, Hercynitic Spinel ("Pleonaste") in Apollo-14 Samples and Its Petrologic Implications. Earth Planet. Sci. Letters, vol. 15, 1972, pp. 376-402.

4-12. Brown, G. M.; Emeleus, C. H.; et al.: Mineral-Chemical Variations in Apollo 14 and Apollo 15 Basalts and Granitic Fractions. Proceedings of the Third Lunar Science Conference, vol. 1, MIT Press (Cambridge, Mass.), 1972, pp. 141-158.

4-13. Wager, L. R.; and Brown, G. M.: Rhum Chemistry and Genesis. Layered Igneous Rocks. W. H. Freeman and Company (San Francisco), 1967, pp. 284-297.

4-14. Duncan, A. R.; Grieve, R. A. F.; and Weill, D. F.: The Life and Times of Big Bertha: Lunar Breccia 14321. Geochim. Cosmochim. Acta, vol. 39, no. 3, 1975, pp. 265-273.

4-15. Bence, A. E.; and Papike, J. J.: Pyroxenes as Recorders of Lunar Basalt Petrogenesis: Chemical Trends Due to Crystal-Liquid Interaction. Proceedings of the Third Lunar Science Conference, vol. 1, MIT Press (Cambridge, Mass.), 1972, pp. 431-469.

4-16. Walker, David; Longhi, John; and Hays, James Fred: Experimental Petrology and Origin of Fra Mauro Rocks and Soil. Proceedings of the Third Lunar Science Conference, vol. 1, MIT Press (Cambridge, Mass.), 1972, pp. 797-818.

4-17. Reid, A. M.; Warner, J. L.; Ridley, W. I.; and Brown, R. W.: Major Element Composition of Glasses in Three Apollo 15 Soils. Meteoritics, vol. 7, Sept. 30, 1972, pp. 395-415.

4-18. Green, D. H.; Ringwood, A. E.; Ware, N. G.; and Hibberson, W. O.: Experimental Petrology and Petrogenesis of Apollo 14 Basalts. Proceedings of the Third Lunar Science Conference, vol. 1, MIT Press (Cambridge, Mass.), 1972, pp. 197-206.

5. U-Th-Pb Systematics of Apollo 16 Samples 60018, 60025, and 64435; and the Continuing Problem of Terrestrial Pb Contamination of Lunar Samples

P. D. Nunes[a], D. M. Unruh[b], and M. Tatsumoto[b]

Uranium, thorium, and lead concentrations and lead isotopic compositions of Apollo 16 breccias 60018 and 64435 and anorthosite 60025 were determined. Serious terrestrial lead contamination of most 60018 separates and of sample 60025 occurred before sample digestion, although no uranium or thorium contamination was detected. The data from essentially uncontaminated breccia 64435, breccia 60018, and a glass separate of breccia 60018 yield uranium-thorium-lead patterns much like those that the authors have found and published for other Apollo 16 rocks. An acid-leach experiment of one of the highly contaminated samples (< 100 mesh, 60018) revealed that the contaminate lead was not easily leachable and that it may have occurred by addition of not-easily-dissolved solids. Analyses of a "clean" NASA saw blade revealed 10 to 11 ppm lead in the saw's cutting edge, which may have been the source of lead contamination.

The lead (Pb) isotopic compositions of Pb and the concentrations of uranium (U), thorium (Th), and Pb were determined in Apollo 16 anorthosite 60025 and breccias 60018 and 64435, collected in the Descartes mountain region in the central lunar highlands.

[a]Department of Geology and Mineralogy, Royal Ontario Museum, Ontario, Canada.

[b]U.S. Geological Survey, Denver, Colorado.

Unfortunately, terrestrial Pb contamination grossly altered the Pb concentrations and U/Pb ratios of many of these samples. An effort was made to discover the source of this contamination.

The relatively uncontaminated samples supplement U-Th-Pb Apollo 16 data previously reported and augment U-Th-Pb patterns already established (refs. 5-1 and 5-2).

ANALYTICAL PROCEDURE

All whole-rock samples were crushed in a stainless steel mortar and analyzed directly. Phase separates of breccia 60018 were obtained by handpicking, sieving, and using a hand magnet.

Samples were dissolved in Teflon bombs. Extraction of the Pb was achieved using a two-step anion exchange technique (ref. 5-1). Total Pb blanks ranged from about 0.5 to 1.9 ng during this study. The U and Th were separated with Dowex 1 X 8, NO_3-form resin (ref. 5-3). The U and Th blanks were less than 0.01 ng.

RESULTS AND DISCUSSION

Concentrations of U, Th, and Pb and the Pb isotopic compositions of breccias 60018 and 64435 and anorthosite 60025 are listed in tables 5-I and 5-II, respectively. Tne U concentrations in breccia 60018 range from ~0.1 ppm (plagioclase concentrate) to ~1.2 ppm (light gray lithic fraction) and probably

reflect varying amounts of potassium, rare-earth elements, and phosphorus (KREEP)[1] component. Plagioclase-pyroxene breccia 64435 contains only about 0.02 ppm U and 0.09 ppm Th – lower than all lunar rocks yet analyzed excluding anorthosites.

Data in tables 5-I and 5-II are graphically displayed on a $^{206}Pb/^{207}Pb$ versus $^{238}U/^{207}Pb$ positive slope variant of the $^{207}Pb/^{206}Pb$ versus $^{238}U/^{206}Pb$ plot (fig. 5-1) of reference 5-4. Also plotted for comparison are breccia 66095 (ref. 5-2), hornfels 65015 (refs. 5-1 and 5-9), anorthosites 60015 (ref. 5-1), 15415 (ref. 5-6), and 67075 (ref. 5-8,), and another analysis of 60025 (ref. 5-5). Except for anorthosites 60015, 67075, and 60025, all Apollo 16 whole-rock samples previously published (refs. 5-1, 5-2, 5-8, and 5-10), fall within error on the solid line drawn in figure 5-1. Chipped samples of hornfels 65015 with a $^{206}Pb/^{204}Pb$ ratio of >2500 (refs. 5-1 and 5-9) and breccia 66095 with a Pb content of ∿15 ppm (ref. 5-2) represent pristine, essentially uncontaminated lunar material. The dashed contamination line in figure 5-1 defines the line along which hornfels 65015 would move if mixed with modern terrestrial Pb. The proximity of anorthosite 60025 and five of the separates of breccia 60018 to this contamination line and the rather low $^{206}Pb/^{204}Pb$ values of these samples (table 5-II) suggest that up to 99 percent of the

[1]Term used to express chemical composition of lunar materials. After Hubbard, N. J.; and Gast, P. W.: Chemical Composition and Origin of Nonmare Lunar Basalts. Proceedings of the Second Lunar Science Conference, vol. 2, MIT Press (Cambridge, Mass.), 1971, p. 999.

TABLE 5-I.- CONCENTRATIONS U, Th, AND Pb IN APOLLO 16 ANORTHOSITE 60025 AND BRECCIAS 60018 AND 64435

Sample	Run	Weight, mg	Concentrations, ppm			Atomic ratios	
			U	Th	Pb	$\frac{^{232}Th}{^{238}U}$	$\frac{^{238}U}{^{204}Pb}$
Anorthosite 60025	1	74.4	0.000594	0.00152	0.0652	2.64	0.581
	[a]2	113.7	.000502	.00108	.0936	2.22	.340
Breccia 60018:							
Whole rock	[a]1	208.9	.801	3.160	1.722	4.08	1378
<100 mesh	1	48.7	.796	3.021	6.643	3.92	9.55
	[a]2	180.5	.381	1.398	1.369	3.79	190
Handpicked glass	[a]1	32.3	.694	2.588	1.827	3.86	353
Magnetics	1	29.8	.433	1.544	1.657	3.68	34.9
Handpicked dark gray	1	39.6	1.055	3.584	2.623	3.51	161
Handpicked light gray	[a]1	88.4	1.209	4.469	2.520	3.82	230
Handpicked white	1	19.11	.1123	.544	.710	5.01	19.4
Breccia 64435	1	58.4	.0226	.0917	.354	4.19	39.2
	[a]2	145.6	.0299	--	.397	--	35.6

[a]Samples totally spiked before digestion.

Pb extracted from these samples is terrestrial. Breccia 64435, breccia 60018, and handpicked glass samples of breccia 60018, on the other hand, lie very close to or on the solid line in figure 5-1; have high $^{206}Pb/^{204}Pb$ ratios (table 5-II); and appear to be negligibly contaminated with terrestrial Pb.

Minimally contaminated samples

When corrected for an assumed primordial Pb (ref. 5-11), the whole-rock and glass analyses of breccia 60018 fall within error on the 4.47- to 3.99-billion-years (b.y.) discordia line defined by other Apollo 16

TABLE 5-II.- ISOTOPIC COMPOSITION OF Pb IN APOLLO 16 SAMPLES 60025, 60018, AND 64435

Sample	Weight, mg	Run	Atomic ratios							
			Observed ratios[a]			Corrected for analytical blank[b,c]				
			$\frac{206_{Pb}}{204_{Pb}}$	$\frac{207_{Pb}}{204_{Pb}}$	$\frac{208_{Pb}}{204_{Pb}}$	$\frac{206_{Pb}}{204_{Pb}}$	$\frac{207_{Pb}}{204_{Pb}}$	$\frac{208_{Pb}}{204_{Pb}}$	$\frac{207_{Pb}}{206_{Pb}}$	$\frac{208_{Pb}}{206_{Pb}}$
Anorthosite 60025										
Whole rock	95.6	P1	18.52	15.72	38.14	18.67	15.78	38.37	0.8456	2.056
	74.4	C1	18.73	15.71	--	18.83	15.74	--	.8361	--
	113.7	[d]C2	18.52	15.64	--	18.54	15.65	--	.8440	--
Breccia 60018										
Whole rock	56.9	P1	436.9	244.3	432.0	643.2	357.1	627.7	0.5552	0.976
	208.9	[d]C1	1119	606.0	--	1356	732.9	--	.5405	--
<100 mesh (magnetics removed)	49.3	P1	25.92	19.58	45.35	26.02	19.65	45.58	.7551	1.752
	48.7	C1	25.94	19.59	--	26.00	19.62	--	.7546	--
	180.5	[d]C2	224.2	124.2	--	239.0	132.0	--	.5523	--
Handpicked glass	71.9	P1	262.3	144.1	272.2	298.2	163.0	307.4	.5466	1.031
	32.3	[d]C1	323.7	219.6	--	403.5	274.2	--	.6762	--
Magnetics	32.5	P1	51.37	32.54	71.41	52.12	32.94	72.35	.6319	1.388
	29.8	C1	50.15	31.71	--	50.82	32.04	--	.6306	--
Handpicked dark gray	40.9	P1	148.1	77.88	169.0	151.7	79.60	173.0	.5248	1.141
	39.6	C1	169.7	88.16	--	174.2	90.32	--	.5185	--
Handpicked light gray	109.2	P1	230.2	110.2	233.2	247.2	117.8	249.5	.4765	1.009
	88.4	[d]C1	216.8	104.3	--	227.7	106.8	--	.4799	--
Handpicked white	40.37	P1	42.88	29.32	66.72	43.78	29.84	67.96	.6816	1.552
	19.11	C1	41.89	28.67	--	43.53	29.58	--	.6795	--
Breccia 64435										
Whole rock	71.0	P1	159.9	198.6	152.8	223.5	280.8	204.8	1.256	0.917
	58.4	C1	150.5	186.1	--	221.1	277.4	--	1.254	--
	145.6	[d]C2	155.2	195.3	--	170.6	215.4	--	1.263	--

[a] ^{208}Pb spike contribution subtracted from Pb concentration data.

[b] The Pb isotopic composition used for blank corrections is $^{206}Pb/^{204}Pb = 18.36$; $^{207}Pb/^{204}Pb = 15.58$; and $^{208}Pb/^{204}Pb = 37.88$.

[c] Analytical total Pb blanks were 1.18 ng for anorthosite 60025 analyses and ranged from 0.48 ng to 1.9 ng for the remaining analyses.

[d] Samples totally spiked before digestion.

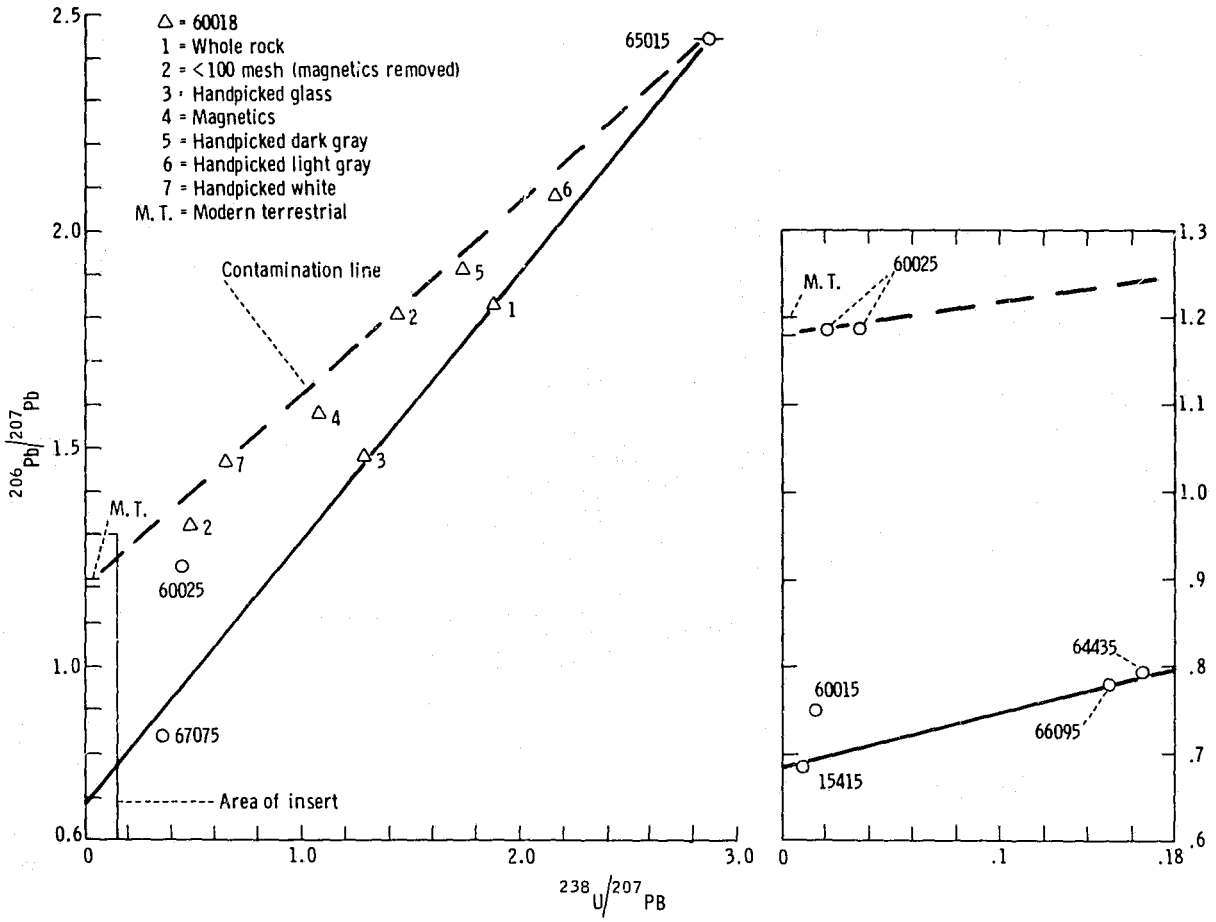

Figure 5-1.- A plot of $^{206}Pb/^{207}Pb$ compared to $^{238}U/^{206}Pb$. New data from 60018, 60025, and 64435 are plotted. The following data are plotted for comparison: 60025 analyzed in reference 5-5, an interior analysis of anorthosite 60015 (ref. 5-1), breccia 66095 (ref. 5-2), anorthosite 15415 (refs. 5-6 and 5-7), anorthosite 67075 (ref. 5-8), and hornfels 65015 (ref. 5-1). Data are corrected for blanks only.

whole-rock U-Pb data excluding anorthosites (refs. 5-1 and 5-9). The 60018 whole-rock analysis is nearly concordant at about 4.42 b.y.[2] The glass contains excess Pb relative to U, which suggests it is either a soil impact melt (i.e., the excess Pb may have been present before glass formation) or the glass somehow gained Pb relative to U after its formation.

Although breccia 64435 contains only ∿0.4 ppm Pb, its very low U and Th contents indicate a severe net enrichment of Pb relative to U and Th. Much like breccia 66095 (ref. 5-2), breccia 64435 apparently gained Pb characterized by a very high $^{207}Pb/^{206}Pb$ ratio of about 1.45. The isotopic character of the excess Pb in 64435 requires that this Pb was produced in a U-rich reservoir very early in the Moon's history when the production rate of ^{207}Pb exceeded that of ^{206}Pb. Model ages of 3.73 to 4.0 b.y. for the introduction of excess Pb into breccia 64435 and of 4.65 to 4.42 b.y. for the production of a U-rich reservoir (μ = 496 to 1115) may be calculated using two- and three-stage U-Th-Pb evolution models, respectively, as discussed at length in reference 5-2.

Despite gross differences in absolute U, Th, and Pb concentrations measured in breccias 64435 (table 5-I)

[2]The constants used are λ_{238} = 0.15369 × 10^{-9} yr^{-1}; λ_{235} = 0.97216 × 10^{-9} yr^{-1} (ref. 5-12); and $^{238}U/^{235}U$ = 137.8 (ref. 5-13). If the U-decay constants of reference 5-14 were used, the ages reported here would be reduced approximately 1.3 percent.

and 66095 (ref. 5-2), both these samples appear to have undergone very similar U-Th-Pb evolution histories.

The Continuing Problem of Terrestrial Pb Contamination of Lunar Samples

Serious terrestrial Pb contamination of some of the Apollo 16 samples has occurred. In this section, the cause of contamination is discussed, and procedures whereby such contamination may be eliminated in the future are recommended.

Contamination of lunar samples by terrestrial Pb has long been a problem to U-Th-Pb investigators. Possible sources of contamination discussed in the literature are as follows.

1. Pb introduced by analytical blanks (currently only a serious problem in very small samples or in samples with very low Pb concentrations such as anorthosites)
2. Mineral-separation techniques (e.g., the heavy-liquid problem reported in ref. 5-7)
3. NASA preparation of the samples (e.g., the contaminated sawdust reported in refs. 5-7 and 5-15)
4. Rocket exhaust contamination possibilities mentioned in reference 5-7
5. Contamination on the lunar surface during sample collection (e.g., the core tube contamination of Apollo 15 and 16 samples reported in refs. 5-8 and 5-16)

Handpicked mineral concentrates and sieve fractions of breccia 60018 and whole-rock analyses of 60025 show strong apparent terrestrial Pb contamination (table 5-III). In particular, the Pb isotopic composition of 60025 determined in the authors' laboratory was indistinguishable from that of modern terrestrial Pb ($^{206}Pb/^{204}Pb \sim 18.5$; measured Pb concentrations = 0.065 and 0.094 ppm). One split of the <100 mesh fraction of 60018 contained 6.6 ppm Pb with a $^{206}Pb/^{204}Pb$ ratio of 26.01; whereas relatively uncontaminated whole-rock and glass samples from this same rock suggest this ratio should be at least 10 times this value[3]. Altogether, three separate splits of the <100 mesh fraction (minus the magnetic component) were analyzed. Two of these splits were analyzed directly (tables 5-I and 5-II), and one was used for an acid-leach experiment (table 5-IV). The gross differences in the measured U, Th, and Pb concentrations and Pb isotope ratios of these three samples reflect considerable heterogeneity among the splits. The acid-leach experiment showed that the residue contained as much Pb as the preceding three acid leaches combined and had a lower $^{206}Pb/^{204}Pb$ ratio than any of the acid leaches (table 5-IV). This finding probably indicates a particulate type of contamination rather than easily dissolved surface contamination.

Interestingly, the Th/U ratios found in the first two nitric acid leaches (steps 2 and 3, table 5-IV) are much higher than the third acid leach (step 4, table 5-IV), which in turn has a lower Th/U ratio than does the residue (step 5, table 5-IV). This pattern was also found in the leach experiment of breccia 66095 (ref. 5-2), and shows that Th is bound in at least two very different sites. Possibly the nitric acid leaches dissolved one or more accessory Th-rich phases such as phosphates.

Because sample 60015 (ref. 5-1) falls outside of error off the U-Pb trend established for other Apollo 16 rock samples (fig. 5-1) in the direction of modern terrestrial Pb, this sample may also exhibit a small degree of terrestrial Pb contamination. Alternatively, this sample may contain a lunar Pb distinctly different from that of most other Apollo 16 samples (ref. 5-1).

The Pb data for 60025 (this report and ref. 5-5) are not sufficiently precise, owing to terrestrial contamination problems, to calculate model ages – rather, these data emphasize that some lunar plagioclase may contain almost no Pb at all.

The large quantity of Pb measured in several of the contaminated samples (especially the first <100 mesh split of 60018 with 6.6 ppm Pb) is impossible to explain by physical or analytical contamination in the authors' laboratory. All samples analyzed by the authors that exhibit significant contamination have one thing in common: they were cut with a bandsaw in the NASA Lunar Receiving Laboratory, although not all samples so dissected were significantly contaminated (table 5-III). To pursue this problem further, the authors requested and received a "clean" saw blade from NASA that had been cleaned as re-

[3]The Pb concentration determinations were made from 10.6 ng and 4.9 ng of total Pb extracted in the case of 60025 and 324 ng Pb extracted in the case of 60018 <100 mesh split 1. Analytical blanks associated with these 60025 and 60018 analyses were 1.18 ng and 1.72 ng, respectively.

TABLE 5-III.- APOLLO 16 SAMPLES ANALYZED BY NUNES AND TATSUMOTO

[Percentage lead contamination estimated by Nunes and Tatsumoto (ref. 5-1) from the degree analyses depart from the U-Pb trend defined by a line joining 66095 and 65015 whole-rock data]

Sample no.	Weight, g	Apparent lead contamination, percent	Any sawed surface?[a]	Comments[a]
60015,46	6.83	13	Yes	Thin chips with sawed surfaces along the narrow edges.
60018,16:	21.67		Yes, on almost all faces	Piece of 1.5-cm-thick slab; sufficient material existed in the slab so that sawed surface could be chiseled off to produce 5-g pieces free of sawed surface.
<100 mesh		77		
Handpicked plagioclase		64		
Magnetic fraction		53		
Handpicked dark gray		32		
Handpicked light gray		12		
Handpicked glass		(b)		
Handpicked whole rock		(b)		
60025,9003	2.81	99	Yes, on about 60% of faces	Sample is all of ,26 furnished by Haskin.
60315,81	3.04	(b)	No	Fresh chips (no sawed or lunar exterior surfaces).
64435,57	10	(b)	Some	Sample obtained from Rosholt; four large interior chips.
65015,52	3.09	(c)	No	Fresh chip.
66095,41	4.85	(c)	No	Rock was not sawed.
67015,11	5.08	(b)	No	Rock was not sawed.
67015,12	4.96	(b)	No	Rock was not sawed.
68415,63	3.48	(b)	~50% sawed surface	

[a] Sawed surface estimates and comments by P. Butler, Jr.

[b] <2% terrestrial Pb contamination.

[c] Assumed to contain no terrestrial Pb.

TABLE 5-IV.- LEAD ISOTOPIC COMPOSITIONS AND U, Th, AND Pb CONTENTS OF ACID LEACHES AND RESIDUE OF A 100 MESH SAMPLE[a] (MAGNETICS REMOVED) OF BRECCIA 60018

Step (b)	Leach description	Run (c)	Pb removed, ng	U removed, ng	Th removed, ng	Atomic ratios[d]									
						Observed			Corrected for blank						
						$\frac{206_{Pb}}{204_{Pb}}$	$\frac{207_{Pb}}{204_{Pb}}$	$\frac{206_{Pb}}{204_{Pb}}$	$\frac{206_{Pb}}{204_{Pb}}$	$\frac{207_{Pb}}{204_{Pb}}$	$\frac{208_{Pb}}{204_{Pb}}$	$\frac{207_{Pb}}{206_{Pb}}$	$\frac{208_{Pb}}{206_{Pb}}$	$\frac{232_{Th}}{238_{U}}$	$\frac{238_{U}}{204_{Pb}}$
1	4 ml water; 4 days	P	1.05	--	--	(23.62)	(18.72)	(48.16)	(27.21)	(20.89)	(55.35)	(0.7677)	(2.034)	--	--
		C	.54	--	--	(23.39)	(18.25)	--	(30.69)	(22.14)	--	(.7214)	--	--	--
2	4 ml 1 normal (1N) nitric acid (HNO_3); 2 days	P	157.2	46.41	509.9	44.04	29.95	89.11	44.31	30.11	89.83	.6794	2.027	--	--
		C	158.8	46.87	515.1	44.66	29.95	--	44.24	30.05	--	.6794	--	11.35	42.1
3	4 ml 16N HNO_3; 3 days	P	254.6	26.99	218.4	51.44	37.89	88.04	51.70	38.07	88.62	.7364	1.714	--	--
		C	296.8	31.45	254.6	51.50	37.93	--	51.64	38.02	--	.7364	--	8.36	16.4
[e]4	2 ml 50% hydrofluoric acid (HF) + 2 ml 16N HNO_3; 3 days	P	400.9	134.7	.958	66.99	39.53	75.23	67.43	39.75	75.77	.5896	1.124	--	--
		C	271.8	91.3	.650	67.16	39.63	--	67.61	39.85	--	.5895	--	.007	53.3
5	4.5 ml 50% HF + 4.5 ml 16N HNO_3; heated overnight (residue dissolution)	P	897.9	219.8	711.0	41.04	26.66	54.16	41.20	26.75	54.43	.6493	1.321	--	--
		C	520.4	127.4	412.0	41.12	26.72	--	41.25	26.78	--	.6493	--	3.34	26.0
	Total		2960	724.9	2623	--	--	--	--	--	--	--	--	--	--
	Apparent ppm of total sample		2.97	.728	2.63	--	--	--	--	--	--	--	--	--	--

[a]The total sample weighed 995.7 mg; ^{208}Pb spike contributions were subtracted from concentration data.

[b]Total Pb blanks were 0.47 ng for leach steps 1, 2, and 3; 1.0 ng for step 4; and 1.7 ng for the step 5 residue dissolution.

[c]P = composition. C = Concentration.

[d]Parentheses indicate significant uncertainty because of the small amounts of lead present.

[e]About one-third of the step 4 leach solution was spilled before dividing and spiking the concentration portion of this solution; thus, the totals of the U, Th, and Pb contents are slightly lower than the true values.

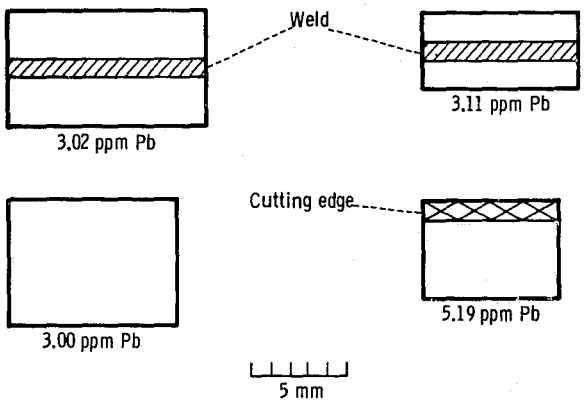

Figure 5-2.- Pieces of NASA steel bandsaw blade that were analyzed for Pb concentration (drawn approximately to scale).

quired by the NASA specification entitled "Lunar Receiving Laboratory Cleaning Procedures for Contamination Control." Four pieces were cut from the blade: two pieces contained varying amounts of the weld but no cutting edge, one piece contained only nonwelded steel, and the fourth piece included some steel and the cutting edge (fig. 5-2). The saw blade samples were cut with an acid-cleaned pair of tinsnips, and all four samples were consecutively washed in twice-distilled acetone for about 10 minutes, in cold, 1.7 normal hydrochloric acid for about 5 minutes, and in five-times-distilled water to remove any surficial Pb. The saw blade samples were then dissolved in hydrochloric acid and nitric acid, and the total samples spiked. Pb separation was achieved with anion exchange columns.

The total Pb contents calculated assuming a $^{208}Pb/^{206}Pb$ sample ratio of 2.063 are shown in figure 5-2. Agreement of the Pb contents of the three saw blade samples with no cutting edge indicates the steel has a uniform Pb content of $\sim$3 ppm regardless of the amount of welded region present. This value compares to the Pb content of 0.6 ppm found (ref. 5-15) for the copper-wire saw blade used in cutting Apollo 12 and 14 rocks.

CONCLUSIONS

The high Pb content of the bandsaw blade sample that includes a portion of the cutting edge ($\sim$5 ppm) indicates Pb is concentrated in the cutting edge, which consists of diamonds cemented in a white bonding material. It is emphasized that the measured Pb contents in these saw blade samples are minimal because of the preliminary acid-washing procedure. Judging from the relative amounts of steel and cutting edge in sample 4, a Pb content of $\sim$10.8 ppm is estimated for the cutting edge material. This quantity of Pb is sufficient to explain all contaminated data. The variable amounts of Pb contamination (from insignificant to much) of bandsaw-cut samples may be explained as varying saw blade particulate contributions to the samples. This variance can explain, for example, why the <100 mesh fraction of 60018 was so highly contaminated (the starting material containing considerable saw-blade-cut surfaces); whereas the whole-rock sample displayed no obvious contamination, perphaps because it was picked from small chunks with no flat (cut) surfaces. Unfortunately, an accurate assessment of the amount of saw blade surface on any given sample dissolved was not made before the realization that these samples were contaminated. In any case, the particulate nature of the contamination, as indicated by the acid-leach experiment and the very high Pb content of at least 10 to 11 ppm found in the cutting edge of the bandsaw blade, indicates that significant Pb contamination of lunar samples during sawing was likely.

To ensure "clean" lunar samples in the future, the following procedures are suggested.

1. Lunar investigators working with Pb should request only chipped samples.

2. When only sawed material is available, enough material should be obtained so that individual investigators may themselves chip away material that displays no sawed surfaces.

3. Sample chunks of cohesive material that are derived from originally sawed samples should be washed in twice-distilled acetone and vibrated ultrasonically to remove any particulate material that may be foreign to the sample. This cleaning should be performed by the individual investigators before crushing and mineral separation.

REFERENCES

5-1. Nunes, P. D.; Tatsumoto, M.; et al.: U-Th-Pb Systematics of Some Apollo 16 Lunar Samples. Proceedings of the Fourth Lunar Science Conference, vol. 2, Pergamon Press (New York), 1973, pp. 1797-1822.

5-2. Nunes, P. D.; and Tatsumoto, Mitsunobu: Excess Lead in "Rusty Rock" 66095 and Implications for an Early Lunar Differentiation. Science, vol. 182, no. 4115, 1973, pp. 916-920.

5-3. Tatsumoto, M.: Isotopic Composition of Lead in Volcanic Rocks from Hawaii, Iwo Jima, and Japan. J. Geophys. Res., vol. 71, no. 6, 1966, pp. 1721-1733.

5-4. Tera, Fouad; and Wasserburg, G. J.: U-Th-Pb Systematics in Three Apollo 14 Basalts and the Problem of Initial Pb in Lunar Rocks. Earth Planet. Sci. Letters, vol. 14, 1972, pp. 281-304.

5-5. Tera, Fouad; and Wasserburg, G. J.: U-Th-Pb Systematics in Lunar Highland Samples from the Luna 20 and Apollo 16 Missions. Earth Planet. Sci. Letters, vol. 17, 1972, pp. 36-51.

5-6. Tatsumoto, M.; Hedge, C. E.; et al.: U-Th-Pb, Rb-Sr, and K Measurements on Some Apollo 15 and Apollo 16 Samples. The Apollo 15 Lunar Samples. Lunar Science Institute (Houston, Tex.) 1972, pp. 391-395.

5-7. Tatsumoto, M.; Hedge, C. E.; Doe, B. R.; and Unruh, D. M.: U-Th-Pb and Rb-Sr Measurements on Some Apollo 14 Lunar Samples. Proceedings of the Third Lunar Science Conference, vol. 2, MIT Press (Cambridge, Mass.), 1972, pp. 1531-1555.

5-8. Silver, L. T.: Uranium-Thorium-Lead Isotopic Characteristics in Regolithic Materials from the Descartes Region. Lunar Science IV, (Abs. of papers presented at the Fourth Lunar Science Conference (Houston, Tex.) Mar. 5-8, 1973), pp. 672-674.

5-9. Tera, Fouad; Papanastassiou, D. A.; and Wasserburg, G. J.: Isotopic Evidence for a Terminal Lunar Cataclysm. Earth Planet. Sci. Letters, vol. 22, 1974, pp. 1-21.

5-10. Nunes, P. D.: Pb Loss From Apollo 17 Glassy Samples and Apollo 16 Revisited. Proceedings of the Sixth Lunar Science Conference, vol. 2, Pergamon Press (New York), 1975, pp. 1491-1499.

5-11. Tatsumoto, Mitsunobu; Knight, Roy. J.; and Allegre, Claude J.: Time Differences in the Formation of Meteorites as Determined from the Ratio of Lead-207 to Lead-206. Science, vol. 180, no. 4092, 1973, pp. 1279-1283.

5-12. Fleming, E. H., Jr.; Ghiorso, A.; and Cunningham, B. B.: The Specific Alpha-Activities and Half-Lives of U^{234}, U^{235}, and U^{236}. Phys. Rev., series 2, vol. 88, no. 3, 1952, pp. 642-652.

5-13. Rosholt, J. N.; and Tatsumoto, M.: Isotopic Composition of Uranium and Thorium in Apollo 11 Samples. Proceedings of the Apollo 11 Lunar Science Conference, vol. 2, Pergamon Press (New York), 1970, pp. 1499-1502.

5-14. Jaffey, A. H.; Flynn, K. F.; et al.: Precision Measurement of Half-Lives and Specific Activities of ^{235}U and ^{238}U. Phys. Rev. C, vol. 4, no. 5, 1971, pp. 1889-1906.

5-15. Tatsumoto, M.; Knight, R. J.; and Doe, B. R.: U-Th-Pb Systematics of Apollo 12 Lunar Samples. Proceedings of the Second Lunar Science Conference, vol. 2, MIT Press (Cambridge, Mass.), 1971, pp. 1521-1546.

5-16. Silver, Leon T.: Uranium-Thorium-Lead Isotopes and the Nature of the Mare Surface Debris at Hadley-Apennine. The Apollo 15 Lunar Samples. Lunar Science Institute (Houston, Tex.), 1972, pp. 388-390.

NASA-Langley, 1977